

Ruthenium-Catalyzed Transformations of Alcohols: Mechanistic Investigations and Methodology Development

Makarov, Ilya; Madsen, Robert; Fristrup, Peter

Publication date:
2013

Document Version
Publisher's PDF, also known as Version of record

[Link back to DTU Orbit](#)

Citation (APA):

Makarov, I., Madsen, R., & Fristrup, P. (2013). Ruthenium-Catalyzed Transformations of Alcohols: Mechanistic Investigations and Methodology Development. Technical University of Denmark, Department of Chemical Engineering.

DTU Library

Technical Information Center of Denmark

General rights

Copyright and moral rights for the publications made accessible in the public portal are retained by the authors and/or other copyright owners and it is a condition of accessing publications that users recognise and abide by the legal requirements associated with these rights.

- Users may download and print one copy of any publication from the public portal for the purpose of private study or research.
- You may not further distribute the material or use it for any profit-making activity or commercial gain
- You may freely distribute the URL identifying the publication in the public portal

If you believe that this document breaches copyright please contact us providing details, and we will remove access to the work immediately and investigate your claim.

Ruthenium-Catalyzed Transformations of Alcohols: Mechanistic Investigations and Methodology Development

PhD Thesis

Ilya S. Makarov

March 2013



Department of Chemistry
Technical University of Denmark

Ruthenium-Catalyzed Transformations of Alcohols: Mechanistic Investigations and Methodology Development

Ilya S. Makarov

Preface

THE WORK PRESENTED IN THIS DISSERTATION was carried out during my PhD study at the Department of Chemistry, Technical University of Denmark from December 2009 to February 2013 under the joint supervision of Professor Robert Madsen and Associate Professor Peter Fristrup. The work was financed by the Danish Council for Independent Research – Technology and Production Sciences.

First and foremost, I would like to express my profound gratitude to my supervisors for hosting me in their research groups and giving a great opportunity to work on fascinating projects in the field of organometallic and computational chemistry and also for inspiring me to work harder and produce more results.

I would like to thank Agnese Maggi, Amanda Birgitte Sølvhøj, Camilla Arboe Jennum, Esben Olsen, Linda Reeh Lorenz-Petersen, Györgyi Osztrovszky, Stig Holden Christensen, Thomas Hauch Fenger, Casper Junker Engelin, Alessandro Corozzi and the rest of the Madsen and Fristrup groups for making my work at DTU enjoyable.

Anne Hector and Charlotte Held Gotfredsen are acknowledged for their invaluable help with recording and processing NMR spectra, Tina Gustafsson for giving me a chance to learn how to operate the GC and GC-MS instruments in our building, Janne Borg Rasmussen and Brian Ekman-Gregersen for the fact that my research has never been stopped because of the lack of the chemicals I needed, Jan Patrick Scholer for excellently crafted glassware and the rest of the staff at our Department for maintaining good working environment in the building.

Esben Taarning, Martin Spangsborg Holm and Christian Mårup Osmundsen are acknowledged for introducing me to heterogeneous catalysis and assisting me during the external stay at Haldor Topsøe A/S.

Two persons, without whom I cannot imagine my life in Denmark and without whom I would have never come to be here, deserve a special gratitude. They are my very close friends, Alexandra Zakharova and Vitaly Komnatnyy. Thank you very much for practical help and emotional support, numerous

discussions, for praise and critic, marvelous jokes and biting irony. I will miss all these days we lived together.

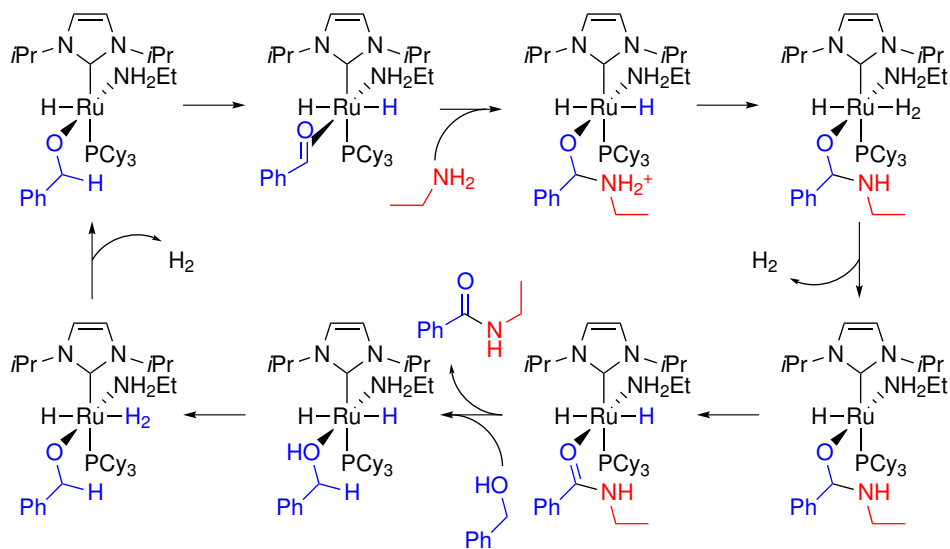
Last but not least I would like to thank my parents, Galina and Stanislav, for supporting me and giving me vital energy every time I come back to Russia.

Kongens Lyngby, March 2013

Ilya S. Makarov

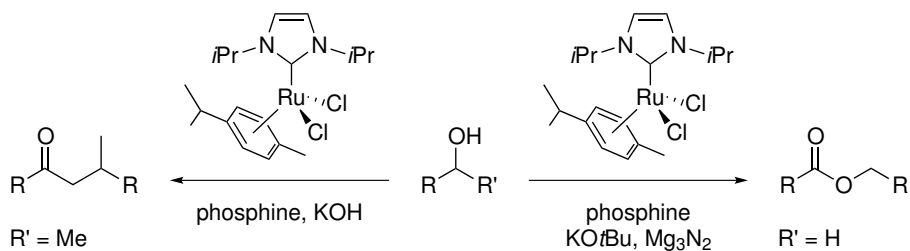
Abstract

THE MECHANISM OF THE RUTHENIUM-CATALYZED dehydrogenative synthesis of amides from alcohols and amines was studied in detail by employing the combination of experimental and theoretical techniques. The Hammett study revealed that a small positive charge is formed at the benzylic position in the transition state of the turnover-determining step. The value of the kinetic isotope effect of 2.29 ± 0.15 indicated that the C–H bond breakage is not the rate-determining step, but that it is one of several slow steps in the catalytic cycle. Experiments with deuterium-labeled alcohols and amines revealed that ruthenium-dihydride species are involved in the catalytic cycle. These experimental results were used in the DFT/MO6 computational study and a plausible catalytic cycle was proposed. Both *cis*-dihydride and *trans*-dihydride intermediates were considered, but when the theoretical turnover frequencies were obtained from the calculated energies, it was found that only the *trans*-dihydride pathway was in agreement with the experimentally determined frequencies.



The proposed catalytic cycle was used for an *in silico* search for more effective carbene ligands. The study showed that the ruthenium complexes with dimethoxyisopropylidene and pyridilidene ligands could be more active than $\text{RuCl}_2(\text{iPr})(p\text{-cymene})$ used in the mechanistic investigation. Two analogs of the calculated complexes were synthesized but were not isolated in a pure form. The amidation reaction catalyzed by a mixture containing the *N*-ethyl pyridilidene-substituted ruthenium complex afforded the amide in 38% yield. It indicated that *in silico* ligand screening might be used for catalyst optimization if it is combined with a more comprehensive experimental study.

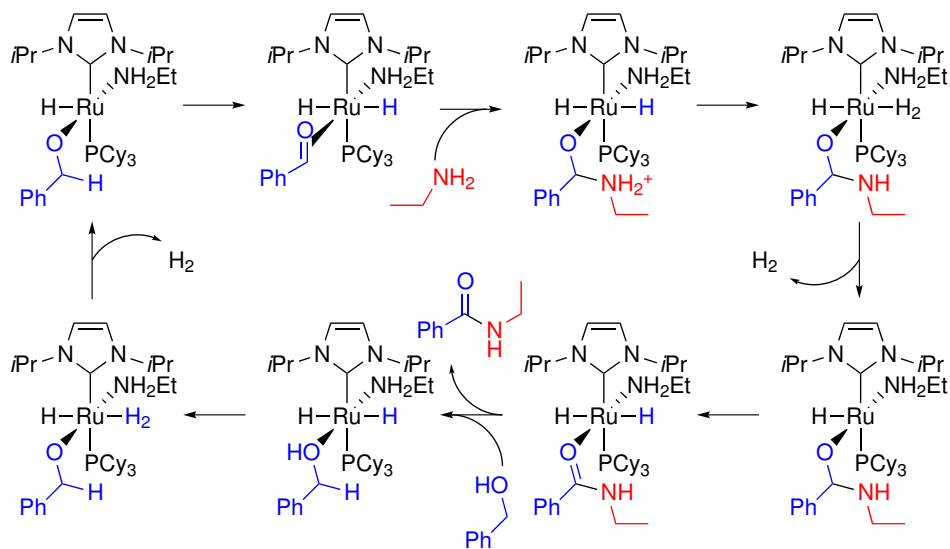
An improved protocol was developed for the ruthenium-catalyzed dehydrogenative self-coupling of primary alcohols to give esters. Addition of 16.7 mol% of Mg_3N_2 to the reaction mixture gave esters from aliphatic alcohols in similar yields but at lower temperature as compared with previously a reported catalytic system. This additive also suppressed the decarbonylation of aromatic alcohols. A previously unknown ruthenium-catalyzed dehydrogenative Guerbet reaction with secondary alcohols to give ketones was discovered. The reaction conditions were optimized and the scope and the limitations were studied. It was found that only acyclic 2-methyl carbinols and simple cyclic alcohols underwent this transformation. It was shown that the reaction proceeded via the oxidation–aldol condensation–reduction pathway and that the active ruthenium species was a dihydride.



During the external stay at Haldor Topsøe A/S, the transformation of acetaldehyde over zeolite-type heterogeneous catalysts was studied. It was shown that tin-Beta zeolite was only capable of producing crotonaldehyde in low yields. Several other heterogeneous catalysts were tested (Al-Beta, Ti-Beta, Sn-MCM-41, TS-1) but none of them demonstrated substantially higher activity in the studied transformation.

Resumé

MEKANISMEN FOR DEN RUTHENIUM-KATALYSEREDE dehydrogenative fremstilling af amider fra alkoholer og aminer er blevet studeret indgående ved at anvende en kombination af eksperimentelle og teoretiske teknikker. Hammett studier viste, at der opbygges en lille positiv ladning på den benzylliske position i overgangstilstanden tilhørende det turn-over bestemmende trin. En kinetisk isotop effekt på 2.29 ± 0.15 indikerer, at kløvningen af C–H bindingen ikke er det hastighedsbestemmende trin, men at det blot er et blandt adskillige langsomme trin i den katalytiske cyklus. Eksperimenter med deuteriummærkede alkoholer og aminer viste, at ruthenium-dihydrid forbindelser er indblandet i den katalytiske cyklus. Disse eksperimentelle resultater blev anvendt i DFT/MO6 beregninger og en plausibel katalytisk cyklus er blevet fremsat. Både cis-dihydrid og trans-dihydrid intermediater blev overvejet, men med fastsættelsen af de teoretiske turn-over frekvenser ud fra de beregnede energier står det klart, at kun trans-dihydrid ruten stemmer overens med de eksperimentelt bestemte frekvenser.



List of Abbreviations

*	in the name of a basis set: polarization functions are placed on all atoms except for transition metals, H, and He
ACS	American Chemical Society
Ad	Adamantyl
B3LYP	Becke gradient-exchange correction and Lee-Yang-Parr correlation functional with 3 parameters
Bn	Benzyl
bp	Boiling point
br. s.	Broad singlet
Bu	Butyl
Cy	Cyclohexyl
DABCO	1,4-Diazabicyclo[2.2.2]octane
DFT	Density functional theory
DNA	Deoxyribonucleic acid
d	Doublet
dd	Doublet of doublets
dppe	1,2-Bis(diphenylphosphino)ethane
ECP	Effective core potential
ESI	Electrospray ionization
Et	Ethyl

FID	Flame ionization detector
GCMS	Gas chromatography–Mass-spectrometry
GGA	Generalized gradient approximation
HF	Hartree-Fock
HRMS	High resolution mass spectrometry
Hex	<i>n</i> -Hexyl
<i>l</i> Pr	1,3-Diisopropylimidazol-2-ylidene
KIE	Kinetic isotope effect
KHMDS	Potassium bis(trimethylsilyl)amide
LACVP	Los Alamos National Laboratory, including outermost core orbitals with 6-31G set for atoms not described by ECPs
LDA	Local density approximation
LSDA	Local spin density approximation
MOX	Minnesota 200x
MPVO	Meerwein-Ponndorf-Verley reduction–Oppenauer oxidation reactions
m	Multiplet
Me	Methyl
Mes	Mesityl (1,3,5-trimethylphenyl)
NHC	<i>N</i> -heterocyclic carbene
<i>n</i>	Normal
NMR	Nuclear magnetic resonance
OMS	Octahedral molecular sieves
Ph	Phenyl
Pr	Propyl

py	Pyridine
quint	Quintet
RDS	Rate-determining step
SCF	Self-consistent field
<i>sec</i>	Secondary
s	Singlet
TDI	TOF-determining intermediate
TDS	TOF-determining transition state
TEOS	Tetraethyl orthosilicate
TEP	Tolman electronic parameter
TOF	Turnover frequency
TS-1	Titanium silicate 1
TS	Transition state
<i>t</i>	Tert
TEAOH	Tetraethylammonium hydroxide
THF	Tetrahydrofuran
UHPLC	Ultra high performance liquid chromatography
ZPE	Zero-point energy

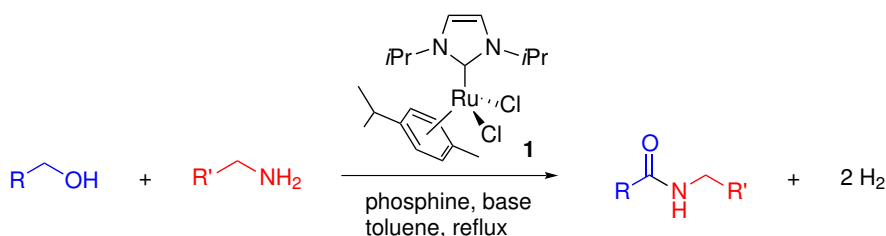
Contents

1	Mechanistic Study of the Amidation Reaction	1
1.1	Introduction	2
1.1.1	Metal-Catalyzed Amide Synthesis	2
1.1.2	Ruthenium-Catalyzed Amidation Reactions	5
1.1.3	Hammett Study	8
1.1.4	Kinetic Isotope Effect	12
1.1.5	Energetic Span Model	15
1.1.6	Density Functional Theory	18
1.2	Experimental Study	21
1.2.1	Hammett Study	21
1.2.2	Determination of the Reaction Order	23
1.2.3	Experiments with Deuterated Substrates	26
1.2.4	Kinetic Isotope Effect	29
1.2.5	NMR Experiments	30
1.2.6	Miscellaneous Experiments	33
1.2.7	Summary of the Experimental Study	35
1.3	Computational Study	36
1.3.1	Orientation of Ligands	36
1.3.2	Calculations on the Catalytic Cycle	39
1.3.3	Geometric Parameters of the Reaction Intermediates	43
1.3.4	Modeling of the Hammett Study	44
1.3.5	Theoretical Kinetic Isotope Effect	46
1.3.6	Summary of the Theoretical Study	47
1.3.7	Computational Details	47
1.4	Conclusions	48
1.5	Experimental Part	49
2	<i>In Silico</i> Screening for More Effective Carbene Ligands for the Amidation Reaction	51
2.1	Introduction	52
2.2	Search for More Effective Ligands	53

2.3	Conclusion	59
2.4	Experimental Section	60
3	Self-Coupling of Primary and Secondary Alcohols	65
3.1	Introduction	66
3.1.1	Ruthenium-Catalyzed Esterification Reactions	66
3.1.2	Ruthenium-Catalyzed Alkylation Reactions Involving Alcohols	71
3.2	Optimization of the Esterification Reaction	74
3.3	Study of the Dehydrogenative Guerbet Reaction with Secondary Alcohols	79
3.3.1	Optimization of the Reaction Conditions	79
3.3.2	Scope and Limitations of the Reaction	81
3.3.3	Mechanistic Investigation	84
3.4	Conclusion	86
3.5	Experimental Part	87
4	Study of the Acetaldehyde Transformations over Zeolite-Type Hetero- geneous Catalysts	93
4.1	Introduction	94
4.2	Results	97
4.3	Conclusion	100
4.4	Experimental Part	101
4.4.1	General Methods	101
4.4.2	Synthesis of the Catalysts	101
4.4.3	Performing the Reactions	102
5	Bibliography	105
A	Publications prepared during the PhD study	113

1 Ruthenium–*N*-Heterocyclic Carbene Catalyzed Coupling of Primary Alcohols with Amines. Mechanistic Investigation.

THIS PART OF THE DISSERTATION discusses the mechanistic investigation of the ruthenium-catalyzed dehydrogenative coupling of primary alcohols with amines to form amides which was recently discovered in the Madsen group (Scheme 1.1).¹ The aim of this work is to understand how the amidation reaction works and to create a plausible model which can be used to improve the reaction and to find better conditions based on *in silico* screening. The investigation is divided into two parts: an experimental study (which includes a Hammett study, determination of the reaction orders, determination of the kinetic isotope effect and some others) and a theoretical study (which includes density functional theory calculations).



Scheme 1.1: Ruthenium-catalyzed dehydrogenative coupling of primary alcohols with amines to form amides.

¹NORDSTRØM, L. U.; VOGT, H.; MADSEN, R. *J. Am. Chem. Soc.* **2008**, *130*, 17672–17673.

1.1 Introduction

1.1.1 Metal-Catalyzed Amide Synthesis

The amide bond is one of the key linkages in organic chemistry. It is found in peptides, artificial polymers, drugs and biologically-active compounds. For example, 9 out of 53 small molecule drugs, whose sales in 2003 exceeded \$1 billion, contained an amide.² Not surprisingly, a great variety of methods for the synthesis of amides have been discovered over past 150 years.^{3,4} There are examples of coupling reactions (mostly based on the reaction between an amine and a carboxylic acid derivative), rearrangements (e.g. Curtius, Beckmann)^{5,6} and some others. Most of these reactions have the same problem: they are performed in a non-atom-economical fashion, *i.e.* require additional reagents which do not end up in the products. In 2007, the ACS and Green Chemistry Institute together with several global pharmaceutical corporations ranked “Amide formation avoiding poor atom economy reagents” as a number one transformation for which they would prefer better reagents.⁷

This is a point where enzymatic and catalytic procedures come into play. Both of these methods are considered “green” and atom-economic because only small amount of catalyst or enzyme are needed to make the reaction work efficiently. We will leave the enzymes to enzymologists and focus on catalytic procedures.

There are several possibilities to obtain amides with the help of metal catalysis. Most of these methods employ alcohols or aldehydes as starting materials but nitriles, esters and the corresponding carboxylic acids can be used as well. A noteworthy example of the transformation of esters to amides was published by Gupta and coworkers.⁸ They reported that benzoyl esters can be converted to amides in high yields with only 1 mol% of zinc dust as

²CAREY, J. S.; LAFFAN, D.; THOMSON, C.; WILLIAMS, M. T. *Org. Biomol. Chem.* **2006**, *4*, 2337–2347.

³*The Amide Linkage: Structural Significance in Chemistry, Biochemistry, and Materials Science*; GREENBERG, A., BRENNEMAN, C. M., LIEBMAN, J. F., Eds.; Wiley-Interscience: New York, 2000.

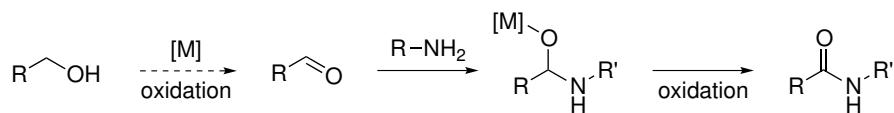
⁴PATTABIRAMAN, V. R.; BODE, J. W. *Nature* **2011**, *480*, 471–479.

⁵SMITH, P. A. S. In *Organic reactions*, 1946; Vol. 3.

⁶GAWLEY, R. E. In *Organic reactions*, 1988; Vol. 35.

⁷CONSTABLE, D. J. C.; DUNN, P. J.; HAYLER, J. D.; HUMPHREY, G. R.; LEAZER, JR., J. L.; LINDERMAN, R. J.; LORENZ, K.; MANLEY, J.; PEARLMAN, B. A.; WELLS, A.; ZAKS, A.; ZHANG, T. Y. *Green Chem.* **2007**, *9*, 411–420.

⁸ARORA, R.; PAUL, S.; GUPTA, R. *Can. J. Chem.* **2005**, *83*, 1137–1140.



Scheme 1.2: Metal-catalyzed amide synthesis from an alcohol or an aldehyde and an amine.

a catalyst under microwave irradiation in 2–8 min. Moreover, the batch of the catalyst can be reused 6 times after washing with aqueous solution of HCl. Rhodium-catalyzed hydrolysis of nitriles gives access to primary amides and allows to conduct this reaction at ambient temperature and without use of strong acids or bases as opposed to a non-catalytic variants.⁹ Nitriles can also react with amines to give amides. In 1986, Murahashi and coworkers published the first example of this transformation catalyzed by $\text{RuH}_2(\text{PPh}_3)_4$ (3 mol%).¹⁰

Several oxidation steps are involved in the synthesis of amides from an alcohol or an aldehyde (Scheme 1.2). The alcohol is first oxidized to the aldehyde which then reacts with the amine and the resulting hemiaminal is oxidized further to the amide. The oxidation steps may require external oxidants but in some cases these reactions may proceed with the liberation of hydrogen gas.

Examples of the catalyst systems used in various amidation reactions are listed in Figure 1.1. The system **a** was successfully applied to the amidation of aldehydes with amine salts. In this case *t*BuOOH was used as an external oxidant.¹¹ Neodymium complex **b** catalyzed the coupling of aldehydes with amines to give amides at room temperature with a catalyst loading of only 1 mol%.¹² However, the aldehyde was used in excess because it also played the role of the oxidant. Another example with amidation of aldehydes was reported by Williams *et al.*¹³ They used 5 mol% of $\text{NiCl}_2 \cdot 6\text{H}_2\text{O}$ (system **c**) and one equivalent of hydroxylamine (which may be considered as an oxidant) to first convert an aldehyde to a nitrile which then reacted with an amine and water to give an amide.

In 1991, Murahashi and coworkers published the first example of the dehydrogenative coupling of an alcohol with an amine to give an amide. They

⁹GOTO, A.; ENDO, K.; SAITO, S. *Angew. Chem. Int. Ed.* **2008**, *47*, 3607–3609.

¹⁰MURAHASHI, S.-I.; NAOTA, T.; SAITO, E. *J. Am. Chem. Soc.* **1986**, *108*, 7846–7847.

¹¹EKOUE-KOVI, K.; WOLF, C. *Chem. Eur. J.* **2008**, *14*, 6302–6315.

¹²QIAN, C.; ZHANG, X.; ZHANG, Y.; SHEN, Q. *J. Organomet. Chem.* **2010**, *695*, 747–752.

¹³ALLEN, C. L.; DAVULCU, S.; WILLIAMS, J. M. J. *Org. Lett.* **2010**, *12*, 5096–5099.

1.1 Introduction

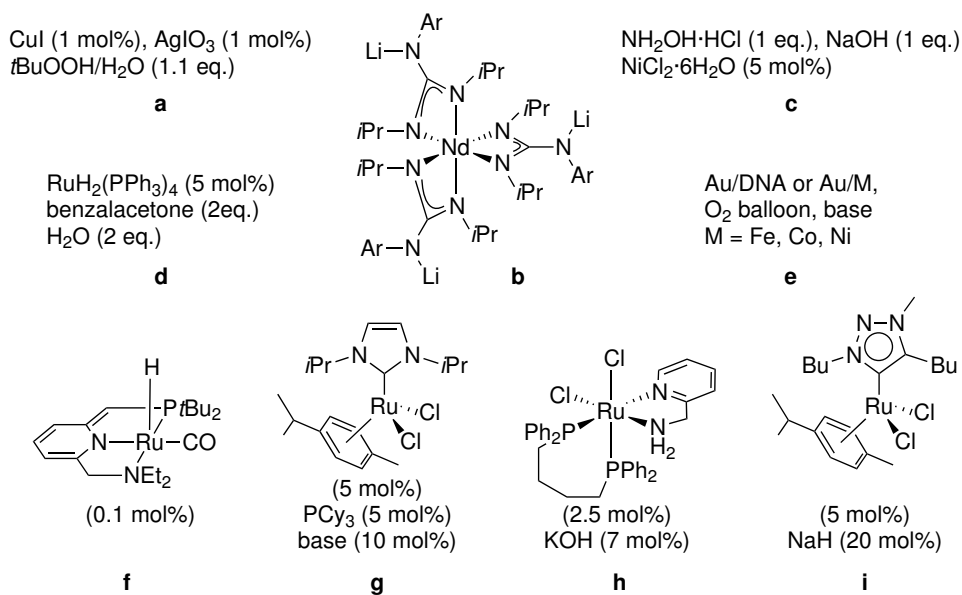


Figure 1.1: Examples of catalytic systems used in various amidation reactions.

reported the synthesis of lactams catalyzed by system **d** from aminoalcohols in the presence of benzalacetone as a hydrogen acceptor.¹⁴ Not only homogeneous catalytic systems can be used for the amidation of alcohols, but also several bimetallic gold-based heterogeneous catalysts as well as Au/fish sperm DNA were shown to successfully produce amides from alcohols and amines in the oxidative atmosphere (systems **e**).^{15,16}

The most “green” and wasteless, and consequently attractive, way of synthesizing amides from an alcohol and an amine is an acceptorless coupling, *i.e.* a reaction which produces hydrogen gas as the only by-product.

Both homogeneous and heterogeneous variants of this transformation have been discovered over the past several years. The first report, published by the Milstein group in 2007, introduced PNN-pincer complex **f** as an effective catalyst for the amide synthesis from alcohols and amines with the liberation of dihydrogen.¹⁷ One year later, the Madsen group reported a similar amidation procedure catalyzed by *N*-heterocyclic carbene-based ruthenium

¹⁴NAOTA, T.; MURAHASHI, S.-I. *Synlett* **1991**, 1991, 693–694.

¹⁵WANG, Y.; ZHU, D.; TANG, L.; WANG, S.; WANG, Z. *Angew. Chem. Int. Ed.* **2011**, *50*, 8917–8921.

¹⁶SOULÉ, J.-F.; MIYAMURA, H.; KOBAYASHI, S. *J. Am. Chem. Soc.* **2011**, *133*, 18550–18553.

¹⁷GUNANATHAN, C.; BEN-DAVID, Y.; MILSTEIN, D. *Science* **2007**, *317*, 790–792.

complexes (one of them is shown in Figure 1.1, complex **g**).¹ The amidation with ruthenium–NHC complexes was subsequently studied in more detail in the following years.^{18,19} Other examples of complexes that can catalyze coupling of a primary alcohol and an amine are compounds **h** and **i** which were reported to catalyze formation of lactams²⁰ and amides²¹, respectively. There have also been published several examples of heterogeneous catalysts for the acceptorless amidation reaction, such as Ag/Al₂O₃ and Au/hydrotalcite catalytic systems.^{22,23}

1.1.2 Ruthenium-Catalyzed Amidation Reactions

The complexes **f** and **g** are very much alike in terms of the substrate scope but have pronounced differences in reactivity. The systems **h** and **i** have not been studied in much detail, since it was only shown that complex **h** was able to catalyze the dehydrogenative cyclization of aminoalcohols to give lactams²⁰ and the amidation with the compound **i** was exemplified only by coupling of benzylamine with 2-phenylethanol.²¹ For that reason these complexes will be excluded from the discussion.

Both complex **f** and **g** perform best in the coupling of primary aliphatic and aromatic alcohols with primary amines to give amides in almost quantitative yields. The reaction is sensitive to steric parameters of the reactants: branching in either the β -position of the alcohol or the β -position of the amine leads to lower yields. The reactions with secondary amines as well as aniline require higher temperature and give the corresponding amides in lower yields in comparison with primary amines. Additional heteroatoms, such as oxygen or nitrogen, do not influence the reactivity unless they are incorporated in a bulky group. Unsaturated alcohol hex-5-en-1-ol was converted to the saturated amide in the coupling catalyzed by system **g** in high yield, which shows that the complex is also active in a hydrogenation reaction. Aminoalcohols with the relatively distant OH and NH₂ groups are converted into lactams in

¹NORDSTRØM, L. U.; VOGT, H.; MADSEN, R. J. *Am. Chem. Soc.* **2008**, *130*, 17672–17673.

¹⁸GHOSH, S. C.; MUTHAIAH, S.; ZHANG, Y.; XU, X.; HONG, S. H. *Adv. Synth. Catal.* **2009**, *351*, 2643–2649.

¹⁹DAM, J. H.; OSZTROVSZKY, G.; NORDSTRØM, L. U.; MADSEN, R. *Chem. Eur. J.* **2010**, *16*, 6820–6827.

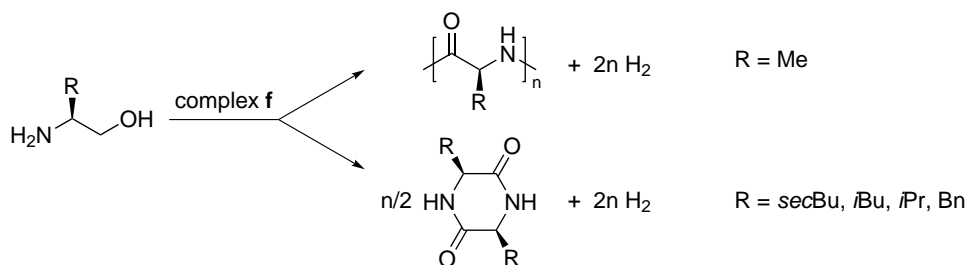
²⁰NOVA, A.; BALCELLS, D.; SCHLEY, N. D.; DOBEREINER, G. E.; CRABTREE, R. H.; EISENSTEIN, O. *Organometallics* **2010**, *29*, 6548–6558.

²¹PRADES, A.; PERIS, E.; ALBRECHT, M. *Organometallics* **2011**, *30*, 1162–1167.

²²SHIMIZU, K.-I.; OHSHIMA, K.; ATSUSHI, S.; SATSUMA, A. *Chem. Eur. J.* **2009**, *15*, 9977–9980.

²³ZHU, J.; ZHANG, Y.; SHI, F.; DENG, Y. *Tetrahedron Lett.* **2012**, *53*, 3178–3180.

1.1 Introduction



Scheme 1.3: Peptide synthesis catalyzed by complex **f**.

good yields,^{17,19} whereas β -aminoalcohols are self-coupled in the presence of complex **f** to give either polypeptides or cyclic dipeptide depending on the size of the substituent in the aminoalcohol (Scheme 1.3).²⁴ Attempts to self-couple glycine derivatives using complex **g** failed.

The scope of these complexes is not limited to substrates with one OH and NH_2 group. Diamines are successfully acylated with primary alcohols to give diamides in high to excellent yields.¹⁷ Complex **f** catalyzes formation of polyamides from diols and diamines. This reaction was reported to proceed with $> 99\%$ conversion and give polyamides with 30–50 repeated units and a polydispersity index of approximately 2.²⁵

The only type of amide which cannot be synthesized with use of these complexes is the primary amide. Attempts to couple NH_3 or its equivalents with primary alcohols in the presence of catalyst **g** did not lead to formation of an amide and resulted only in self-coupling of the alcohol to give the corresponding ester.¹⁹ Primary amides can be obtained by metal-catalyzed coupling of alcohols with ammonia in the presence of manganese oxide based octahedral molecular sieves ($\text{KMn}_8\text{O}_{16}$, OMS-2).²⁶

In some cases the amidation reaction does not perform well and by-products are formed. If the reaction catalyzed by pincer complex **f** occurs in a moderate yield then the remaining alcohol is self-coupled to the ester. Phenethyl 2-phenylacetate was also a major by-product in the coupling of

¹⁷GUNANATHAN, C.; BEN-DAVID, Y.; MILSTEIN, D. *Science* **2007**, 317, 790–792.

¹⁹DAM, J. H.; OSZTROVSZKY, G.; NORDSTRØM, L. U.; MADSEN, R. *Chem. Eur. J.* **2010**, 16, 6820–6827.

²⁴GNANAPRAKASAM, B.; BALARAMAN, E.; BEN-DAVID, Y.; MILSTEIN, D. *Angew. Chem. Int. Ed.* **2011**, 50, 12240–12244.

²⁵ZENG, H.; GUAN, Z. *J. Am. Chem. Soc.* **2011**, 133, 1159–1161.

²⁶YAMAGUCHI, K.; KOBAYASHI, H.; OISHI, T.; MIZUNO, N. *Angew. Chem. Int. Ed.* **2012**, 51, 544–547.

2-phenylethanol with aniline and BnNHMe catalyzed by complex **g** (yields of the amide were 35 and 65%, correspondingly), however, in other cases no major by-product was detected.

From a mechanistic point of view, the amidation proceeds via β -hydride elimination, amine addition and a second β -hydride elimination (Scheme 1.1). It was shown that neither esters nor imines are intermediates in this transformation.¹⁹ An aldehyde formed after the first β -hydride elimination stays coordinated to the ruthenium atom as was demonstrated by a cross-over experiment. The coupling of *p*-methylbenzyl alcohol and hexylamine with benzaldehyde added after 3 h yielded *N*-hexyl-*p*-methylbenzamide and *N*-hexylbenzamide in a ratio of 10:1 and the rest of benzaldehyde was converted to the corresponding imine.¹⁹ More likely, benzaldehyde is first reduced to benzyl alcohol which then is coupled with the amine to give the amide. In 2010, Hong and coworkers reported that the mixture of an alcohol and an aldehyde can be converted to two amides under the conditions which are similar to those used in the cross-over experiment (ruthenium–NHC complex was formed *in situ* from RuH₂(PPh₃)₄, di-*iso*-propylimidazolium salt and NaH).²⁷ In our laboratory, the reaction with system **g** was not reproducible, so we have no explanation for this observation.

After an aldehyde is formed, it is attacked by an amine to form a zwitterionic intermediate which can either stay coordinated, eliminate H₂ providing a free site for the second β -hydride elimination or dissociate from the ruthenium center to give an imine. The latter is possible to achieve by slightly changing the amidation catalytic systems. Replacing the NEt₂ group in complex **f** with the *Pt*Bu₂ group and replacing PCy₃ with DABCO and removing the base from system **g** transform these complexes into good catalysts for the imination reaction (Scheme 1.4).^{28,29}

Finally, a few remarks about the physical properties of the catalysts and their activity are appropriate. Complex **f** is sensitive to air, hence, requires conducting all the operations connected with the catalyst (synthesis, storing, amidation reaction) in inert atmosphere, *i.e.* in a glove-box. This is not always desirable. Complex **g** is air-stable, can be prepared on gram-scale and does not require special handling but is less active than complex **f**. Comparable

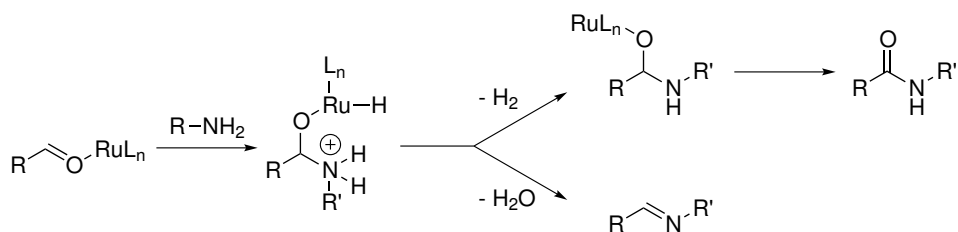
¹⁹DAM, J. H.; OSZTROVSZKY, G.; NORDSTRØM, L. U.; MADSEN, R. *Chem. Eur. J.* **2010**, *16*, 6820–6827.

²⁷MUTHAIAH, S.; GHOSH, S. C.; JEE, J.-E.; CHEN, C.; ZHANG, J.; HONG, S. H. *J. Org. Chem.* **2010**, *75*, 3002–3006.

²⁸GNANAPRAKASAM, B.; ZHANG, J.; MILSTEIN, D. *Angew. Chem. Int. Ed.* **2010**, *49*, 1468–1471.

²⁹MAGGI, A.; MADSEN, R. *Organometallics* **2012**, *31*, 451–455.

1.1 Introduction



Scheme 1.4: Formation of an imine or an amide from the same zwitterionic intermediate.

yields are achieved with 0.1 mol% of complex **f** after 8–12 h and 5 mol% of complex **g** after 24 h. It seems obvious that the former catalyst is much more active than the latter, but this comparison is not completely correct because the reactant concentrations are not taken into account. In the case of the Milstein catalyst **f**, the alcohol and the amine concentration is 3.3 M and in the case of catalyst **g** only 0.5 M. This fact means that, in theory, if the reaction is first order in both alcohol and amine, then just conducting the amidation reaction with complex **g** under the conditions identical to those reported in the Milstein paper,¹⁷ will make complex **g** almost 50 times more “active”. We will return to the comparison of the reactivities of these catalysts later (Section 1.2.6 on page 33).

1.1.3 Hammett Study

More than 75 years ago Louis Hammett published a paper where he quantified the relationship between the substituents in the *meta* or the *para* position in a benzene ring and the rates of the reactions which take place in a side chain of a benzene ring:³⁰ He separated the effect of the substituents into two constants: σ which depends only on the substituent and ρ which depends only on the reaction conditions. Thus, the difference in the reactivity of a substituted compound X and a non-substituted compound H is:

$$\lg(K_X) - \lg(K_H) = \sigma\rho \quad (1.1)$$

Which can be transformed to:

$$\lg\left(\frac{K_X}{K_H}\right) = \sigma\rho \quad (1.2)$$

¹⁷GUNANATHAN, C.; BEN-DAVID, Y.; MILSTEIN, D. *Science* **2007**, *317*, 790–792.

³⁰HAMMETT, L. P. *J. Am. Chem. Soc.* **1937**, *59*, 96–103.

Equation 1.2 is now known as the Hammett equation. This equation describes a linear free-energy relationship between equilibrium constants K of the reactions with substituted and non-substituted benzene derivatives. It holds not only for K but also for rate constants k . In practice, the Hammett equation is used, for example, to determine the charge built-up in the rate-determining step (RDS) in the reaction which takes place in a side chain of the benzene ring. One can measure the rate of the reactions with substrates featuring electron-donating or electron-withdrawing groups and plot the relative reactivities $\lg\left(\frac{K_X}{K_H}\right)$ versus substituent constants σ . The slope of the graph (which is also called the Hammett plot) yields the reaction constant ρ which can be:

1. positive ($\rho > 0$). This means that the substrates with electron-withdrawing groups react faster than the non-substituted compound and that a negative charge is built up during the reaction.
2. negative ($\rho < 0$). This is the opposite case to the previous one. The substrates with electron-donating groups react faster and a positive charge is built up.
3. neutral ($\rho = 0$). This means that no charge is built up in RDS. This case is rare.

The magnitude of ρ indicates the sensitivity of the reaction to the electronic nature of the substituent and how large the charge built-up is in the transition state: the larger the absolute value the more pronounced is the charge that is formed in RDS.

Hammett plots are not always linear. Usually, a sharp change in the ρ value is associated with a change in the mechanism or in the geometry of the transition state in the RDS.³¹ Another reason for a non-linearity could be that the Hammett equation does not account for strong resonance interactions between a substituent and a reaction center, for steric effects of a substituent. This led to the modification of the Hammett equation and the development of the new equations: Swain-Lupton (Equation 1.3),³² Yukawa-Tsuno (Equations 1.4 and 1.5),³³ Taft (Equation 1.6)³⁴ and some others.

³¹WILLIAMS, A., *Free Energy Relationships in Organic and Bio-Organic Chemistry*; Royal Society of Chemistry: Cambridge, 2003.

³²SWAIN, C. G.; LUPTON, E. C. *J. Am. Chem. Soc.* **1968**, *90*, 4328–4337.

³³YUKAWA, Y.; TSUNO, Y. *Bull. Chem. Soc. Jpn.* **1959**, *32*, 965–971.

³⁴TAFT, R. W. *J. Am. Chem. Soc.* **1952**, *74*, 3120–3128.

$$\lg \left(\frac{k_X}{k_H} \right) = \sigma \rho \quad \text{where } \sigma = f\tilde{\mathfrak{F}} + r\mathfrak{R} \quad (1.3)$$

$$\lg \left(\frac{k_X}{k_H} \right) = \rho (\sigma + r (\sigma^+ - \sigma)) \quad (1.4)$$

$$\lg \left(\frac{k_X}{k_H} \right) = \rho (\sigma + r (\sigma^- - \sigma)) \quad (1.5)$$

$$\lg \left(\frac{k_s}{k_{\text{CH}_3}} \right) = \rho^* \sigma^* + \delta E_s \quad (1.6)$$

These equations introduce different empirical parameters which account for one or another aspect of the reaction. Out of all the parameters only those of the Yukawa-Tsuno equation (σ^+ and σ^-) are widely used because it was shown many times that they give better correlation than the Swain $\tilde{\mathfrak{F}}$ and \mathfrak{R} . Parameters σ^+ and σ^- also “often afford insight into the reaction mechanism which is lost when the normalized Swain constants are used.”³⁵ One of the reasons is that σ^+ was designed and measured specifically for reactions which are known to proceed with the formation of a positive charge (and σ^- for reactions with a negative charge), whereas Swain constants are more general and less specific.

There are several methods for determining the relative reactivity. The classical one is to conduct a reaction with each substituted substrate separately and then find the relative reactivity by dividing a rate (or an equilibrium) constant of the reaction by the value for a non-substituted substrate. This method has several drawbacks. First, it is hard to ascertain that all the reactions are conducted under exactly the same conditions (the same concentration of the reactants, same temperature, same pressure, etc.). Second, the rate constants are usually measured under the conditions which are far from those used for the normal reaction. For example, if one wants to keep the concentration of a reactant constant and measure a pseudo first-order rate constant, a large excess of this reactant should be used. This widely used technique can cause problems in metal-catalyzed reactions since under such conditions absolutely different catalytically active species can be formed. Finally, measuring a rate for the separated reactions usually require at least three experiments for each substrate to get reliable and statistically significant results.

Another method for measuring the relative reactivities is to conduct competition experiments: equimolar mixture of a substituted (X) and a non-substituted

³⁵HANSCH, C.; LEO, A.; TAFT, R. W. *Chem. Rev.* **1991**, *91*, 165–195.

reactant (H) is introduced into the reaction and then the concentration of these two compounds is followed during the reaction. Relative reactivity can be derived assuming that both of the compounds react according to the same mechanism. The rates of the two reactions are:

$$\frac{d[X]}{dt} = k_X [X]^n [\text{other reactants}]^m \quad (1.7)$$

$$\frac{d[H]}{dt} = k_H [H]^n [\text{other reactants}]^m \quad (1.8)$$

dividing Equation 1.7 by Equation 1.8 gives:

$$\frac{d[X]}{d[H]} = \frac{k_X [X]^n}{k_H [H]^n}$$

for the first order reaction ($n = 1$), it can be written as:

$$\frac{d[X]}{d[H]} = \frac{k_X [X]}{k_H [H]}$$

after the separation of variables and integration:

$$\ln \frac{[X]_0}{[X]} = \frac{k_X}{k_H} \ln \frac{[H]_0}{[H]} \quad (1.9)$$

Equation 1.9 demonstrates that relative reactivities can be obtained as the slope of the line when $\ln \frac{[X]_0}{[X]}$ is plotted against $\ln \frac{[H]_0}{[H]}$.

The method of the competition experiments has several advantages in comparison with the classical method. Two reactions are conducted in the same reaction flask which guarantees exactly the same conditions. The reactions can be conducted with normal amounts of the reactants and they do not require any specific treatment. In addition, the total number of experiments can be slightly reduced because there is no need to do the measurements with the non-substituted compound alone.

In summary, the Hammett study is a powerful tool which is extensively used in mechanistic investigations.^{36–40}

³⁶RASMUSSEN, T.; JENSEN, J. F.; OSTERGAARD, N.; TANNER, D.; ZIEGLER, T.; NORRBY, P.-O. *Chem. Eur. J.* **2002**, *8*, 177–184.

³⁷KEINICKE, L.; FRISTRUP, P.; NORRBY, P.-O.; MADSEN, R. *J. Am. Chem. Soc.* **2005**, *127*, 15756–15761.

³⁸FRISTRUP, P.; KREIS, M.; PALMELUND, A.; NORRBY, P.-O.; MADSEN, R. *J. Am. Chem. Soc.* **2008**, *130*, 5206–5215.

³⁹DEPREZ, N. R.; SANFORD, M. S. *J. Am. Chem. Soc.* **2009**, 11234–11241.

⁴⁰LEE, D.-H.; KWON, K.-H.; YI, C. S. *Science* **2011**, *333*, 1613–1616.

1.1.4 Kinetic Isotope Effect

The kinetic isotope effect (KIE) shows how the isotope substitution changes the reaction rate. This is a useful tool for studying reaction mechanisms and allows to ascertain whether a specific bond is broken during the rate-determining step. Usually in organic chemistry, the KIE is measured for compounds in which a hydrogen atom in the bond under consideration is replaced with a deuterium atom. In such a case, the KIE is calculated as a ratio of two rate constants $k_{\text{H}}/k_{\text{D}}$. There are several classifications of the KIE, such as: primary or secondary, normal or inverse. To explain an origin of the kinetic isotope effect, the primary the KIE will be discussed, *i.e.* when the C–H/C–D bond breakage occurs in the rate-determining step.

Consider a homolytic dissociation of a C–H and a C–D bond. The activation energy for this process is a difference between the dissociation limit and the lowest energy state (Figure 1.2), which is the zeroth ($n = 0$ in Equation 1.10) for up to 99% of C–H bonds at 300 K and is called the zero-point energy (ZPE).

$$E_n = \left(n + \frac{1}{2}\right) h\nu \quad \text{where } n = 0, 1, 2, \dots \quad (1.10)$$

Any chemical bond can be described as a spring with a mass attached at both ends, and consequently, a stretching vibrational frequency of this bond can be modeled by the classic equation for the stretching of a spring (Equation 1.11). Combining Equation 1.10 and Equation 1.11, we can see that ZPE is inversely proportional to the square root of the reduced mass (m_r). Since m_r for a C–D bond is larger than for a C–H bond ($m_r^{\text{CH}} = 1.08$, $m_r^{\text{CD}} = 1.71$), ZPE for the former is lower. This also means that the activation energy (E_a) is higher for a C–D bond and its dissociation proceeds slower making the KIE greater than 1.

$$\nu = \frac{1}{2\pi} \sqrt{\frac{k}{m_r}} \quad \text{where } m_r = \frac{m_1 m_2}{m_1 + m_2} \quad (1.11)$$

Assuming that the bond is completely broken in the transition state, the maximum value of the KIE can be estimated using Equation 1.12. At 300 K the KIE for a C–H bond with a vibrational frequency at 3000 cm^{-1} is approximately 6.5.

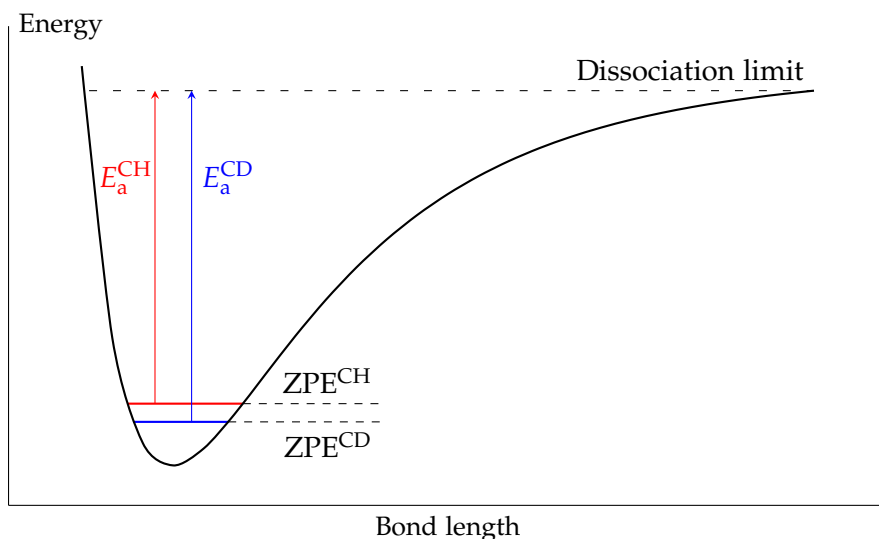


Figure 1.2: Complete dissociation of C–H and C–D bonds.

$$\begin{aligned}
 KIE_{full} &= \frac{k_H}{k_D} = \exp\left(-\frac{E_a^{CH} - E_a^{CD}}{RT}\right) \\
 &= \exp\left(-\frac{E_{lim} - ZPE^{CH} - (E_{lim} - ZPE^{CD})}{RT}\right) \\
 &= \exp\left(\frac{ZPE^{CH} - ZPE^{CD}}{RT}\right) = \exp\left(\frac{\Delta ZPE_{react}}{RT}\right) \quad (1.12)
 \end{aligned}$$

Examples of the complete breakage of a bond at the transition state are rare and the value of a primary KIE is normally lower than 6.5. Usually, the bond is only partially broken or another bond starts forming simultaneously at the transition state. If a bond is not completely broken, then it has different zero-point energies for the C–H and C–D cases (like in the ground state) but the bond in the transition state is weaker, which is why the ZPE difference is smaller (Figure 1.3). The activation energy is still higher for the deuterated substrate than for the non-deuterated counterpart but the difference in the activation energies is lower than in the case of the complete dissociation which results in smaller values of the kinetic isotope effect (Equation 1.13).

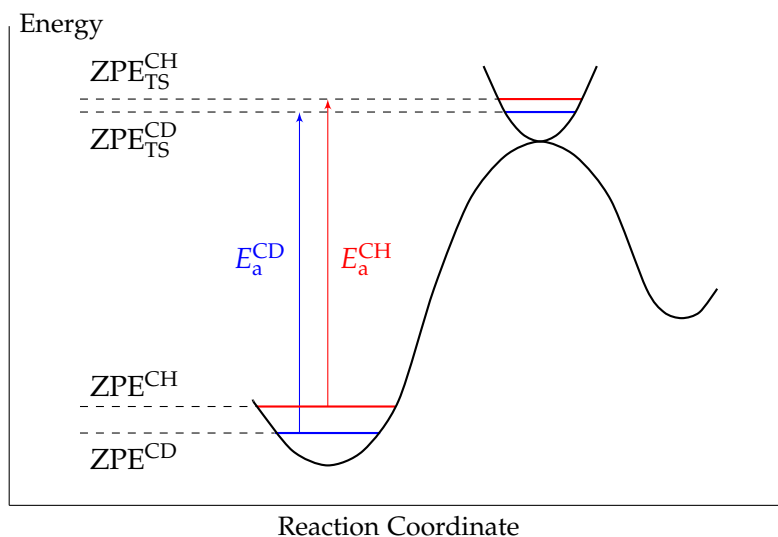


Figure 1.3: Partial dissociation of C–H and C–D bonds.

$$\begin{aligned}
 KIE_{part} &= \frac{k_H}{k_D} = \exp\left(-\frac{E_a^{CH} - E_a^{CD}}{RT}\right) \\
 &= \exp\left(-\frac{ZPE_{TS}^{CH} - ZPE^{CH} - (ZPE_{TS}^{CD} - ZPE^{CD})}{RT}\right) \\
 &= \exp\left(\frac{ZPE^{CH} - ZPE^{CD} - (ZPE_{TS}^{CH} - ZPE_{TS}^{CD})}{RT}\right) \\
 &= \exp\left(\frac{\Delta ZPE_{react} - \Delta ZPE_{TS}}{RT}\right) < KIE_{full} \quad (1.13)
 \end{aligned}$$

Equation 1.13 helps to connect and compare an experimental KIE with a theoretical one by using zero-point energies from the calculations.

There are three common ways of measuring the kinetic isotope effect:

1. Conducting two experiments, one for the substrate with a C–H bond and one for the substrate with a C–D bond, and measuring rate constants for each of them
2. Conducting a competition experiment between a deuterated and non-deuterated substrates and measuring the KIE based on the relative

amount of products formed from each of the substrates or based on disappearance of the starting materials

3. Conducting an intramolecular competition experiment with a substrate which has hydrogen and deuterium atoms in the identical positions. In this case the KIE can also be calculated based on relative amount of product resulting from functionalization of the C–H or the C–D bonds.

These methods could give different values of KIE for the same reaction depending on the relative position of the rate-determining step (RDS) and the C–H breakage step. Comparing KIE values obtained by two or three of the methods, valuable information about the mechanism of the reaction and the position of the elementary steps relative to each other can be obtained. For example, if these two steps coincide, then the KIE will be observed in all three experiments. However, if RDS precedes a C–H cleavage step and the substrate with the bond of interest is not involved in this step, then the KIE will be observed only with the second and third methods. This is due to the fact that the product distribution is defined by the difference in rates of a C–H bond cleavage regardless of whether this is the RDS or not. In the first method, the rate of the reactions will be identical for deuterated and non-deuterated substrates resulting in the absence of a KIE. More details and analysis of other possible reaction scenarios can be found in a recent publication by Simmons and Hartwig.⁴¹

In summary, the kinetic isotope effect is a simple yet powerful method for studying reaction mechanisms which provides important information about which bond is broken during the reaction and when.⁴²

1.1.5 Energetic Span Model

For our study we need a tool which could link experimental kinetic data with theoretically-obtained parameters, for example, energy and also could be used for predicting reactivity of certain catalytic systems. In the Section 1.1.4 there was derived an equation which allows to calculate kinetic isotope effect based on theoretical zero-point energy of reactants and transition state. Unfortunately, it is useful only for verifying a proposed catalytic cycle but not for predicting reactivity. Fortunately, there have been developed several

⁴¹SIMMONS, E. M.; HARTWIG, J. F. *Angew. Chem. Int. Ed.* **2012**, *51*, 3066–3072.

⁴²GÓMEZ-GALLEGO, M.; SIERRA, M. A. *Chem. Rev.* **2011**, *111*, 4857–4963.

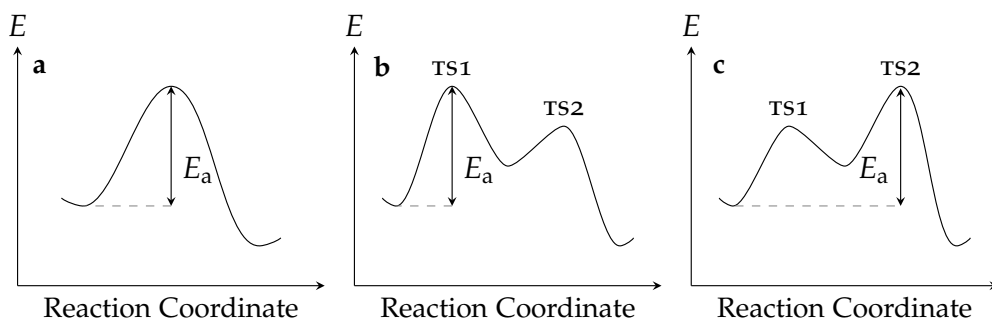


Figure 1.4: Energy profiles for one- or two-step transformations.

methods for such a prediction. One of them, the so-called “energetic span model”, will be discussed in this section.

In 1884, Svante Arrhenius, based on his experimental observations, proposed a simple relationship between the reaction rate and temperature which is now known as the Arrhenius rate law (Equation 1.14). This equation also finds use in theoretical chemistry because it links the activation energy of the reaction with its rate.

$$k = A \exp\left(-\frac{E_a}{RT}\right) \quad (1.14)$$

For an elementary reaction there is only one transition state and the rate is determined by the energy difference between a reactant and a transition state which equals to the activation energy of the reaction (E_a , Figure 1.4a). For a transformation which consists of two elementary reactions, E_a could be determined by either of the transition states. If TS1 is higher in energy than TS2, then E_a is equal to the activation energy of the first elementary step which, owing to this, is called the rate-determining step (Figure 1.4b). If TS2 is higher in energy than TS1, then E_a is equal to a sum of the activation energy of the second step and the difference in energies between a product and a reactant of the first elementary reaction (Figure 1.4c). In this case, the second step is the RDS even though it is not only its activation energy that determines the overall rate.

The concept of the rate-determining step only applies to reactions which operate under non-steady state conditions because, by definition, steady state approximation implies that each step of the reaction has equal rate. As a consequence, all of them determine the overall reaction rate. This situation is common in catalytic processes when the steady state approximation holds true

during the most part of the reaction. To be able to analyze kinetics of catalytic reactions based on calculated energies, Jutand and Amatore introduced a term “the energetic span of the cycle” (δE) which is a difference in energy between the highest and the lowest points of the catalytic cycle.⁴³ This expression is derived by combining the Arrhenius equation with the Boltzmann distribution for the intermediate (I_n) which precedes the TS with the highest energy in the cycle:

$$\begin{aligned} r &= k [I_n] = [I_n] \exp\left(-\frac{E_a^n}{RT}\right) = [I_{low}] \exp\left(-\frac{E_a^n}{RT}\right) \exp\left(-\frac{\Delta E}{RT}\right) \\ &= [I_{low}] \exp\left(-\frac{E_a^n + \Delta E}{RT}\right) = [I_{low}] \exp\left(-\frac{\delta E}{RT}\right) \end{aligned} \quad (1.15)$$

where $[I_{low}]$ is the concentration of the compound with the lowest energy, ΔE is the energy difference between I_{low} and I_n , and E_a^n is the activation energy of the n th step.

As we can see, the energetic span resembles the activation energy of the process in Figure 1.4c. However, for the catalytic reaction we also must keep in mind that the end of the first cycle is the beginning of the second cycle. For the exothermic reaction this leads to a situation when the starting point of a new cycle is below the original one by the reaction energy, E_r . As the reaction proceeds, the energy of a new cycle drops which makes it difficult to choose I_{low} for Equation 1.15. To take the cyclic nature of the process into account, Shaik and coauthors modified the definition of the energetic span and proposed a way of calculating the turnover frequency (TOF) (Equations 1.16 and 1.17).⁴⁴

$$\delta E = \begin{cases} \Delta G_{TDTS} - \Delta G_{TDI} & \text{if TDTS appears after TDI} \\ \Delta G_{TDTS} - \Delta G_{TDI} + \Delta G_r & \text{if TDTS appears before TDI} \end{cases} \quad (1.16)$$

$$\text{TOF} = \frac{k_B T}{h} \exp\left(-\frac{\delta E}{RT}\right) \quad (1.17)$$

Here, two new terms are introduced: TDTS (TOF-determining transition state) and TDI (TOF-determining intermediate) which are the species that maximize the energetic span of the cycle. From Equation 1.17 we can conclude

⁴³AMATORE, C.; JUTAND, A. J. *Organomet. Chem.* **1999**, 576, 254–278.

⁴⁴KOZUCH, S.; SHAIK, S. *Acc. Chem. Res.* **2011**, 44, 101–110.

that the lower the energetic span, the higher the TOF and the faster the reaction. As was shown in the literature, TDTS and TDI are usually (but not necessarily) the highest and the lowest in the entire cycle.⁴⁴

Even though modern computational methods (such as density functional theory calculations) have advanced a lot, it is still a challenging task to obtain accurate Gibbs free energies and, as a consequence, precise values for the turnover frequency. In spite of this, relative TOFs can be used to compare different catalytic systems or pathways of a reaction if all optimizations are carried out at the same level of calculations.

A program called AUTOF was created for calculating energetic span and TOF based on the theoretically obtained energy profile of a reaction.^{45–47}

To summarize, the energetic span model provides a link between experiments and theoretical calculations by means of the turnover frequency. The model can also be used for computational search of better catalytic systems.

1.1.6 Density Functional Theory

One of the major goals of theoretical chemistry is to determine the electronic structure of a molecule (*i.e.* the wave function associated with electrons and their energies) because it implies its chemical properties.⁴⁸ There have been developed several methods for obtaining the electronic structure over past 100 years and almost all of them are based on the Schrödinger equation which, in the simplest form, is represented in Equation 1.18.

$$E\Psi = \hat{H}\Psi \quad (1.18)$$

By solving this equation, both the wave function (Ψ) and the energy of a system can be obtained. Because of extreme complexity of the mathematical operations required for these calculations, the equation can be solved analytically (exactly) only for a wave function with one particle (for example, proton). For the larger systems there have been developed various approximations. One of them replaces an n -body system by the single-body, assuming that each of its particles moves in a self-consistent field (SCF) created by the other

⁴⁴KOZUCH, S.; SHAIK, S. *Acc. Chem. Res.* **2011**, *44*, 101–110.

⁴⁵KOZUCH, S.; SHAIK, S. *J. Am. Chem. Soc.* **2006**, *128*, 3355–3365.

⁴⁶KOZUCH, S.; SHAIK, S. *J. Phys. Chem. A* **2008**, *112*, 6032–6041.

⁴⁷UHE, A.; KOZUCH, S.; SHAIK, S. *J. Comp. Chem.* **2011**, *32*, 978–985.

⁴⁸LEACH, A. R., *Molecular Modelling: Principles and Applications*, 2nd ed.; Pearson Education Limited: 2001.

particles of the system. This is a central concept of the Hartree-Fock (HF) method which has found a wide application in chemistry because it allows for obtaining quite accurate results in a relatively short time.⁴⁹

Another *ab initio* approach to finding the electronic structure of a molecule is based on the electron density distribution and is now known as density functional theory (DFT). As was proven by Kohn and coworkers the energy of a system is uniquely determined by its electron density.^{50,51} In principle, DFT could give exact energy of a system but again due to very complex mathematics various approximations have to be used in order to work with this theory.

Initial approximations, such as local density approximation (LDA) and local spin density approximation (LSDA) did not allow to obtain accurate results in comparison with the HF theory mostly because they did not take into account the fact that the electron density varies in a molecule. The situation changed after Axel Becke suggested the gradient-corrected approximation with correct asymptotic behavior⁵² which is now known as the generalized gradient approximation (GGA). The same year Lee, Yang and Parr reported a gradient corrected correlation functional⁵³ which in combination with the Becke correction gave a new DFT method called BLYP which surpassed the HF in the quality of calculations.

$$E_{xc}^{B3LYP} = (1 - a) E_x^{LDA} + aE_x^{HF} + b\Delta E_x^B + (1 - c) E_c^{LDA} + cE_c^{LYP} \quad (1.19)$$

Further research in this direction led to a new, so-called, hybrid functional B3LYP⁵²⁻⁵⁴ which is still popular and widely used. It is hybrid because, as can be seen in Equation 1.19, the energies due to the Becke correction (ΔE_x^B) and the LYP correlation (E_c^{LYP}) functionals are mixed with some exact exchange energy from the HF method (E_x^{HF}). The advantage of this mixing is that systematic errors of the two method are partially canceled.

In spite of the fact that the DFT methods in general give better results in comparison with the HF methods,⁵⁵ they are still not ideal and have several drawbacks due to the approximations used. Probably the most significant

⁴⁹JENSEN, J. H., *Molecular Modeling Basics*; CRC Press: 2010.

⁵⁰HOHENBERG, P.; KOHN, W. *Phys. Rev.* **1964**, *136*, B864–B871.

⁵¹KOHN, W.; SHAM, L. J. *Phys. Rev.* **1965**, *140*, A1133–A1138.

⁵²BECKE, A. D. *Phys. Rev. A* **1988**, *38*, 3098–3100.

⁵³LEE, C.; YANG, W.; PARR, R. G. *Phys. Rev. B* **1988**, *37*, 785–789.

⁵⁴BECKE, A. D. *J. Chem. Phys.* **1993**, *98*, 5648–5652.

⁵⁵KOHN, W.; BECKE, A. D.; PARR, R. G. *J. Phys. Chem.* **1996**, *100*, 12974–12980.

in relation to our study is that DFT fails to correctly describe van der Waals interactions.^{56,57} There are several ways to overcome this problem, such as including additive terms⁵⁸ or developing new functionals which account for dispersion,^{59,60} here only the latter will be discussed.

In 2008, Zhao and Truhlar reported a new family of functionals which was a successor of another family M05: M06, M06-HF, M06-L and M06-2X – as the authors wrote about them “with a broad applicability in chemistry”.^{59,61} Each of these functional was designed for specific needs, for example, M06 – for calculations on main group elements, organometallics, kinetics and non-covalent bonds. As of February 2013, the original paper in *Theoretical Chemistry Accounts* has been cited almost 2000 times (according to SciFinder) which indicates that these functionals are really finding their place in modern computational chemistry. M06 is a hybrid functional with 27% of HF exchange, it is not purely *ab initio* because it includes several parameters optimized to better fit real-world energetic databases including four for transition metals. It is worth noting that this functional was also successfully used in our research group.⁶²

⁵⁶KOHN, W.; MEIR, Y.; MAKAROV, D. *Phys. Rev. Letters* **1998**, *80*, 4153–4156.

⁵⁷DOBSON, J. F.; MCLENNAN, K.; RUBIO, A. *Aust. J. Chem.* **2002**, *54*, 513–527.

⁵⁸GRIMME, S. *J. Comp. Chem.* **2004**, *25*, 1463–1473.

⁵⁹ZHAO, Y.; TRUHLAR, D. G. *Acc. Chem. Res.* **2008**, *41*, 157–167.

⁶⁰AVERKIEV, B. B.; ZHAO, Y.; TRUHLAR, D. G. *J. Mol. Catal. A* **2010**, *324*, 80–88.

⁶¹ZHAO, Y.; TRUHLAR, D. G. *Theor. Chem. Acc.* **2008**, *120*, 215–241.

⁶²BANTREIL, X.; PRESTAT, G.; MORENO, A.; MADEC, D.; FRISTRUP, P.; NORRBY, P.-O.; PREGOSIN, P. S.; POLI, G. *Chem. Eur. J.* **2011**, *17*, 2885–2896.

1.2 Experimental Study

Reproducibility is one of the biggest issues in all kinetic measurements. The quality and the purity of the reactants, solvents and glassware used in the study should guarantee that it will yield a reproducible result. We started the mechanistic study with the catalytic system discovered earlier in our laboratory: 5 mol% of **1**, 5 mol% of PCy₃ and 10 mol% of KO*t*Bu. In the early stage of our study it was found that it was hard to get the same results from seemingly identical experiments. It was found that all the samples of the commercially available PCy₃ from various suppliers contained impurities such as phosphine oxide and phosphites. PCy₃ could be purified by recrystallization but after a short period it got oxidized again. To solve this problem we employed the method proposed by Netherton and Fu and substituted PCy₃ with its salt PCy₃·HBF₄ (**2**).⁶³

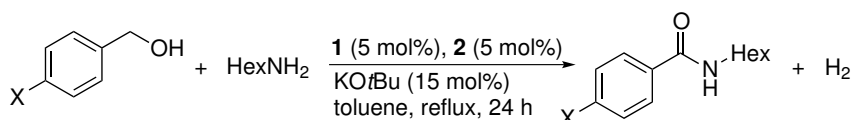
Half-molar concentration of an alcohol and an amine was the optimal for the most of the substrates because the reaction was complete in 24 h and proceeded with a sufficient initial rate. Thus, the mechanistic study was performed with the following experimental system: 5 mol% of **1**, 5 mol% of **2**, 15 mol% of KO*t*Bu, 2–5 mL of 0.5 M toluene solution of an alcohol and an amine.

1.2.1 Hammett Study

Before performing any kinetic measurements the amidation of hexylamine **5** was carried out with different *para*-substituted benzyl alcohols **6a–k**. In most cases the reactions proceeded cleanly and gave the corresponding amides **11a–g** in high yields after 24 h (entries 1–7 in Table 1.1). Unfortunately, the alcohols with electron-withdrawing groups (except for **6b**) could not tolerate the amidation conditions. The reaction with *para*-chlorobenzyl alcohol **6h** gave several byproducts due to dehalogenation of the alcohol, and some amount of imine was formed as well. Nitro-group of **6i** and cyano-group of **6j** were reduced under these conditions which led to the formation of different compounds. Alcohol **6k** did not give any product detectable by GCMS.

Next, the competition experiments between **6a** and six *para*-substituted alcohols **6b–g** were performed (Scheme 1.5). The rate of the amidation was measured based on the disappearance of the alcohols assuming that they did not participate in side reactions and were converted only into the amides.

⁶³NETHERTON, M. R.; FU, G. C. *Org. Lett.* **2001**, *3*, 4295–4298.

Table 1.1: Amidation of *para*-substituted benzyl alcohols **6a–g**.

Entry	Alcohol	X	Yield ^a [%]
1	6a	H	90
2	6b	CF ₃	70
3	6c	F	80
4	6d	Me	94
5	6e	OMe	100
6	6f	SMe	88
7	6g	NMe ₂	100
8	6h	Cl	0
9	6i	NO ₂	0
10	6j	CN	0
11	6k	COOMe	0

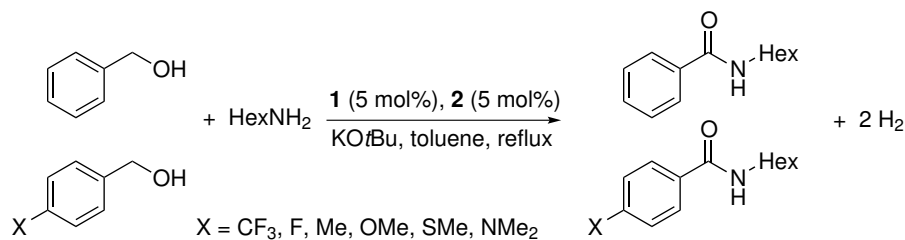
^a – isolated yield after 24 h

From these experiments it was possible to determine the relative reactivity of **6b–g** compared to the parent benzyl alcohol. Assuming that all these reactions have the same mechanism and are first order with respect to the alcohol, the relative reactivities can be obtained ($k_{rel} = \frac{k_X}{k_H}$) by using Equation 1.9 on page 11. We plotted $\ln \frac{[X]_0}{[X]}$ against $\ln \frac{[H]_0}{[H]}$ and these plots resulted in good linear correlations for all the *para*-substituted benzyl alcohols (Figure 1.5). These results support our assumption about the order of the reaction with respect to the alcohol.

Next, the Hammett plot was constructed based on the relative reactivities and different σ values (Figure 1.6). The experimental data correlated best with the σ^+ values³⁵ which yielded the reaction constant $\rho = -0.154$. Some of the relative reactivities gave good correlation with σ^\bullet values⁶⁴ which might indicate that radical intermediates are formed during the amidation reaction. To test this the

³⁵HANSCH, C.; LEO, A.; TAFT, R. W. *Chem. Rev.* **1991**, *91*, 165–195.

⁶⁴CREARY, X.; MEHRSHAIKH-MOHAMMADI, M. E.; McDONALD, S. J. *Org. Chem.* **1987**, *52*, 3254–3263.



Scheme 1.5: Competition experiments for the amidation of **6a** versus that of *para*-substituted benzyl alcohols **6b–g**.

reaction was conducted in the presence of cyclohexa-1,4-diene (1 equivalent with respect to the alcohol) as a radical scavenger and it was found that it had almost no influence on the amide formation (small amount of imine was formed probably due to some impurities in the scavenger). This experiment demonstrated that radical species are not involved in the catalytic cycle.

The value of the reaction constant ρ of -0.154 indicates that a small positive charge is formed at the benzylic position of the alcohol in the transition state of the RDS. The amide formation most likely proceeds through two consecutive β -hydride eliminations: transformations of an alcohol to an aldehyde and a hemiaminal to an amide. Either of these steps is a good candidate for the RDS because in both cases a partial positive charge is built-up in the transition state.

1.2.2 Determination of the Reaction Order

The next step was to determine the reaction order with respect to the reactants (Figure 1.7). The initial-rate method was employed and the rates measured based on the formation of an amide as opposed to the Hammett study where the reaction was monitored by the disappearance of the alcohol. The reason is that at the early stage of the reaction the change in the concentration can be measured more precisely for the amide than for the alcohol.

Hexylamine **5** and benzyl alcohol **6a** were used as substrates for determining order in the amine. The concentration of **5** was varied from 0.2 M to 0.5 M while keeping the concentration of **6a** (0.5 M) and the ruthenium catalyst **1** (0.025 M) constant. The initial rates (r_{init}) were plotted against the amine concentrations to give a straight line (Figure 1.7a) which indicated that the amidation reaction is first order in the amine.

The reaction is also first order in alcohol as it was shown in the Hammett study (Section 1.2.1). Next, we examined the order in the catalyst. Initial

1.2 Experimental Study

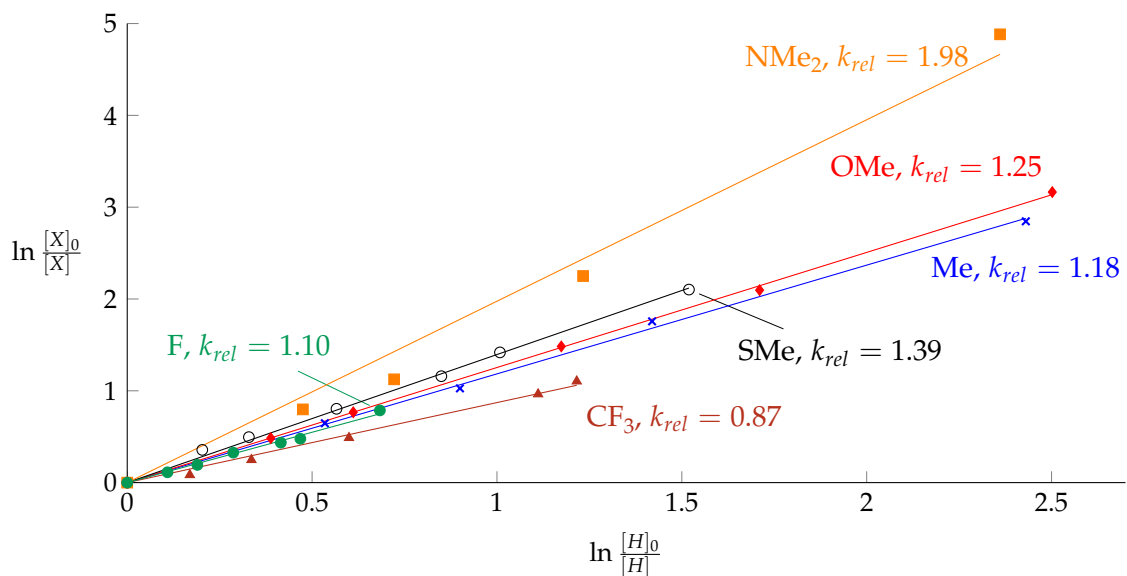


Figure 1.5: Kinetic data for the amidation of *para*-substituted benzyl alcohols **6b–g** in competition with **6a**.

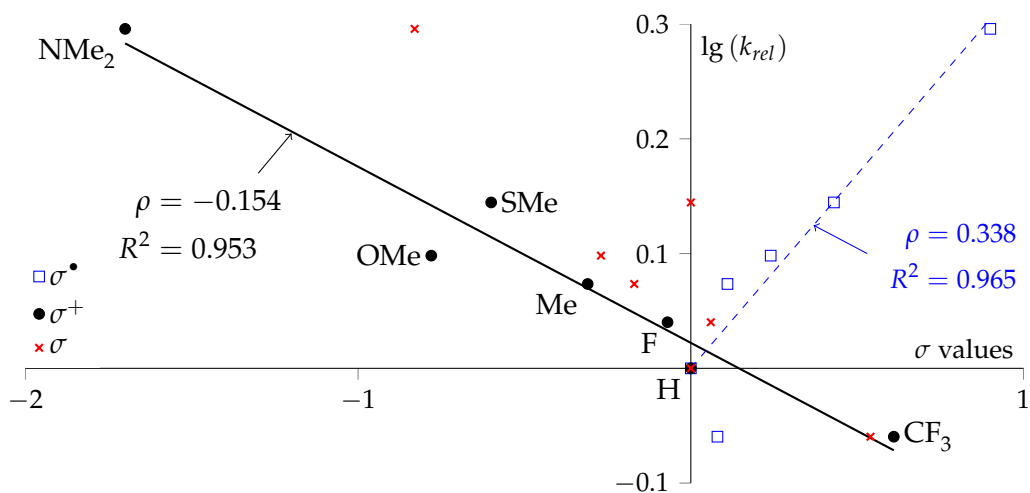


Figure 1.6: Hammett plots constructed using different sets of σ values.

experiments showed that at low catalyst loadings (≤ 2 mol% or 10 mM) the amidation either had a long initiation time or did not proceed at all which made it impossible to obtain reproducible results. At higher loadings, (≥ 6 mol%), the reaction was also accompanied by substantial uncertainties. To overcome these obstacles the experimental procedure was altered and the reaction performed as follows: complex **1**, $\text{PCy}_3 \cdot \text{HBF}_4$ (**2**) and $\text{KO}t\text{Bu}$ were refluxed in toluene for 45 min before the solution of the alcohol and the amine was added. To test if these alterations have changed the mechanism of the reaction we repeated the experiments from Figure 1.7a and observed the same linear dependence. Following the modified procedure, concentration of **1** was varied from 5 to 37 mM while keeping the concentration of the alcohol and the amine constant (0.5 M). Plotting the obtained rate values against the catalyst concentration in double-logarithmic coordinates gave a straight line with a slope of 1.511 which means that the order of the amidation reaction in ruthenium is 1.5 (Figure 1.7c). However, if the conditions of the experiment are considered more carefully, it is likely that this order is not correct. When varying amount of complex **1**, the concentration of all the reactants is not kept constant because the amount of $\text{PCy}_3 \cdot \text{HBF}_4$ and $\text{KO}t\text{Bu}$ also varies. As it was previously shown, in racemization of chiral alcohols mediated by a ruthenium–NHC complex similar to **1** *tert*-butoxide is involved only in the initiation step of the reaction and does not otherwise interfere with the catalytic cycle.⁶⁵ We assume that it plays similar role in the amidation reaction and is only needed for the formation of a catalytically-active species which takes place when **1** is premixed with **2** and $\text{KO}t\text{Bu}$. As a consequence, it does not influence the rate of the reaction.

To better understand the role of PCy_3 , we studied its influence on the rate of the reaction. The amount of **2** was varied from 0 to 5 mM (and of $\text{KO}t\text{Bu}$, accordingly) while keeping concentration of all other reactants constant (alcohol and amine – 0.2 M, **1** – 0.01 M) and it was found that the order in a phosphine is 0.5 (Figure 1.7b).

Taking all this information into account, the rate equation can be written as follows:

$$r = k[\text{alcohol}][\text{amine}][\text{PCy}_3]^{0.5}[\mathbf{1}]^n \quad (1.20)$$

To eliminate possible uncertainties due to slight variations in the alcohol, amine or phosphine concentrations in different experiments, the rate in

⁶⁵Bosson, J.; Poater, A.; Cavallo, L.; Nolan, S. P. J. *Am. Chem. Soc.* **2010**, *132*, 13146–13149.

1.2 Experimental Study

Equation 1.20 was normalized as follows:

$$r' = \frac{r}{[alcohol][amine][PCy_3]^{0.5}} = k[1]^n \quad (1.21)$$

The order in ruthenium was calculated using Equation 1.21 and it was found that it equals 1 (Figure 1.7d). The final rate equation for the amidation reaction is:

$$r = k[alcohol][amine][1][PCy_3]^{0.5} \quad (1.22)$$

Based on Equation 1.22 it can be concluded that most likely no polymeric ruthenium species are involved in the reaction and that PCy₃ is not always coordinated to ruthenium throughout the catalytic cycle.

1.2.3 Experiments with Deuterated Substrates

Initially, we wanted to determine the kinetic isotope effect (KIE) by performing competition experiments similar to those used in the Hammett study. It was rapidly discovered that if an equimolar mixture of benzyl alcohol (**6a**) and α,α -*d*₂-**6a** was introduced into the reaction with hexylamine under the amidation conditions, a rapid scrambling of hydrogen and deuterium occurred. Unfortunately, it made it impossible to use competition experiments for measuring the KIE but it demonstrated an unexpected behavior of the reaction which was studied in details.

From the experiments in the previous section it is clear that hexylamine and benzyl alcohol are not the best substrates for the kinetic measurements in terms of reproducibility but for the sake of consistency all the orders were determined with the same alcohol and amine. This section also deals with kinetic measurements and to make our life easier we decided to change the substrates and use 2-phenylethanol (**7**) and benzylamine (**8**) instead.

To determine the source of the scrambled atoms the amidation reaction was performed with various deuterated and non-deuterated compounds. First candidate for the source of the hydrogen was toluene. The amidation reaction was made between **7** and **8** in toluene-*d*₈ (Table 1.2, entry 1) and measured the amount of mono-, di- and non-deuterated **7** over time by GCMS. This experiment demonstrated that the solvent did not exchange its hydrogen atoms with the reactants (Figure 1.8).

Next, an experiment with non-deuterated **7** and **8**-*d*₂ (entry 2) was performed which showed that after 24 h the hydrogen–deuterium ratio almost

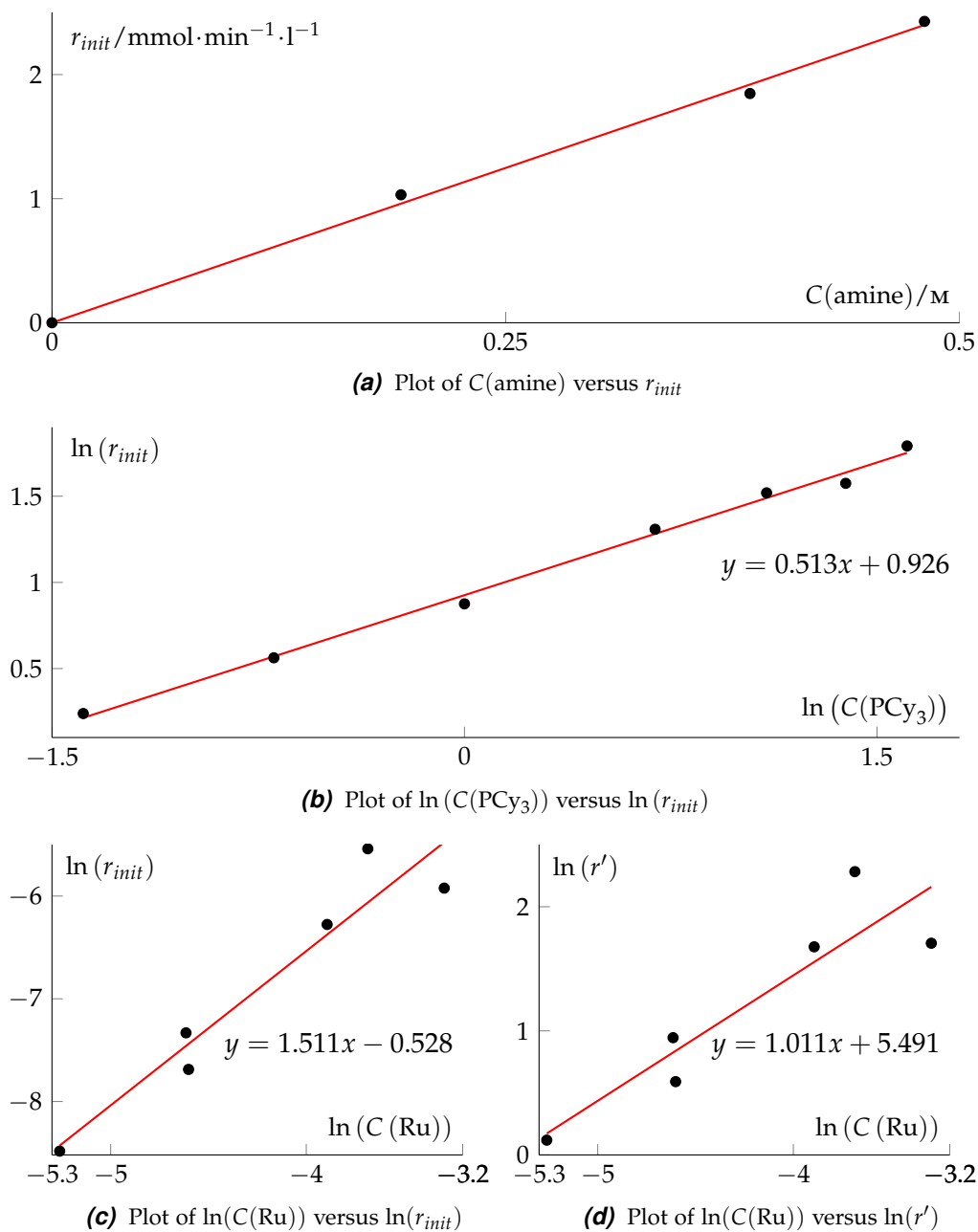
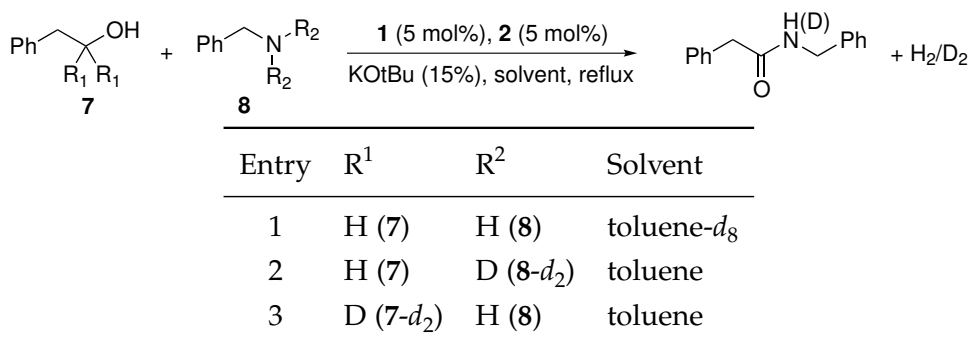


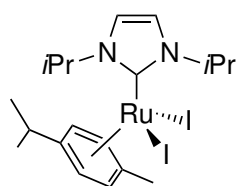
Figure 1.7: Determination of the reaction order with respect to the reactants.

Table 1.2: Experiments to determine the position of the scrambled atoms.

approached the ratio of 3:2 (Figure 1.8). This indicates that the total number of the exchangeable protons in the system is 5.

Finally, in the reaction between 7-*d*₂ and 8 the hydrogen–deuterium ratio rapidly equilibrated around the same ratio of 3:2 (entry 3 and Figure 1.8). The fact that the scrambling had started before the amide was formed implies that there is a reversible step at the beginning of the catalytic cycle. More likely, this step is a β-hydride elimination leading to the formation of an aldehyde.

Analyzing these results we can conclude that the five exchangeable hydrogen atoms in the system are: two protons of the NH₂ group, two from the α-position and one from the OH group of the alcohol. More importantly, the scrambling implies that the amidation reaction operates through the so-called “dihydride” mechanism, *i.e.* a ruthenium–dihydride species is involved in the catalytic cycle.

**Figure 1.9:** Structure of the complex 1-*I*₂.

The dihydride mechanism means that the two chlorine atoms are not bound to ruthenium during the catalytic cycle. To gain further support for this idea we synthesized a diiodo-analog of the complex 1 – RuI₂IiPr(*p*-cymene) (1-*I*₂, Figure 1.9) and used it in the reaction. It was previously shown that similar diiodo-complexes can catalyze the amidation reaction although giving usually lower yields, probably, due to the lower stability of these complexes.^{19,66}

When the initial rate of the reaction with 1-*I*₂ as the pre-catalyst was measured,

¹⁹DAM, J. H.; OSZTROVSKY, G.; NORDSTRØM, L. U.; MADSEN, R. *Chem. Eur. J.* **2010**, *16*, 6820–6827.

⁶⁶ZHANG, Y.; CHEN, C.; GHOSH, S. C.; LI, Y.; HONG, S. H. *Organometallics* **2010**, *29*, 1374–1378.

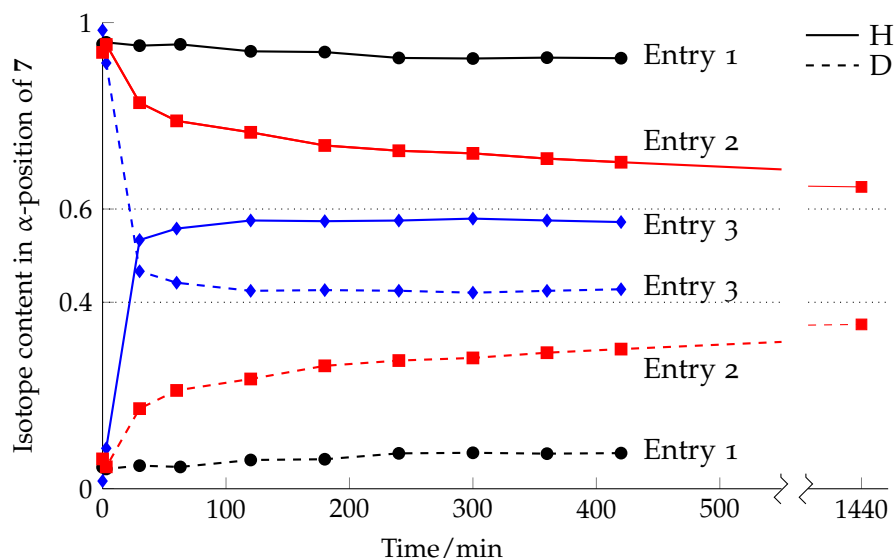


Figure 1.8: Experiment with deuterium-labeled substrates.

a value of $3.09 \text{ mM} \cdot \text{min}^{-1}$ was obtained which was essentially the same as in the case of dichloride compound **1**. This fact supports our idea that no halogen atoms are bound to ruthenium in the catalytic cycle.

To summarize, it was found that under the amidation conditions hydrogen atoms from α -position and the OH group of the alcohol and the NH_2 group of the amine can be scrambled and that the reaction operates via the dihydride mechanism.

1.2.4 Kinetic Isotope Effect

As it was shown in the previous section, competition experiments could not be used for determining the KIE. Therefore, the only other option was to perform two separate reactions: one with deuterated substrates and one with non-deuterated – and measuring their rates. To do this, a special deuterated alcohol was needed which would contain deuterium in the α -position and the OH group.

First, an analog of **7** with three deuterium atoms BnCD_2OD was synthesized. An IR spectrum of this compound showed that it contained a significant amount of BnCD_2OH . In spite of this fact, the rate constant of the amidation reaction as measured with this partly deuterated compound to give the value

1.2 Experimental Study

of the initial rate of $(1.260 \pm 0.050) \text{ mM} \cdot \text{min}^{-1}$, which then yielded the KIE value of 1.785 ± 0.172 . Unfortunately, all attempts to obtain the alcohol with higher deuterium content in the OH group failed. Because of this we had to use commercially available alcohols.

The reaction with perdeuteroethanol gave unreproducible results due to the low boiling point of the alcohol. Next, perdeutero-1-butanol ($\text{C}_4\text{D}_9\text{OD}$, **9-*d*₁₀**) was investigated and it yielded satisfactory data in terms of reproducibility. The initial rate of the reaction between **9-*d*₁₀** and BnND_2 (**8-*d*₂**) was $(6.44 \pm 0.02) \text{ mM} \cdot \text{min}^{-1}$. Even though substrates with deuterium atoms at the exchangeable positions were used, the real value of the initial rate might be lower because in these experiments $\text{PCy}_3 \cdot \text{HBF}_4$ was used as a phosphine source which upon deprotonation gave *t*BuOH which in turn might exchange its proton with the OD or ND_2 groups. Unfortunately, it was impossible to quantify how big the influence of these protons was, but we assumed that since only 5 mol% was used, the real value of the initial rate should not be dramatically lower. In the case of the non-deuterated analogs, **8** and **9**, the initial rate was $(14.77 \pm 0.96) \text{ mM} \cdot \text{min}^{-1}$. These values gave an experimental KIE of 2.29 ± 0.15 .

Since the KIE value is greater than unity, the breakage of the C–H bond has an impact on the overall rate of the reaction but is only one of several slow steps in the catalytic cycle.

1.2.5 NMR Experiments

At this point of the study, quite a few kinetic parameters of the amidation reaction were available which could later on be compared with the calculated ones but the information about the structure of the species involved in the catalytic cycle was still lacking (apart from that some of them were dihydridic). To fill this gap we undertook an NMR study of the reaction.

First, we studied whether *p*-cymene is coordinated to ruthenium during the reaction. $\text{RuCl}_2\text{LiPr}(\textit{p}\text{-cymene})$ (**1**) has very low solubility in toluene but it is soluble enough to give a relatively good NMR spectrum which has a singlet at 1.9 ppm assigned to a methyl group of the coordinated *p*-cymene. After the beginning of the reaction another singlet at 2.15 ppm (methyl group of free *p*-cymene) appeared and the signal at 1.9 ppm disappeared. After 10 min the amount of free *p*-cymene reached the value of the amount of **1** used for the reaction (Figure 1.10). This means that all *p*-cymene decoordinates from ruthenium at the very beginning of the reaction.

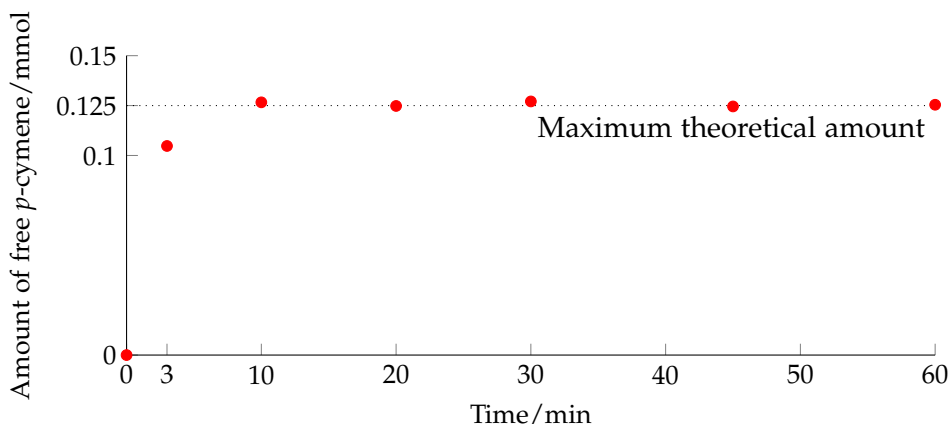


Figure 1.10: Amount of free *p*-cymene present in the solution during the amidation reaction.

Next step was to elucidate the structures of the intermediates. The reaction in an NMR tube was monitored at 70 °C and 40 mol% catalytic loading with various substrates and phosphines. To reduce the number of unwanted signals, the reaction was performed in C₆D₆ with RuCl₂LiPr(benzene) (**10**, Figure 1.11). This experiment demonstrated that no free aldehyde was formed in the solution. It proved the proposed earlier idea that the aldehyde formed during the reaction stays coordinated to the ruthenium center.¹⁹ Unfortunately, this was the only useful information we could obtain from the experiment. Next, PCy₃ was replaced with PPh₃ and ethanol together with benzyl amine were used to free the region between 0 and 2 ppm from extra signals and, probably, get an insight into what was happening with the *iso*-propyl groups of the NHC during the reaction. Several doublets as well as multiplets were found in that region (Figure 1.12). They could be assigned to the Me groups of the *iso*-propyl group attached to the NHCs of the various intermediates, but it was hard to say anything more specific.

More useful information was found in the hydride part of the spectrum, *i.e.* from -7 ppm to -20 ppm. Since the signals in this region did not overlap

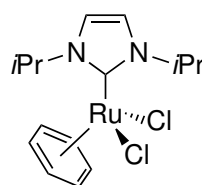


Figure 1.11: Structure of the complex **10**.

¹⁹DAM, J. H.; OSZTROVSZKY, G.; NORDSTRØM, L. U.; MADSEN, R. *Chem. Eur. J.* **2010**, *16*, 6820–6827.

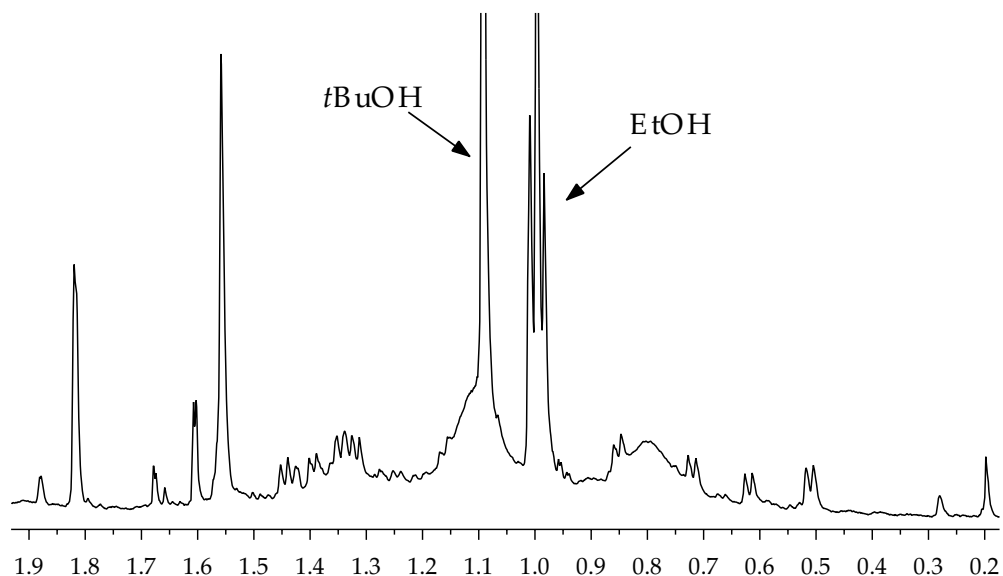


Figure 1.12: A part of the NMR spectrum of the reaction mixture.

with the solvent and reactant signals, it was decided to perform the reaction with the usual system but still with a high catalytic loading: 40 mol% of **1** and $\text{PCy}_3 \cdot \text{HBF}_4$, 120 mol% of $\text{KO}t\text{Bu}$, 2-phenylethanol and benzylamine in toluene- d_8 . After 3 h, several clusters of hydride signals were observed including low-intensity signals at -7.44 ppm and -7.54 ppm, very low-intensity ones in the range -10.66 ppm to -11.13 ppm, high-intensity doublets from -17.41 ppm to -17.89 ppm ($^2J_{\text{P-H}} = 20$ Hz), as well as a high-intensity doublet at -18.04 ppm ($^2J_{\text{H-H}} = 7.1$ Hz). These observations clearly revealed that several hydride species were formed during the amidation reaction what was also in accordance with previously reported data.⁶⁶ Moreover, the doublet at -18.04 ppm showed that there was a dihydride species that did not contain a phosphine ligand. The doublets from -17.41 ppm to -17.89 ppm and their coupling constants suggested the presence of ruthenium–hydride complexes in which one phosphine group is coordinated *cis* to the hydride atom.⁶⁷ Over time, the intensity of the signals decreased and some of them disappeared.

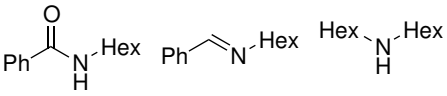
Finally, an experiment was conducted in a usual manner (in refluxing toluene- d_8) in a Schlenk tube with 20 mol% of **1** and after 30 min analyzed a

⁶⁶ZHANG, Y.; CHEN, C.; GHOSH, S. C.; LI, Y.; HONG, S. H. *Organometallics* **2010**, *29*, 1374–1378.

⁶⁷LEE, H. M.; SMITH, D. C.; HE, Z.; STEVENS, E. D.; YI, C. S.; NOLAN, S. P. *Organometallics* **2001**, *20*, 794–797.

Table 1.3: Product distribution in the reaction between benzyl alcohol and hexylamine in various solvents.

$\text{Ph-CH}_2\text{-OH} + \text{Hex-NH}_2 \xrightarrow[\text{solvent, 15 mol\% KOtBu}]{\text{1, 5 mol\%, 2, 5 mol\%}}$



Solvent	T, °C	Amide ^a	Imine ^a	Di-Hex-amine ^a
Toluene	110	90	5	0
Benzene	80	40	0	0
<i>n</i> -Octane	125	20	50	5
THF	66	25	0	0
2-Me-THF	80	50	0	0
1,4-Dioxane	101	60	0	0
<i>t</i> BuOH	82	30	10	0
2-methyl-2-pentanol	120	20	50	5
CH ₂ Cl ₂	40	0	5	0
<i>sym</i> -C ₂ H ₄ Cl ₂	84	0	0	0
<i>sym</i> -C ₂ H ₂ Cl ₄	120	0	0	0
PhCl	140	0	20	20

^a – GCMS yield after 24 h, in %.

sample by ¹H and ³¹P NMR. In the proton spectrum several additional signals to those listed above were observed: a singlet at –9.70 ppm, a doublet at –15.04 ppm (²J_{P-H} = 22.5 Hz), and signals around –17.8 ppm. These signals also showed the presence of ruthenium species with a phosphine coordinated *cis* to hydride. The phosphorous spectrum revealed a group of signals in the range 46–51 ppm, a low-intensity signal at 57.2 ppm, and a high-intensity signal at 10 ppm which corresponded to free PCy₃. Other low-field signals could be assigned to ruthenium species with a coordinated phosphine.

1.2.6 Miscellaneous Experiments

The experiments described in this section are not a part of the mechanistic study but provided more general knowledge about the reaction itself.

The reaction between benzyl alcohol and hexylamine was studied under

1.2 Experimental Study

the amidation conditions in different solvents and formation of three products was observed: an amide, an imine or a dimerized amine (Table 1.3). It is known that the reaction performs best in toluene. No byproducts were formed in benzene but the rate of the amidation reaction was lower in comparison with toluene due to the lower boiling point of benzene. In contrast to these two solvents, a reaction in *n*-octane gave all the three possible products with prevalence of imine. The explanation for this could be that aromatic solvents can play the role of ligand and stabilize some reactive intermediates whereas *n*-octane cannot. This idea was also supported by the experiments in polar aprotic solvents which could be a ligand as well, such as THF, 2-Me-THF, 1,4-dioxane: the amide is the only product in these solvents and the yield of the reactions depends only on the reaction temperature. Tertiary alcohols seem to interfere with the intermediates giving lower yields of the amide and some amount of the imine. Finally, several chlorinated solvents were tested but none of these proved to be suitable for this reaction, more likely, due to the oxidative insertion of Ru into C–Cl bond which resulted in deactivation of the catalyst or due to low reaction temperature (in CH₂Cl₂).

Since one of the goals of this work was to develop a better catalyst for the amidation reaction, it was important to understand the activity of the catalyst in comparison with other known complexes (discussed in Section 1.1.2 on page 5).

First, the reaction was conducted under the conditions similar to those reported by Milstein and coworkers¹⁷: 0.1 mol% of the catalyst, 0.1 mol% of PCy₃·HBF₄, 0.3 mol% of KO^tBu, 3.33 M solution of benzylamine and 1-butanol in toluene. When all these reactants were mixed together and refluxed for 24 h, almost no amide was formed due to the low concentration of the ruthenium precatalyst. As a consequence, the catalytically active species were formed very slowly if they were generated at all. To form an active catalyst, **1** was refluxed with the phosphine and the base in a small volume of toluene for 45 min and after that added the solution of the alcohol and the amine (as in Section 1.2.2 when determining orders of the reaction). Under these conditions we obtained the corresponding amide in 5% yield after 24 h, which demonstrated that our system was less active than the Milstein system (for comparison, Milstein reported 97% yield after 7 h for benzylamine and 1-pentanol). However, after the substrates had been changed to hexylamine and 2-phenylethanol and the catalytic loading had been increased to 0.75 mol%, the amide was obtained in 80% yield after 18 h. With 1 mol% of **1**, the complete conversion was

¹⁷GUNANATHAN, C.; BEN-DAVID, Y.; MILSTEIN, D. *Science* **2007**, *317*, 790–792.

achieved after 18 h. Other reported catalytic systems are less active than ours: the coupling catalyzed by 4 mol% of the diamine–diphosphine ruthenium complex (**h** in Figure 1.1 on page 4) gives 21–95% of lactams after 4–16 h,²⁰ while with 5 mol% of 1,2,3-triazolyldeneyl ruthenium complexes (**i** in the same figure) amides are synthesized in 40–65% after 15 h.²¹

Finally, we employed the knowledge about the reaction orders to lower the catalytic loading while retaining the same reactivity. As was found in Section 1.2.2, increasing the concentration of PCy₃ accelerates the reaction, the amidation was therefore performed with 0.5 mol% of **1** and a Ru:P ratio of 1:5 instead of the usual 1:1. Under these conditions the reaction between hexylamine and 2-phenylethanol gave 65% of the amide after 18 h.

1.2.7 Summary of the Experimental Study

In summary, during the experimental study it was found that:

1. A small positive charge is formed in the transition state in the rate-determining step.
2. The reaction is first order in the alcohol, the amine and the catalyst and has an order of 0.5 in the phosphine
3. The KIE is 2.29 ± 0.15 .
4. No halogen atoms are bound to the ruthenium center during the reaction.
5. Ruthenium–dihydride species are involved in the catalytic cycle.
6. *para*-Cymene is not coordinated to ruthenium during the reaction.
7. A phosphine is bound to some intermediates and its orientation is *cis* relative to the hydride.
8. Protons from the α -position and the OH group of the alcohol and the NH₂ group of the amine can be scrambled under the amidation conditions.

²⁰NOVA, A.; BALCELLS, D.; SCHLEY, N. D.; DOBEREINER, G. E.; CRABTREE, R. H.; EISENSTEIN, O. *Organometallics* **2010**, *29*, 6548–6558.

²¹PRADES, A.; PERIS, E.; ALBRECHT, M. *Organometallics* **2011**, *30*, 1162–1167.

1.3 Computational Study

At this point of the study it was already possible to propose a plausible mechanism for the amidation reaction which accounted for all the observed facts. For better understanding of the catalytic cycle we undertook an extensive theoretical investigation on the reaction.

For calculating energy of a species a method suggested by Wertz was chosen which, as shown in Equation 1.23, employs a combination of gas-phase energy (E_{scf}) with solution-phase energy (E_{solv}) and Gibbs free energy (ΔG).⁶⁸ This approach allows to take into account contribution of a solvent without calculating solution-phase Gibbs free energy. It has been successfully applied in several studies of transition metal-catalyzed reactions.^{38,69,70}

$$\Delta G_{\text{tot}} = E_{\text{solv}} - E_{\text{scf}} + \Delta G \quad (1.23)$$

1.3.1 Orientation of Ligands

From the experimental study we knew that *p*-cymene dissociates off during the first minutes of the reaction creating three vacant coordination sites. NMR also showed that hydride species were involved in the catalytic cycle and that a phosphine was coordinated to some of them. It was also shown that in the presence of an alcohol and a base, chloride atoms bound to ruthenium can be substituted with a hydride and an alkoxide.^{71,72} Based on these observations we suggest that NHC, hydride, phosphine and alkoxide are the ligands that coordinate to the ruthenium center in the beginning of the catalytic cycle. Attaching these four ligands to ruthenium creates a 14-electron complex which has two empty sites. One of the empty sites has to be in the *cis* position to the alkoxide for the β -hydride elimination to occur. The second free site could be occupied by any of the ligands present in the reaction mixture: an amine, an alcohol, an additional phosphine, something else or it could stay empty throughout the reaction. To find it out energy for various ligand orientations were calculated as well as energies of the species with different ligands.

³⁸FRISTRUP, P.; KREIS, M.; PALMELUND, A.; NORRBY, P.-O.; MADSEN, R. *J. Am. Chem. Soc.* **2008**, *130*, 5206–5215.

⁶⁸WERTZ, D. *J. Am. Chem. Soc.* **1980**, *102*, 5316–5322.

⁶⁹LAU, J. K. C.; DEUBEL, D. V. *J. Chem. Theory Comput.* **2006**, *2*, 103–106.

⁷⁰FRISTRUP, P.; TURSKEY, M.; MADSEN, R. *Org. Biomol. Chem.* **2012**, *10*, 2569–2577.

⁷¹ARANYOS, A.; CSJERNYIK, G.; SZABÓ, K. J.; BÄCKVALL, J.-E. *Chem. Commun.* **1999**, *2*, 351–352.

⁷²SOLARI, E.; GAUTHIER, S.; SCOPELLITI, R.; SEVERIN, K. *Organometallics* **2009**, *28*, 4519–4526.

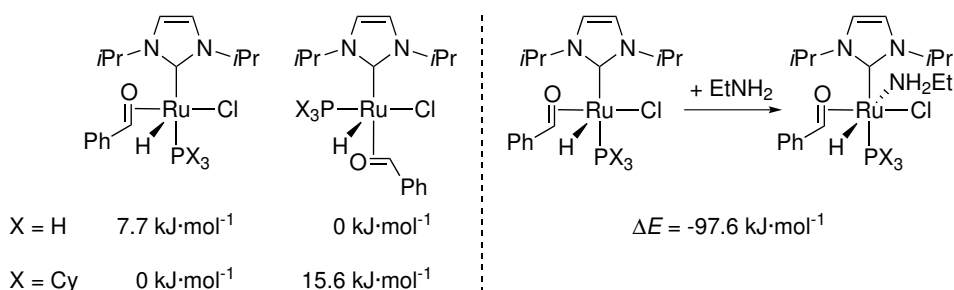


Figure 1.13: Lowest-energy ligands orientation (left) and an amine coordination (right).

The calculations (DFT/B3LYP) were started with a simplified system in comparison with the real setup: PCy₃ was replaced with PH₃, ethylamine and benzyl alcohol were employed as reactants, and 1,3-diisopropylimidazol-2-ylidene (*i*Pr) as a permanent carbene ligand. Initial calculations were carried out without knowing that a dihydride species took part in the reaction. As a consequence, it was assumed that only one chlorine atom was substituted. First, stability of a supposed intermediate after the first β -hydride elimination was studied. It was found that in the lowest energy isomer PH₃ was *cis* to the carbene but when it was replaced with PCy₃, the *trans* orientation of the phosphine and the carbene became more favorable by 15.6 kJ·mol⁻¹ (Figure 1.13 left). This result demonstrated that the two largest ligands tended to be situated as far from each other as possible. Next, it was studied how coordination of various ligands influenced the energy of the species and found that the most energy gain was obtained if EtNH₂ was bound to the ruthenium atom (Figure 1.13 (right)).

Next, a catalytic cycle for the amidation reaction was proposed (Figure 1.14). Ruthenium alkoxide **14a** enters the cycle and undergoes β -hydride elimination to give a hydridic species **14b** with a coordinated aldehyde which after the addition of an amine transforms to a charged hemiaminal-like species **14c**. After the proton abstraction by the hydride and elimination of hydrogen gas, an empty site is created on the ruthenium center. Then, second β -hydride elimination occurs to give a coordinated amide **14f** which gets replaced by another molecule of the alcohol. After the abstraction of the proton from its O–H bond by the hydride and elimination of the second molecule of dihydrogen the first species of the cycle is formed again.

Since it was not determined whether a chloride was coordinated to the ruthenium atom during the cycle, the energy of the intermediates with sub-

1.3 Computational Study

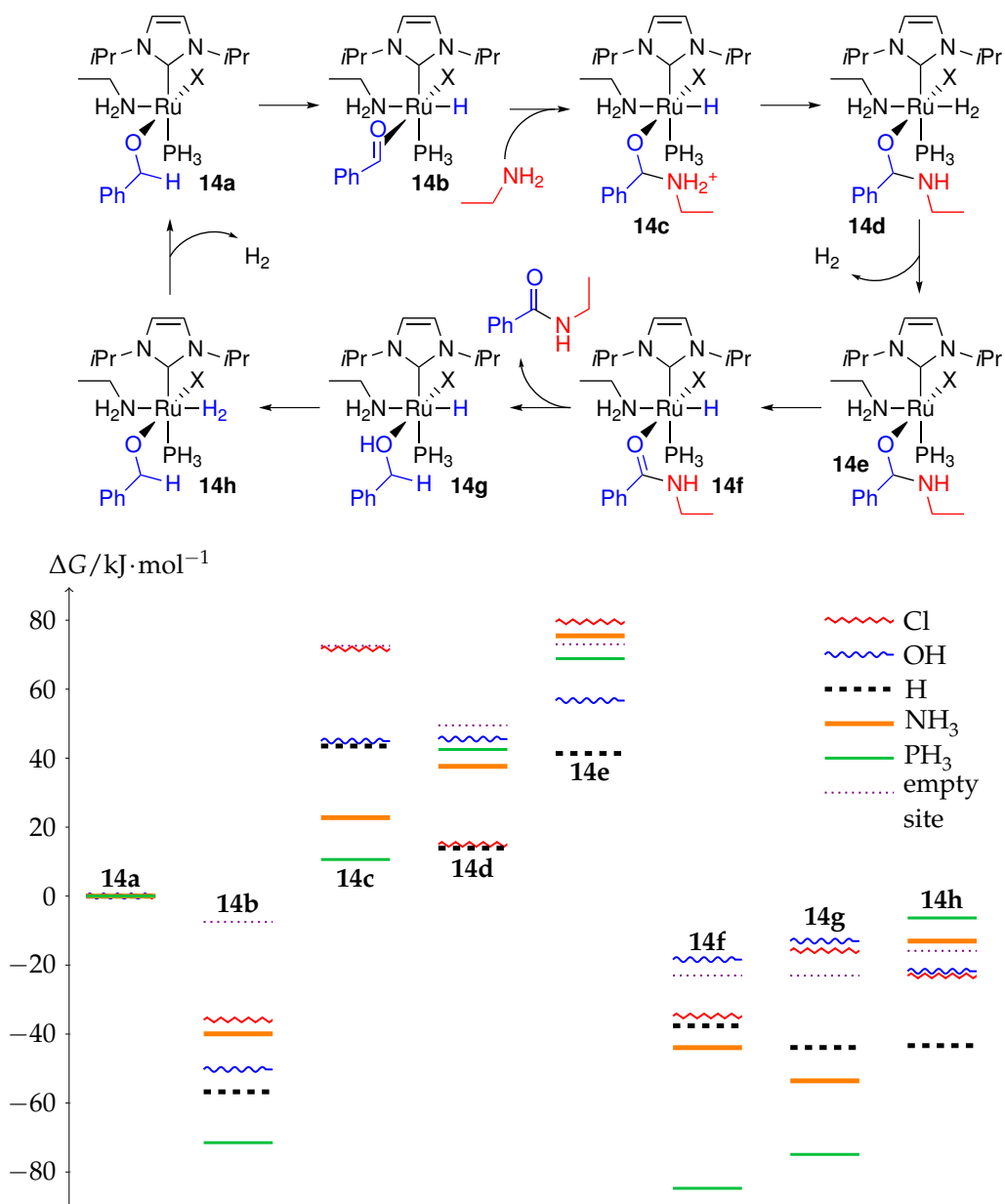


Figure 1.14: Proposed catalytic cycle with different ligands ($X = \text{Cl}, \text{OH}, \text{H}, \text{NH}_3, \text{PH}_3$ or an empty site) and energy profiles for the cycles with these ligands.

stituents different from chloride was calculated (Figure 1.14). To make the calculations faster, the simplest possible ligands were used, *i.e.* OH instead of an alkoxide, NH₃ instead of an amine. Even though these calculations did not include the transition states, they still allowed to estimate the relative stability of the species with different substituents. The calculations revealed that the second molecule of an amine or a phosphine is unlikely to be coordinated to the ruthenium center whereas any of the other three ligands could be bound to ruthenium (or the site could be empty) throughout the catalytic cycle.

To distinguish between these possibilities, a study of the cycles including all transition states for each of the ligands was undertaken. At the very beginning of this study there unexpectedly appeared problems when searching for the transition states: the TS optimizations yielded either a starting molecule or a product of the transformation. Even if the resulting structure differed from the reactant and the product, its calculated IR spectrum never had a negative frequency. Addition of polarization and diffuse functions to the basis set did not help and only after changing the functional from B3LYP to M06 it was possible to obtain correct structure of the transition states for the complexes with X = H.

At this point of the study, the hydrogen scrambling was discovered in the experiments with deuterium-labeled substrates, and that is why the calculations for all the possible ligands were not completed. Further work was carried out assuming that the ligand X is hydride and that the reaction operates via a dihydride mechanism.

1.3.2 Calculations on the Catalytic Cycle

Two important changes had been made since the beginning of the theoretical study: the functional had been changed from B3LYP to M06 and a chlorine ligand had been replaced with a hydride in the model. To verify that the chosen orientation of the ligands was still the lowest-energy configuration, the energy of the possible isomers was calculated again but this time using PCy₃ as a phosphine. The calculations revealed that two isomers of the alkoxide complex with NHC and PCy₃ *trans* to each other had almost the same energy ($\Delta\Delta G_{\text{tot}}(\mathbf{15a}-\mathbf{15b}) = 5.8 \text{ kJ}\cdot\text{mol}^{-1}$), hence either of these species could be formed at the beginning of the reaction and start their own catalytic cycle (Figure 1.15).

According to the relative orientation of two hydride ligands during the cycle, we will refer to the pathway **a** as the *cis*-pathway and to **b** as the *trans*-pathway.

1.3 Computational Study

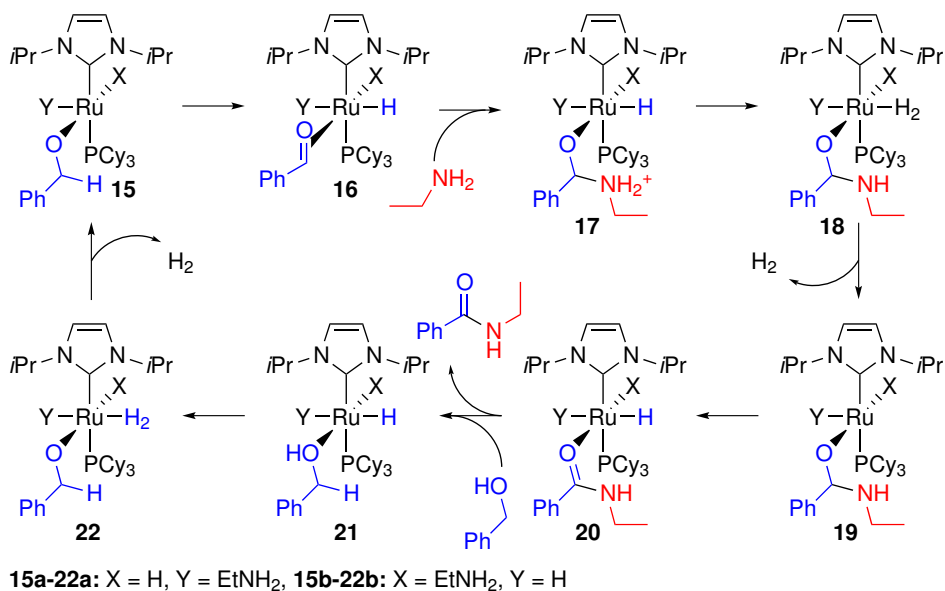


Figure 1.15: Proposed catalytic cycle (**a:** *cis*-dihydride route, **b:** *trans*-dihydride route).

To distinguish between these possible pathways, the entire catalytic cycle was calculated starting from either species **15a** or **15b** (Figure 1.16).

From the experiments with the deuterated substrates (Figure 1.8 on page 29) it was known that deuterium scrambling took place at the very beginning of the reaction and before the formation of the amide. It was also observed that the rate of the exchange was much higher than the rate of the amide formation. In the experiment with the α,α -dideuteroalcohol 8% of deuterium was exchanged with hydrogen after 3 min, whereas no amide was detected by GCMS after the same time. These observations suggest that the deuterium scrambling occurs in the first β -hydride elimination step when a dihydride species (**16**) is formed. The calculations show that the formation of species **16a** is exothermic ($\Delta G_{\text{tot}}^{\text{react}} = 28.6 \text{ kJ}\cdot\text{mol}^{-1}$), whereas the formation of species **16b** is endothermic ($\Delta G_{\text{tot}}^{\text{react}} = 50.3 \text{ kJ}\cdot\text{mol}^{-1}$). Moreover, the activation energy for the reverse reaction was lower in the case of species **16b** ($\Delta\Delta G_a(\mathbf{16a}-\mathbf{16b}) = 30.4 \text{ kJ}\cdot\text{mol}^{-1}$). It should also be noted that the difference in energy between the preceding (**TS1**) and subsequent (**TS2**) transition states for intermediate **16** is higher in the case of the *trans*-pathway ($\Delta G_a(\mathbf{TS2b}-\mathbf{TS1b}) = 48.9 \text{ kJ}\cdot\text{mol}^{-1}$, $\Delta G_a(\mathbf{TS2a}-\mathbf{TS1a}) = 18.5 \text{ kJ}\cdot\text{mol}^{-1}$). All these facts suggested that after the first β -hydride elimination a *trans*-dihydride species **16b** was

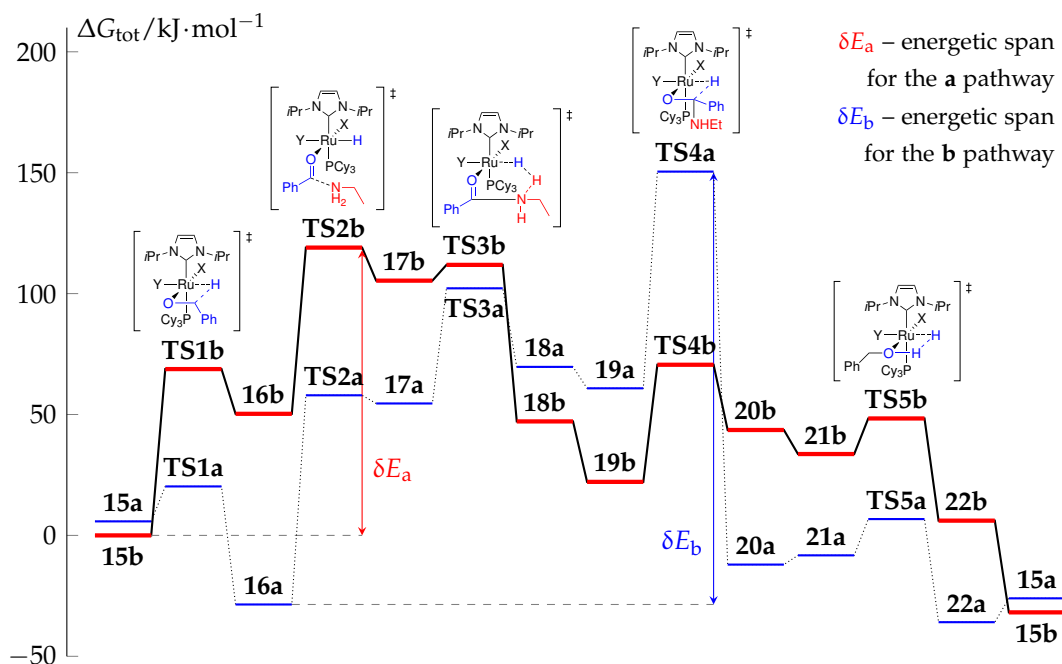


Figure 1.16: Energy profile for *cis*- and *trans*-pathways.

likely to be formed. Consequently, the equilibrium between deuterated and non-deuterated substrates would be determined by the *trans*-pathway in the first β -hydride elimination step.

Next, we applied the energetic span model to these catalytic cycles in order to verify whether the reaction operates via the **b** pathway. Calculations in the AUTOF program revealed that for the *cis*-pathway a dihydride species with a coordinated aldehyde (**16a**) is the TDI and the transition state for the second β -hydride elimination (**TS4a**) is the TDTs. The energetic span for this route is $\Delta E_a = 189.1 \text{ kJ}\cdot\text{mol}^{-1}$. For the *trans*-pathway the starting alkoxide species (**15b**) is the TDI and the transition state for an amine addition step (**TS2b**) is the TDTs. The energetic span was found to be $\Delta E_b = 119.0 \text{ kJ}\cdot\text{mol}^{-1}$. The TOF values derived from these energetic spans are $1.04 \times 10^{-8} \text{ h}^{-1}$ for the **a** pathway and $7.38 \times 10^{-1} \text{ h}^{-1}$ for the **b** pathway which is very close to the average experimental TOF of $8.00 \times 10^{-1} \text{ h}^{-1}$. The fact that the *trans*-route is six orders of magnitude faster than the *cis*-route supports the conclusion that the reaction proceeds mainly via the **b** pathway, and consequently, we can classify the overall mechanism of the reaction as a “*trans*-dihydride mechanism”.

Table 1.4: Energy of EtNH₂ association to form intermediates **15b–22b**.

Intermediate	15b	16b	17b	18b	19b	20b	21b	22b
$\Delta G_{\text{tot}}^{\text{react}}/\text{kJ}\cdot\text{mol}^{-1}$	-35.1	-42.9	-33.4	-65.7	-83.6	-67.6	-107.0	-31.3

Table 1.5: Energy of PCy₃ dissociation from intermediates **15b–22b**.

Intermediate	15b	16b	17b	18b	19b	20b	21b	22b
$\Delta G_{\text{tot}}^{\text{dissoc}}/\text{kJ}\cdot\text{mol}^{-1}$	41.2	-6.4	29.4	61.1	63.7	16.0	43.8	15.7

After the relative orientation of the hydride ligands had been found, the energy of amine association to form the intermediates in the catalytic cycle was calculated in order to confirm the assumption that an amine is coordinated to the ruthenium center throughout the reaction. Our calculations supported our assumption and showed that the formation of all the intermediates is an exothermic process (Table 1.4).

Another important aspect related to the ligand orientation is whether or not a phosphine is bound to the ruthenium atom throughout the catalytic cycle. The order of the reaction in phosphine is 0.5 which indicates that there are one or more steps involving dissociation of phosphine. Calculations revealed that species **16b** is more stable without phosphine whereas all other intermediates have lower energy when a molecule of phosphine is coordinated to ruthenium (Table 1.5). This result might indicate that our initial assumption that PCy₃ is always bound to ruthenium was not correct and the reaction proceeds (at least partly) via species without phosphine starting from intermediate **16b**. Considering this possibility we calculated the activation energy for the amine addition to the species without phosphine and found that this barrier is 21.7 kJ·mol⁻¹ higher than in case of the transformation **16b** → **17b**. Even though the species without phosphine is more stable, the phosphine-free pathway is 15.3 kJ·mol⁻¹ less favorable.

Based on these calculations, we can suggest that intermediate **16b** exists in equilibrium with a species without phosphine. Since this equilibrium takes place between two rate-determining states, the concentration of **16b** will have a strong influence on the overall rate of the reaction. This is also in agreement with the experimental observations, where the addition of phosphine shifts the equilibrium towards intermediate **16b** and increases the overall rate of

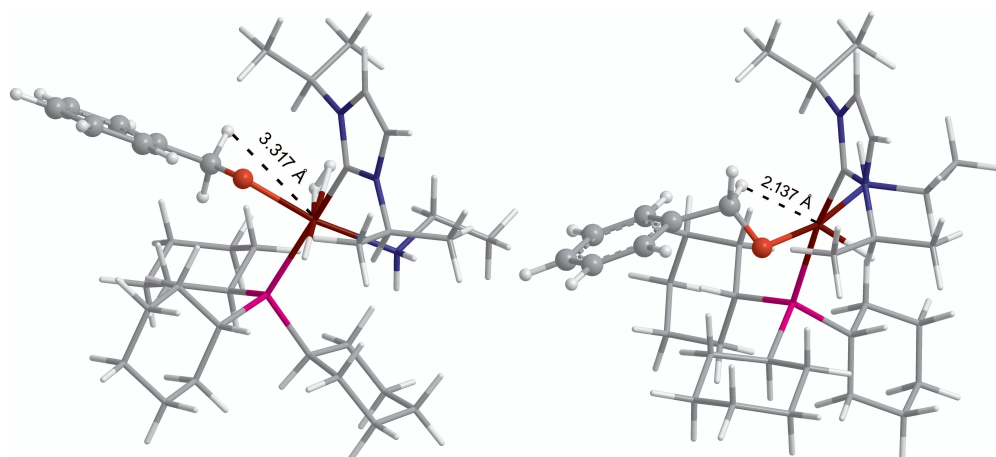


Figure 1.17: Calculated structures of intermediates **22b** (left) and **15b** (right).

the reaction, but the order with respect to phosphine is less than 1 because some phosphine dissociates off. Moreover, the doublet in the proton NMR spectrum at -18.04 ppm can be assigned to the dihydride species that is in equilibrium with **16b** after PCy_3 dissociation.

1.3.3 Geometric Parameters of the Reaction Intermediates

The next step was to have a closer look at geometric details of the species involved in the reaction. All the compounds in the proposed cycle are 18-electron species except for the two which have to have an empty site to undergo β -hydride elimination, namely, **15b** and **19b**. Each of these two intermediates is formed after dissociation of dihydrogen from the corresponding saturated species but neither of them turns into a real 16-electron species. The reason for this is that after H_2 has dissociated off, the corresponding alkoxide changes its mode of coordination from η^1 to η^3 by engaging in an agostic interaction between ruthenium atom and C–H bond (which will be broken during β -hydride elimination). This process leads to shortening of the Ru–H distance in the case of species **15b** from 3.317 Å to 2.137 Å (Figure 1.17). This kind of interactions has been observed previously in the computational studies of the β -hydride elimination with alkoxides.⁷³

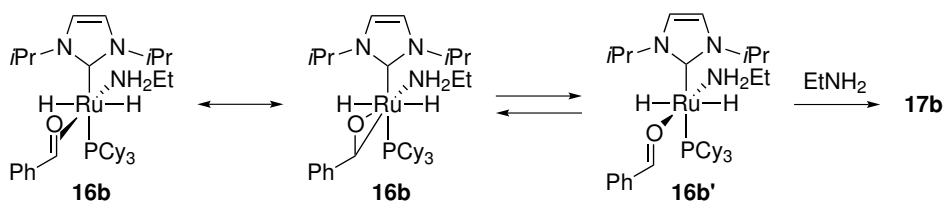
This agostic interaction indicates that the ruthenium center is electron-poor during the catalytic cycle. That is also supported by earlier observations that

⁷³SIEFFERT, N.; BÜHL, M. *J. Am. Chem. Soc.* **2010**, *132*, 8056–8070.

1.3 Computational Study

better electron-donating phosphines and NHC's enhance the reactivity of the ruthenium complexes in the amidation reaction.⁷⁴

After the first β -hydride elimination complex **15b** transforms into species with a coordinated aldehyde **16b**. The calculations show that the aldehyde is bound to ruthenium in η^2 manner through the π -system of the carbonyl group which is in line with a previously reported computational study on similar ruthenium–aldehyde complexes.⁷⁵ It should be noted that the carbonyl carbon atom of the aldehyde is closer to sp^3 rather than to sp^2 -hybridized because the out-of-plane angle for the C–H bond in **16b** is 44° and the C–O bond length is 1.309 Å. For comparison, the out-of-plane angles for the C–H bonds in formaldehyde and methanol are 0° and 54° , the C–O bond lengths are 1.208 Å and 1.420 Å, respectively. These observations imply that species **16b** is more correctly represented by a three-membered oxaruthenacycle. In the presence of the amine, complex **16b** rearranges into aldehyde η^1 -isomer **16b'** which resembles the free aldehyde more than complex **16b**: out-of-plane angle for the C–H bond is 11° and the C–O bond length is 1.235 Å (Scheme 1.6 and Figure 1.18). Compound **16b'** is then attacked by an amine to give intermediate **17b**.



Scheme 1.6: Equilibrium between the isomers of compound **16b**.

1.3.4 Modeling of the Hammett Study

Modeling of the Hammett study is another tool for verifying the proposed catalytic cycle. As was shown in Section 1.3.2 there are two steps between the TDI and the TDTs which determine the overall rate of the reaction, *i.e.* β -hydride elimination and nucleophilic addition of an amine. In terms of the Hammett study, *para*-substituents of the same electronic nature have opposite influence on these steps. Electron-donating groups facilitate the β -hydride

⁷⁴DAM, J. H. *Organometallic Reactions: Development, Mechanistic Studies and Synthetic Applications*, PhD Thesis, Technical University of Denmark, 2009, pp 87–110.

⁷⁵SCHLEY, N. D.; DOBEREINER, G. E.; CRABTREE, R. H. *Organometallics* **2011**, 4174–4179.

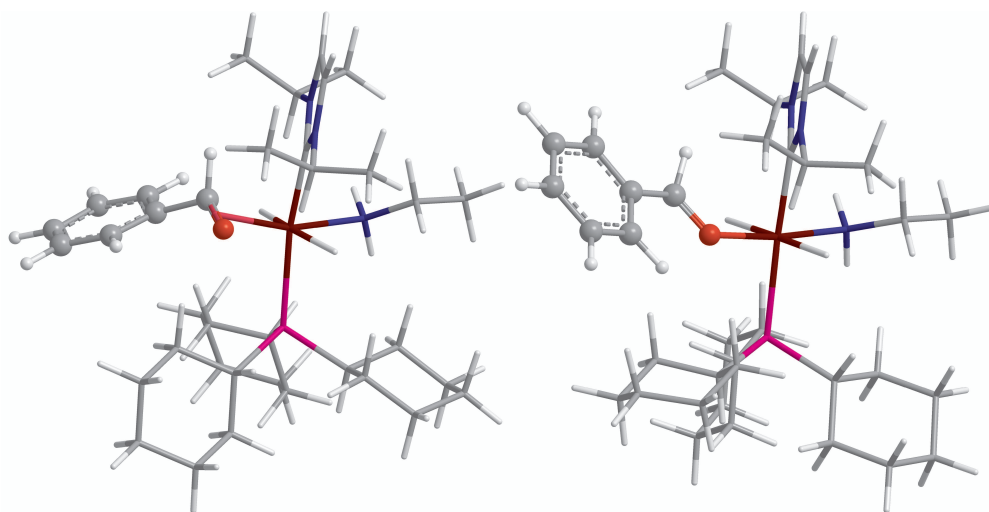


Figure 1.18: Calculated structures of complexes **16b** (left) and **16b'** (right).

elimination by stabilizing a partial positive charge on the carbon atom whereas in the nucleophilic addition these groups increase a negative charge on the carbonyl carbon atom and hence decrease its electrophilicity which slows down the transformation. The calculated energetic barriers for these two steps are almost equal which means that they could contribute equally to the rate limitations of the reaction. Based on this we could expect a small value of ρ in absolute magnitude. The experimental ρ -value of -0.15 is in agreement with this argumentation.

To gain further support for the proposed cycle, the relative reactivity for *para*-substituted benzyl alcohols was calculated ($X = \text{F}, \text{Cl}, \text{CF}_3, \text{Me}, \text{SMe}, \text{OMe}$ and NMe_2) based on the energetic span model (Equation 1.24) and plotted versus σ^+ (Figure 1.19). It should be noted that it was possible to obtain a good correlation only when using gas-phase and solvation energies .

$$\lg \left(\frac{k_X}{k_H} \right) = \frac{\delta E_H - \delta E_X}{2.303RT} \quad (1.24)$$

As can be seen, points from two non-polar substituents (H and Me) do not fit with the overall good correlation. This could be due to the inaccuracy of the solvation model. Having excluded these two points from the correlation, almost identical values of ρ were obtained with the gas-phase and solvation energies: $\rho_{\text{solv}} = -0.73$ and $\rho_{\text{gas phase}} = -0.68$. These values are lower than the experimental one ($\rho = -0.15$) but they have the same sign which indicates

1.3 Computational Study

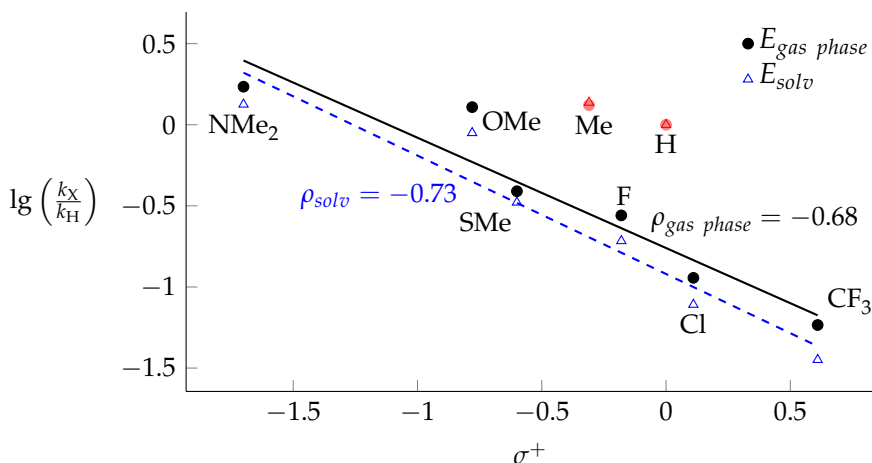


Figure 1.19: Hammett plot with calculated gas-phase and solvation energies. Red points were excluded from the linear regression.

the same trend in reactivity: substrates with electron-donating substituents are more reactive than those with electron-withdrawing substituents.

1.3.5 Theoretical Kinetic Isotope Effect

Another parameter to be compared with the experimental results is the kinetic isotope effect. As it was shown earlier, the KIE could be calculated based on zero-point energies (Equation 1.13 in Section 1.1.4). For these calculations the energetic span model was used again.

First, the calculations for deuterated analogs of the compounds used in the theoretical study were carried out, namely PhCD₂OD and EtND₂. The energetic span for the cycle with the compounds was $\delta G_{\text{tot}}^{\text{D}} = 142.3 \text{ kJ}\cdot\text{mol}^{-1}$ which resulted in a TOF of $1.4 \times 10^{-2} \text{ h}^{-1}$. Calculating the KIE as a ratio of the TOFs of the two cycles yielded a value of 3.78 (Equation 1.25) which was significantly higher than the experimental value of 2.29 ± 0.15 .

$$\text{KIE} = \frac{\text{TOF}_{\text{H}}}{\text{TOF}_{\text{D}}} = 3.78 \quad (1.25)$$

When using the zero-point energy of TDI as ZPE_{react} and TDTS as ZPE_{TS} in Equation 1.13, a much better value of 2.80 (Equation 1.26) was obtained.

$$\text{KIE} = \exp\left(\frac{\Delta\text{ZPE}_{\text{react}} - \Delta\text{ZPE}_{\text{TS}}}{RT}\right) = 2.80 \quad (1.26)$$

Next, PhCD₂OD was replaced in the calculations with C₂D₅OD which more resembled C₄D₉OD used in the experimental study. Ethanol was preferred over butanol to make the calculations faster and to eliminate discrepancy in energies due to the different conformations of butanol. For these compounds we obtain a KIE of 3.30 based on turnover frequencies and 1.99 based on ZPEs. This replacement showed that the substituent on the α carbon atom of the alcohol did have a profound influence on the calculated KIE value. More importantly, it allowed us to obtain the KIE value which was very close to the experimental one. This result provided further support to the proposed catalytic cycle.

1.3.6 Summary of the Theoretical Study

In summary, during the theoretical study the following was calculated:

1. Determined that an amine is a permanent ligand on the ruthenium atom.
2. Found that two hydride ligands are in the *trans*-orientation in the species involved in the reaction.
3. Proposed a catalytic cycle for the amidation reaction and determined its energy profile.
4. Based on the proposed cycle calculated ρ values for the reaction which have the same sign as the experimental one.
5. Obtained a value of the kinetic isotope effect which is in good agreement with the experimental one.

1.3.7 Computational Details

All calculations have been performed in Jaguar⁷⁶ using the M06 or B3LYP functionals in combination with the LACVP* basis set.⁷⁷

All structures were optimized in gas phase, and then the single point solvation energy was calculated for the optimized structures using standard Poisson-Boltzmann solver with parameters suitable for benzene as the solvent (dielectric constant: epsout = 2.284, probe radius: radprb = 2.600). Gibbs free energies were obtained from the vibrational frequency calculations for the gas phase geometries at 298 K and 383 K. All transition states were characterized by the presence of one imaginary vibrational frequency.

⁷⁶ Jaguar, version 7.8, Schrödinger, LLC, New York, NY, 2011.

⁷⁷HAY, P. J.; WADT, W. R. *J. Chem. Phys.* **1985**, *82*, 270–283.

1.4 Conclusions

The ruthenium-catalyzed coupling of a primary alcohol with an amine to give an amide was studied by means of experimental and theoretical methods. The Hammett study revealed that a small positive charge is formed at the benzylic position in the transition state on the turnover-determining step. The small value indicates that the rate of the reaction is not determined by a single elementary step but rather two steps with opposite electronic character both influence the reaction rate. Based on hydrogen–deuterium scrambling we proposed that ruthenium–dihydride species are involved in the catalytic cycle. The kinetic isotope effect was experimentally determined to be 2.29 ± 0.15 , which suggested that breakage of the C–H bond is not the rate-determining step, but that it is one of several slow steps in the catalytic cycle.

These experimental results were supported by the characterization of a plausible catalytic cycle by using DFT/MO6 calculations. Both *cis*-dihydride and *trans*-dihydride intermediates were considered, but when the theoretical turnover frequencies were obtained from the calculated energies, it was found that only the *trans*-dihydride pathway was in agreement with the experimentally determined TOFs.

This study yielded a working model of the amidation reaction which would be further used for *in silico* search for better ligands.

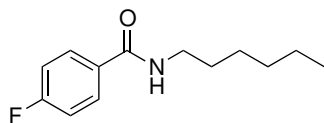
1.5 Experimental Part

General Experimental Methods

All chemicals were obtained from Aldrich and used without further purification. Complexes **1**,¹ **1-I**,¹⁹ (4-(dimethylamino)-phenyl)-methanol **6g**,⁷⁸ 1,1-dideutero-2-phenylethanol (**7-d**₂) were synthesized according to the reported procedures. Complex **10** was synthesized similarly to **1** with the only difference that [RuCl₂(*p*-cymene)]₂ (**3**) was replaced with [RuCl₂(benzene)]₂,⁷⁹ BnND₂ was synthesized by the reaction of BnNH₂ with an excess of D₂O. Toluene was distilled from sodium and benzophenone under an argon atmosphere. All ¹H, ¹³C and ¹⁹F-NMR spectra were recorded on a Varian Mercury 300 instrument (frequencies for ¹H, ¹³C and ¹⁹F are 300 MHz, 75 MHz and 282 MHz, respectively). ³¹P-NMR spectra were recorded on a Varian Unity Inova 500 MHz spectrometer equipped with a 5 mm probe with residual solvent signals as reference. CDCl₃ was used as a solvent for all NMR measurements. Chemical shifts are listed in ppm. IR spectra were obtained on a Bruker alpha-P spectrometer. Column chromatography separations were carried out on silica gel (220–440 mesh). HRMS data were obtained using ultra high performance liquid chromatography-high resolution mass spectrometry (UHPLC-HRMS) on a maXis G3 quadrupole time of flight mass spectrometer (Bruker Daltonics, Bremen) equipped with an electrospray (ESI) source. Reaction kinetics was followed by withdrawing samples from the reaction mixture after certain periods and analyzing them on a Shimadzu GCMS-QP2012S instrument equipped with an Equity-5 column (30 m × 0.25 mm × 0.25 μm) with nonane as the internal standard.

Characterization Data

N-Hexyl 4-fluorobenzamide **11c**



¹H-NMR: δ 0.83–0.96 (m, 3 H), 1.24–1.45 (m, 6 H), 1.54–1.68 (m, 2 H), 3.37–3.49 (m, 2 H), 6.09 (br. s., 1 H), 7.05–7.15 (m, 2 H), 7.72–7.81 (m, 2 H). ¹³C-NMR:

¹NORDSTRØM, L. U.; VOGT, H.; MADSEN, R. J. *Am. Chem. Soc.* **2008**, *130*, 17672–17673.

¹⁹DAM, J. H.; OSZTROVSZKY, G.; NORDSTRØM, L. U.; MADSEN, R. *Chem. Eur. J.* **2010**, *16*, 6820–6827.

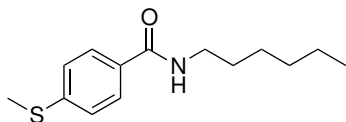
⁷⁸CHAIKIN, S. W.; BROWN, W. G. J. *Am. Chem. Soc.* **1949**, *71*, 122–125.

⁷⁹BENNETT, M. A.; SMITH, A. K. J. *Chem. Soc., Dalton Trans.* **1974**, 233–241.

1.5 Experimental Part

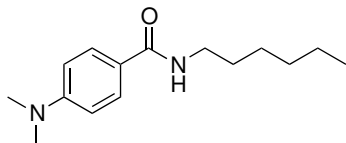
δ 14.2, 22.7, 26.8, 29.8, 31.6, 40.3, 115.5, 115.8, 129.2, 129.3, 166.6. $^{19}\text{F-NMR}$: δ -109.03. **IR** (neat, cm^{-1}) 3329 (N-H), 2962, 2929, 2873, 2853, 1632 (C=O), 1600, 1540, 1497, 1223, 852. **HRMS** (m/z) calcd for $[\text{C}_{13}\text{H}_{19}\text{FNO}+\text{H}]^+$ 224.1451, found 224.1445.

N-Hexyl 4-methylthiobenzamide **11f**



$^1\text{H-NMR}$: δ 0.84–0.94 (m, 3 H), 1.24–1.43 (m, 6 H), 1.54–1.66 (m, 2 H), 2.50 (s, 3 H), 3.39–3.47 (m, 2 H), 6.09 (br. s., 1 H), 7.22–7.27 (m, 2 H), 7.64–7.70 (m, 2 H). $^{13}\text{C-NMR}$: δ 14.3, 15.3, 22.8, 26.9, 29.9, 31.7, 40.3, 125.7, 127.4, 131.2, 143.3, 167.1. **IR** (neat, cm^{-1}) 3329 (N-H), 2957, 2936, 2915, 2870, 2852, 1627 (C=O), 1597, 1485, 1437, 1313, 1270, 1092, 755. **HRMS** (m/z) calcd for $[\text{C}_{14}\text{H}_{22}\text{NOS}+\text{H}]^+$ 252.1422, found 252.1420.

N-Hexyl 4-dimethylaminobenzamide **11g**



$^1\text{H-NMR}$: δ 0.83–0.93 (m, 3 H), 1.23–1.42 (m, 6 H), 1.51–1.64 (m, 2 H), 3.00 (s, 6 H), 1.51–1.64 (m, 2 H), 6.09 (br. s., 1 H), 7.05–7.15 (m, 2 H), 7.72–7.81 (m, 2 H). $^{13}\text{C-NMR}$: δ 14.2, 22.7, 26.8, 29.8, 31.6, 40.3, 115.5, 115.8, 129.2, 129.3, 166.6. $^{19}\text{F-NMR}$: δ -109.03. **IR** (neat, cm^{-1}) 3329 (N-H), 2962, 2929, 2873, 2853, 1632 (C=O), 1600, 1540, 1497, 1223, 852. **HRMS** (m/z) calcd for $[\text{C}_{15}\text{H}_{25}\text{N}_2\text{O}+\text{H}]^+$ 249.1967, found 249.1959.

NMR data for compounds *N*-hexylbenzamide (**11a**), *N*-hexyl 4-(trifluoromethyl)benzamide (**11b**), *N*-hexyl 4-methylbenzamide (**11d**), *N*-hexyl 4-methoxybenzamide (**11e**), *N*-hexyl 2-phenylacetamide (**12**), *N*-benzylbutyramide (**13**) are in accordance with literature values.^{1,13,80,81}

¹NORDSTRØM, L. U.; VOGT, H.; MADSEN, R. *J. Am. Chem. Soc.* **2008**, *130*, 17672–17673.

¹³ALLEN, C. L.; DAVULCU, S.; WILLIAMS, J. M. *J. Org. Lett.* **2010**, *12*, 5096–5099.

⁸⁰JO, Y.; JU, J.; CHOE, J.; SONG, K. H.; LEE, S. *J. Org. Chem.* **2009**, *74*, 6358–6361.

⁸¹ISHIHARA, K.; YANO, T. *Org. Lett.* **2004**, *6*, 1983–1986.

2 *In Silico* Screening for More Effective Carbene Ligands for the Amidation Reaction

IN THE PREVIOUS CHAPTER the mechanism of the amidation reaction was determined and the computational model of the catalytic cycle was created. The next step in improving the reactivity of the catalytic system is to screen different ligands attached to the ruthenium center. A combination of the theoretical and experimental methods was chosen for achieving this goal. It was intended to vary carbene ligands *in silico* and based on the energetic span theory select those which could increase the activity of the catalyst. This approach will save time and resources by eliminating the need to synthesize many ruthenium complexes just to find that they are less active.

2.1 Introduction

It was previously shown that electronic properties on the *N*-heterocyclic carbene ligand had a profound influence on the reactivity of the ruthenium complexes in the amidation reaction.^{1,82} Several carbenes were tested and it was found that the catalysts with imidazole-based carbenes performed best and gave rise to very high yields. On the contrary, complexes with the saturated counterpart **23a**, the triazole-based carbene **23b**, the dimethyl substituted carbene **23c** or the benzene-fused **23d** performed poorly in the reaction (Figure 2.1). These observations suggested that electron-donating ligands should increase the reactivity of the catalyst.

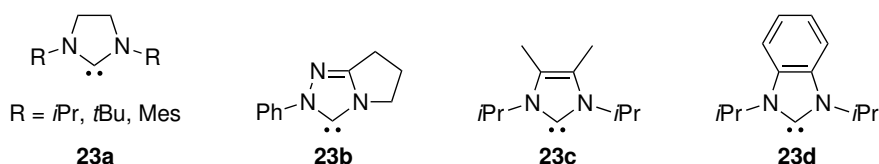


Figure 2.1: Carbene ligands for the ruthenium complexes used in the amidation reaction.

In 1977, Tolman proposed to use the vibrational frequency of the CO bond in the complexes $\text{Ni}(\text{CO})_3\text{L}$ (L is a phosphine) to quantify the ability of various phosphines to donate (or withdraw) electron density to (or from) a metal center.⁸³ It was observed that the better the phosphine is as an electron donor, the lower the measured vibrational frequency was for the corresponding complex. The explanation is that the electron density is donated back from the metal center to the anti-bonding π^* orbital of CO making the C–O triple bond weaker, and consequently, lowering its vibrational frequency. Nowadays, this parameter is known as the Tolman electronic parameter (TEP).

The TEP is utilized to quantify and compare electronic and steric properties not only of phosphines but also of other classes of ligands such as NHCs.⁸⁴ With the help of modern computational methods it is possible to obtain the TEP for the complexes which are not easily available or do not exist. There have been published several theoretical investigations focused on the TEP

¹NORDSTRØM, L. U.; VOGT, H.; MADSEN, R. *J. Am. Chem. Soc.* **2008**, *130*, 17672–17673.

⁸²NORDSTRØM, L. U. *Methods for Transition Metal Catalyzed C–N Bond Formation and Organocatalytic Allylation of Aldehydes*, PhD Thesis, Technical University of Denmark, 2008.

⁸³TOLMAN, C. *Chem. Rev.* **1977**, *77*, 313–348.

⁸⁴KELLY III, R. A.; CLAVIER, H.; GIUDICE, S.; SCOTT, N. M.; STEVENS, E. D.; BORDNER, J.; SAMARDJIEV, I.; HOFF, C. D.; CAVALLO, L.; NOLAN, S. P. *Organometallics* **2008**, *27*, 202–210.

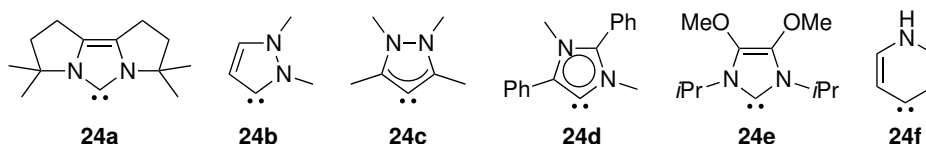


Figure 2.2: Carbenes selected for the screening.

for carbenes including NHCs.^{85–87} It was shown that the ligands **23a–d** had a larger TEP than *i*Pr (the carbene ligand of compound **1**)⁸⁶ which supports the idea that electron-donating properties of the carbene ligands determine the reactivity of the catalyst in the amidation reaction.

2.2 Search for More Effective Ligands

The carbenes from the paper by Gusev⁸⁶ with the TEP lower than the value for *i*Pr were selected for the screening. To further refine the selection, carbenes with bulky substituents next to the carbon atom attached to ruthenium were excluded. The ligands listed in Figure 2.2 were chosen for the initial screening. The energetic span model was used for comparing the results of the calculations. To do this, the *i*Pr ligand was substituted in the TDI (**15b**) and TDTS (**TS2b**) of the proposed cycle and after the optimization the energetic span was calculated.

To test this method the energetic span was calculated for the species with carbene **23a** (R = *i*Pr) which was experimentally shown to be a worse ligand for the amidation reaction than *i*Pr. The energetic span for ligand **23a** was 127.3 kJ·mol⁻¹ which is 8.3 kJ·mol⁻¹ larger than for *i*Pr which was an indication that the reaction should be slower. This result was in line with the observed reactivity, hence the energetic span model can be employed for the comparison.

Table 2.1 shows that four out of six selected ligands lower the energetic span of the amidation reaction. However, as it can be seen from the ratio of the turnover frequencies derived from the energetic spans, only three of these carbenes (**24b**, **24e** and **24f**) significantly increase the rate of the reaction. Moreover, it was previously shown that with carbene **24b** the yields of the amidation reaction after 3 and 24 hours were lower than with the ruthenium

⁸⁵GUSEV, D. G. *Organometallics* **2009**, *28*, 763–770.

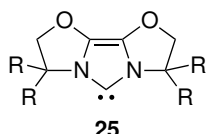
⁸⁶GUSEV, D. G. *Organometallics* **2009**, *28*, 6458–6461.

⁸⁷TONNER, R.; FRENKING, G. *Organometallics* **2009**, *28*, 3901–3905.

Table 2.1: Calculated Energetic Spans for Ruthenium Complexes with Carbenes **24a–24e**.

Carbene	24a	24b	24c	24d	24e	24f	IiPr
$\delta G/\text{kJ}\cdot\text{mol}^{-1}$	295.4	106.1	113.7	141.0	109.2	101.7	119.0
$\frac{TOF_{carb}}{TOF_{iPr}}$	$8.7\cdot 10^{-25}$	58.2	5.3	$1\cdot 10^{-3}$	21.9	229.4	1

catalyst **1**.⁷⁴ Probably, it was due to a lower stability of the complex with this ligand. As a consequence, only two carbenes (**24e**, **24f**) were studied further.

**25**

a: R = H
b: R = Me

Figure 2.3: Structure of IBiox carbene.

A literature search revealed that no ruthenium complexes with either of the two selected carbenes were known, and moreover, no transition-metal-complexes with the dimethoxy carbene **24e** have ever been synthesized. Dimethoxyimidazolium salts which could be used as a precursor for these complexes has not been reported either. The only known type of carbenes with two oxygen atoms at the double bond of an NHC is carbenes derived from bisoxazolines (IBiox, **25**, Figure 2.3) which were reported by Glorius and coworkers as effective ligands for palladium-catalyzed cross-coupling reactions.^{88,89} It was decided to synthesize analogs of compound **1** with the IBiox ligand and test them in the amidation reaction.

All the reported IBiox carbenes have substituents at the 3 and the 7 positions (R-groups in Figure 2.3) which is undesirable for the amidation reaction. Because of this it was decided to synthesize, first, previously unknown non-substituted IBiox carbene **25a**. Following the procedure by Butula and Karlović⁹⁰ bis(oxazoline) **29a** was obtained from aminoalcohol **26a** in 48% yield over 3 steps (Scheme 2.1). Cyclization with chloromethyl pivalate and silver triflate (procedure i)⁸⁸ did not lead to imidazolium salt **30a** neither did the reaction with chloromethyl ethyl ether (procedure ii).⁹¹

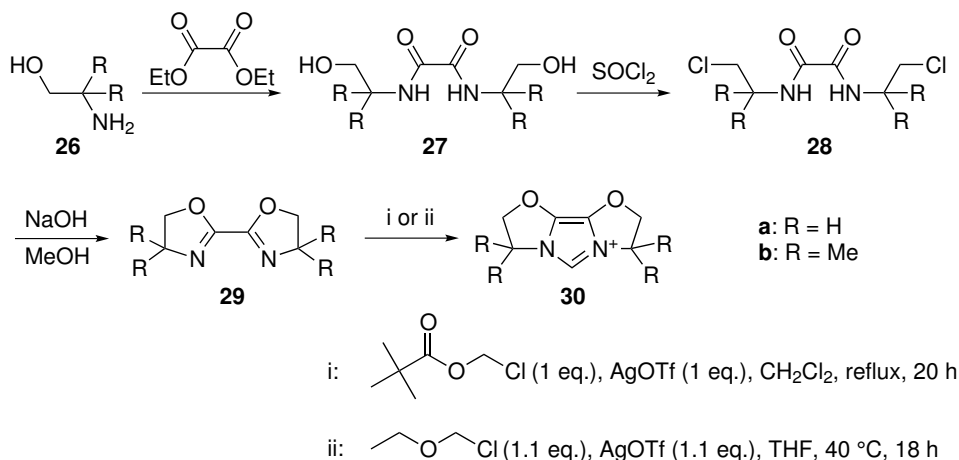
⁷⁴DAM, J. H. *Organometallic Reactions: Development, Mechanistic Studies and Synthetic Applications*, PhD Thesis, Technical University of Denmark, 2009, pp 87–110.

⁸⁸ALTENHOFF, G.; GODDARD, R.; LEHMANN, C. W.; GLORIUS, F. *Angew. Chem. Int. Ed.* **2003**, *42*, 3690–3693.

⁸⁹ALTENHOFF, G.; GODDARD, R.; LEHMANN, C. W.; GLORIUS, F. *J. Am. Chem. Soc.* **2004**, *126*, 15195–15201.

⁹⁰BUTULA, I.; KARLOVIĆ, G. *Liebigs Ann. Chem.* **1976**, 1455–1464.

⁹¹LEVY, J.-N.; LATHAM, C. M.; ROISIN, L.; KANDZIORA, N.; DI FRUSCIA, P.; WHITE, A. J. P.;



Scheme 2.1: Synthesis of IBiox precursors.

To save time and instead of trying other cyclization conditions it was decided to synthesize tetramethyl bis(oxazoline) **30b** following the reported procedure.⁸⁸ Triflate salt **30b** was obtained in 33% yield over four steps. This salt reacted with NaH in THF to give a solution of free carbene **25b** which was then mixed with ruthenium dimer [RuCl₂(*p*-cymene)]₂ (**3**) but this led to decomposition of the reactants and no desired complex Ru(IBioxMe)Cl₂(*p*-cymene) **31** was isolated (Figure 2.4). Performing the amidation reaction in a way that the active catalyst was formed *in situ* by refluxing salt **30b** with [RuCl₂(*p*-cymene)]₂, KO^{*t*}Bu and PCy₃·HBF₄ for 45 min in toluene followed by addition of a solution of benzylamine and 2-phenylethanol did not yield the corresponding amide after 24 h. Because of these experimental obstacles further attempts to obtain complex **31** were stopped.

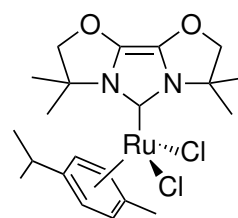


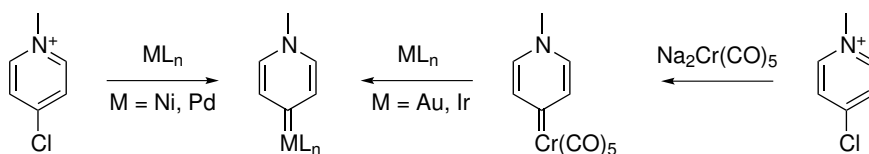
Figure 2.4: Structure of complex **31**.

The next carbene in the investigation was a derivative of pyridilidene. There have been reported several methods for synthesis of metal complexes featuring this kind of ligands (Scheme 2.2). One of them is a direct oxidative insertion of low-valent metal complexes into a C–Cl bond of chloropyridinium salts.

WOODWARD, S.; FUCHTER, M. J. *Org. Biomol. Chem.* **2012**, *10*, 512–515.

⁸⁸ALTENHOFF, G.; GODDARD, R.; LEHMANN, C. W.; GLORIUS, F. *Angew. Chem. Int. Ed.* **2003**, *42*, 3690–3693.

2.2 Search for More Effective Ligands



Scheme 2.2: Methods for synthesis of pyridilidene-substituted complexes.

This approach was successfully applied for synthesizing palladium catalysts for various cross-coupling reactions.^{92,93} Another method is a carbene transfer from a chromium-pentacarbonyl-carbene complex to different metals such as gold or rhodium. This is more versatile approach in comparison to the oxidative addition because it allows to obtain complexes without a chlorine atom attached to a metal center.⁹⁴

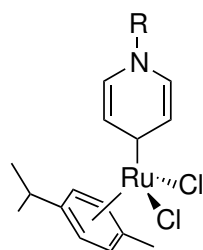


Figure 2.5: Structure of complex **32**.

Unfortunately, neither of these approaches could be used to obtain ruthenium catalyst **32** (Figure 2.5). There were no suitable ruthenium complexes which would insert into a C–Cl bond of chloropyridinium salts to give **32** while the reported yields over the two steps for the second method were inappropriately low (approximately 3%). Because of this we directed our eyes towards the methods for synthesis of NHCs and chose the one which employed decarboxylation of imidazolium carboxylates.^{95,96} This allowed to get the corresponding transition metal (including ruthenium) complexes in high yield under mild conditions. Before doing any experiments the formation of compound **32** from the corresponding betaine was studied computationally.

For comparison, the formation energy of complex **1** from imidazolium carboxylate **33** was calculated along with the formation energy of complex **32** (Scheme 2.3). The calculations showed that the formation of free carbenes *i*Pr and **24f** with a loss of CO₂ was an endothermic process. The formation

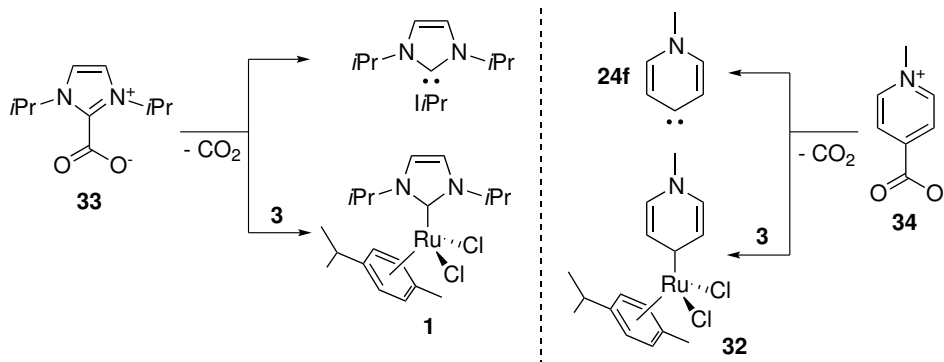
⁹²RAUBENHEIMER, H. G.; CRONJE, S. *Dalton Trans.* **2008**, 1265–1272.

⁹³SCHUSTER, O.; YANG, L.; RAUBENHEIMER, H. G.; ALBRECHT, M. *Chem. Rev.* **2009**, *109*, 3445–3478.

⁹⁴STRASSER, C. E.; STANDER-GROBLER, E.; SCHUSTER, O.; CRONJE, S.; RAUBENHEIMER, H. G. *Eur. J. Inorg. Chem.* **2009**, 1905–1912.

⁹⁵VOUTCHKOVA, A. M.; APPELHANS, L. N.; CHIANESE, A. R.; CRABTREE, R. H. J. *Am. Chem. Soc.* **2005**, *127*, 17624–17625.

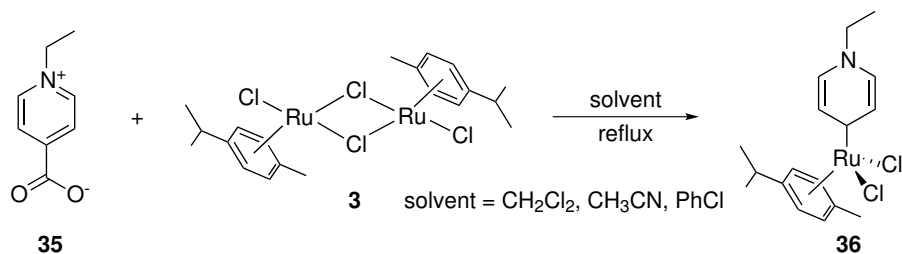
⁹⁶DRÖGE, T.; GLORIUS, F. *Angew. Chem. Int. Ed.* **2010**, *49*, 6940–6952.



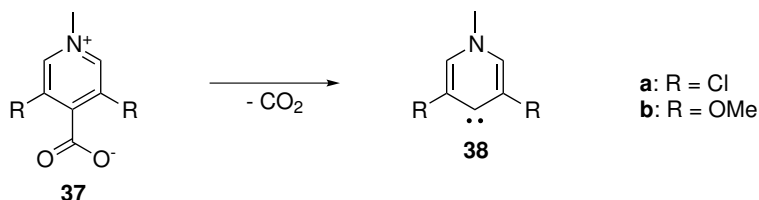
Scheme 2.3: Formation of the ruthenium complexes from the corresponding betaines.

energy for the former was $37.8 \text{ kJ}\cdot\text{mol}^{-1}$ whereas for the latter this value was $121.4 \text{ kJ}\cdot\text{mol}^{-1}$ indicating that **24f** was less stable, and consequently, more reactive. At the same time, the reactions between ruthenium dimer **3** and betaines **33** and **34** to give complexes **1** and **32** were highly exothermic with the energy gain of $117.1 \text{ kJ}\cdot\text{mol}^{-1}$ and $165.4 \text{ kJ}\cdot\text{mol}^{-1}$, correspondingly.

The calculations gave analogous results for these systems which made it possible to expect the similar reactivity in the real-world experiments. Refluxing ruthenium dimer **3** with *N*-ethylpyridinium carboxylate **35** in dichloromethane, however, did not yield the desired compound **36** (Scheme 2.4). This was probably due to the low boiling point of CH_2Cl_2 . The same reaction performed in acetonitrile gave an inseparable mixture of the initial complex **3** and, most likely, compound **36**. It was not possible to determine the structure of the second product based on NMR spectra of the mixture. In spite of this fact, the mixture was used as a catalyst in the amidation reaction between benzylamine and 2-phenylethanol which gave amide in 38% yield after 24 h. Inspired by this result



Scheme 2.4: Synthesis of pyridilidene complex **36**.

Table 2.2: Energy of CO₂ dissociation from various betaines.

R	Ad	Cl	Cy	F	<i>i</i> Pr	Me	OMe	Ph	<i>t</i> Bu
$E_{\text{diss}}/\text{kJ}\cdot\text{mol}^{-1}$	53.6	-53.4	73.5	-51.5	21.3	42.7	-39.7	58.0	-11.3

we undertook further attempts to purify the mixture of the complexes and isolate compound **36**. Varying solvents and their ratio for column chromatography did not result in better separation of the compounds. Performing the reaction between betaine **35** and ruthenium dimer **3** at higher temperature in boiling chlorobenzene did not afford the desired complex in a more pure form either.

One of the possible reasons why all these syntheses failed could be the high instability of the formed carbene **24f**. To find more stable pyridilidenes the dissociation of carbon dioxide from various substituted betaines to give carbenes was studied computationally (Table 2.2). The study showed that introduction of heteroatoms into the positions adjacent to the carbene center favored the dissociation reaction and stabilized the obtained carbene.

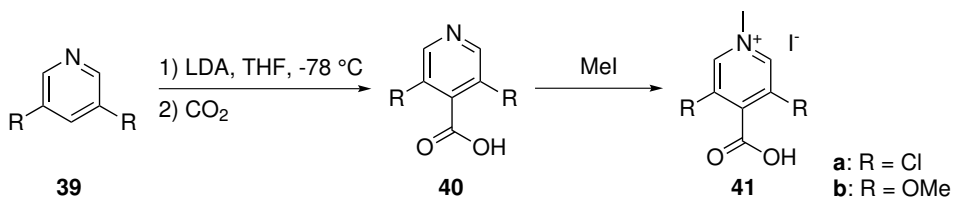
For the experimental study 3,5-dichloropyridine **39a** was chosen as a starting substrate because it could be used to synthesize both compounds **37a** and **37b**. Following the reported procedures^{97,98} hydroiodide **41a** was obtained in 32% yield over two steps (Scheme 2.5). This compound was reacted with ruthenium dimer **3** in the presence of 1 equivalent of KOH in refluxing dichloromethane, acetonitrile or chlorobenzene but neither of these reactions afforded desired ruthenium complex with carbene **38a**.

Next, it was attempted to synthesize the corresponding dimethoxy analog. Carboxylic acid **40b** was synthesized from 3,5-dichloropyridine **39a** in two steps: first, chlorine atoms were replaced with methoxy groups by the reaction with sodium and potassium methoxides to give 3,5-dimethoxypyridine **39b**.⁹⁹

⁹⁷MARZI, E.; BIGI, A.; SCHLOSSER, M. *Eur. J. Org. Chem.* **2001**, 1371–1376.

⁹⁸BUNCEL, E.; KEUM, S.-R. *Tetrahedron* **1983**, *39*, 1091–1101.

⁹⁹PHILLIPS, S. T.; REZAC, M.; ABEL, U.; KOSSENJANS, M.; BARTLETT, P. A. *J. Am. Chem. Soc.* **2002**, *124*, 58–66.



Scheme 2.5: Synthesis of *N*-methylpyridinium carboxylic acids.

The product of the first step was reacted further with LDA and CO₂ to give acid **40b** in 17% yield over two steps.

Unfortunately, at this point of the study it was decided to stop working on this project because of lack of time and it seemed it required much effort to get promising results. Moreover, at the same time another more successful project started and it was decided to focus entirely on that. The next chapter discusses the new project in more detail.

2.3 Conclusion

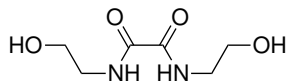
Carbene ligands for the catalyst in the amidation reaction were studied computationally. The initial selection of the ligands was done by using the Tolman electronic parameter and then the energetic span was calculated for the reactions catalyzed by the complexes with the chosen carbenes. Several ligands gave substantially lower energetic span than the carbene used in the experimental mechanistic investigation and they were selected for the more thorough study. It demonstrated that NHC with two oxygen atoms attached to the double bond of the carbene as well as a pyridilidene ligand could dramatically improve the reactivity of the ruthenium catalyst in the amidation reaction.

Approaches for synthesizing analogs of these carbenes were proposed and tested but none of them afforded pure ruthenium complexes with new ligands. However, it was shown that the reaction catalyzed by impure complex with a pyridilidene ligand gave the amide in 38% yield.

Even though only several ligands were screened computationally the study yielded a working catalyst for the amidation reaction. It indicated that *in silico* ligand screening might be used for catalyst optimization if it is combined with a more comprehensive experimental study.

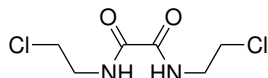
2.4 Experimental Section

N,N'-bis(2-hydroxyethyl)oxalamide **27a**



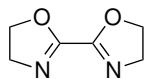
The experimental procedure was adapted from the work of Butula and Karlović.⁹⁰ Diethyloxalate (5.85 g, 40 mmol) was dissolved in toluene (40 mL) and 2-aminoethanol (4.89 g, 80 mmol) was slowly added. Upon the addition a white precipitate was forming. A stirring bar was added, a condenser attached and the flask was placed into an oil bath ($T = 80\text{ }^{\circ}\text{C}$). After 1.5 h the mixture was cooled to room temperature, solvent was decanted off and a yellowish precipitate was recrystallized from ethanol (approx. 100 mL) to give white precipitate. It was filtered, washed with cold ethanol ($2 \times 10\text{ mL}$) and dried *in vacuo*. Yield 6.2 g (88%). After some time additional 550 mg precipitated from the mother liquor. Overall yield 6.75 g (96%). $^1\text{H-NMR}$ (300 MHz, $\text{DMSO-}d_6$): δ 3.20 (q, 4 H, $^3J_{\text{H-H}} = 6.2\text{ Hz}$), 3.44 (t, 4 H, $^3J_{\text{H-H}} = 6.2\text{ Hz}$), 4.74, (br. s., 2 H), 8.55–8.59 (m, 2 H).

N,N'-bis(2-chloroethyl)oxalamide **28a**



The experimental procedure was adapted from the work of Butula and Karlović.⁹⁰ Thionyl chloride (10 mL, 138 mmol) was added dropwise to the stirring suspension of compound **27a** (4 g, 23 mmol) in toluene (25 mL). A condenser was attached and the flask was placed into an oil bath ($T = 120\text{ }^{\circ}\text{C}$). After 2 h of reflux the reaction mixture was cooled to room temperature and the white precipitate was filtered off, washed with toluene ($2 \times 10\text{ mL}$) and recrystallized from ethyl acetate to give a white crystalline solid. Yield 4.37 g (90%). $^1\text{H-NMR}$ (300 MHz, $\text{DMSO-}d_6$): δ 3.48 (q, 4 H, $^3J_{\text{H-H}} = 6.3\text{ Hz}$), 3.69 (t, 4 H, $^3J_{\text{H-H}} = 6.3\text{ Hz}$), 8.95–8.99 (m, 2 H)

4,4',5,5'-tetrahydro-2,2'-bioxazole **29a**

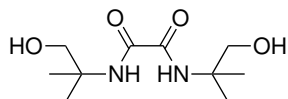


The experimental procedure was adapted from the work of Butula and Karlović.⁹⁰ Solution of NaOH (800 mg, 20 mmol) in MeOH (20 mL) was added to a flask

⁹⁰BUTULA, I.; KARLOVIĆ, G. *Liebigs Ann. Chem.* **1976**, 1455–1464.

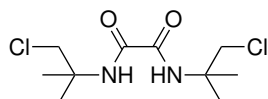
with compound **28a** (2.13 g, 10 mmol) and a stirring bar. A condenser was attached and the flask was placed into an oil bath ($T = 90\text{ }^{\circ}\text{C}$). After 1 h of reflux the reaction mixture was cooled to room temperature and a white precipitate was filtered off. The filtrate was evaporated *in vacuo* and the resulting sticky substance was recrystallized from MeOH to give a white precipitate. Yield 780 mg (56%). $^1\text{H-NMR}$ (300 MHz, $\text{DMSO-}d_6$): δ 3.92 (t, 4 H, $^3J_{\text{H-H}} = 9.6\text{ Hz}$), 4.34 (t, 4 H, $^3J_{\text{H-H}} = 9.6\text{ Hz}$).

N,N'-bis(1-hydroxy-2-methylpropan-2-yl)oxalamide **27b**



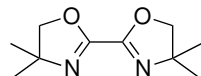
Was synthesized analogously to **27a** where 2-amino-2-methylpropan-1-ol (7.12 g, 80 mmol) was used instead of 2-aminoethanol. Yield 8.8 g (95%). The compound was used for the next step without characterization.

N,N'-bis(1-chloro-2-methylpropan-2-yl)oxalamide **28b**



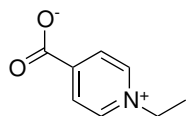
Was synthesized analogously to **28a** where compound **27b** was used instead of **27**. Yield 5.82 g (94%). $^1\text{H-NMR}$ (300 MHz, CDCl_3): δ 1.46 (s, 12 H), 3.79 (s, 4 H), 7.42 (br. s., 2 H).

4,4',4'-tetramethyl-4,4',5,5'-tetrahydro-2,2'-bioxazole **29b**



Was synthesized analogously to **29a** where compound **28b** was used instead of **28a**. Yield 840 mg (43%). $^1\text{H-NMR}$ (300 MHz, CDCl_3): δ 1.35 (s, 12 H), 4.11 (s, 4 H).

1-ethylpyridin-1-ium-4-carboxylate **35**



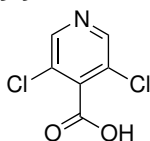
The experimental procedure was adapted from the work of Kosover and Patton.¹⁰⁰ A chromatography column (diameter 2.5 cm) was filled (10 cm) with Dowex-1 resin (Cl-form). It was washed with 1 M solution of NaOH (500 mL)

¹⁰⁰KOSOWER, E.; PATTON, J. J. *Org. Chem.* **1961**, *26*, 1318–1319.

2.4 Experimental Section

and then with distilled water until neutral pH. 1-Ethyl-4-(methoxycarbonyl)pyridin-1-ium iodide (3 g, 10 mmol) was dissolved in water and the solution was poured onto the column. It was washed with water and all fractions were collected and dried on a freeze-dryer to afford a white crystalline precipitate mixed with small amounts of a yellow liquid. This liquid was removed with a pipette and the white precipitate was washed with ethanol and dried *in vacuo*. Yield 1.39 g (92%). ¹H-NMR (300 MHz, D₂O): δ 1.62 (t, 3 H, ³J_{H-H} = 6.7 Hz), 4.65 (q, 2 H, ³J_{H-H} = 6.7 Hz), 8.23, (d, 2 H, J_{H-H} = 5.0 Hz), 8.89, (d, 2 H, J_{H-H} = 5.0 Hz).

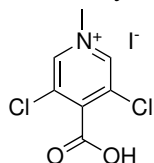
3,5-dichloroisonicotinic acid **40a**



The experimental procedure was adapted from the work of Marzi *et al.*⁹⁷ A 50 mL three-neck round-bottom flask was charged with 3,5-dichloropyridine **39a** (2 g, 13.5 mmol) and a stirring bar. A condenser and a thermometer were attached to the flask and the third neck was closed with a septum. The flask was evacuated and refilled with argon three times. THF (15 mL) was added and after compound **39a** had dissolved the flask was placed into an acetone/dry ice bath ($T = -70^\circ\text{C}$). After 10 min LDA (6.7 mL of a 2 M solution in THF, 13.5 mmol) was slowly added via syringe (within approx. 15 min). During the addition the color of the reaction mixture changed to red-orange. After 2 h at -70°C the reaction mixture was poured onto freshly crashed dry ice. When the mixture warmed to room temperature water (100 mL) was added and the aqueous layer was separated and washed with ether (2×50 mL). The aqueous solution was acidified to pH 1 and extracted with CH₂Cl₂ (3×50 mL). Organic fractions were evaporated and the residue was recrystallized from ethanol to give a yellow powder. Yield 1.03 g (40%). ¹H-NMR (300 MHz, CDCl₃): δ 9.72.

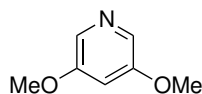
⁹⁷MARZI, E.; BIGI, A.; SCHLOSSER, M. *Eur. J. Org. Chem.* **2001**, 1371–1376.

4-carboxy-3,5-dichloro-1-methylpyridin-1-ium iodide **41a**



The experimental procedure was adapted from the work of Buncel and Keum.⁹⁸ Compound **40a** (1 g, 5.4 mmol) was mixed with CH₃I (2.68 g, 18.9 mmol) in a round-bottom flask. The flask was covered with aluminum foil and placed in an ice/water bath. After 4 days a yellow precipitate was filtered and washed with small amounts of cold ether. The product was dried *in vacuo*. Yield 1.43 g (80%). ¹H-NMR (300 MHz, DMSO): δ 4.32 (s, 3 H), 9.35 (s, 2 H).

3,5-dimethoxypyridine



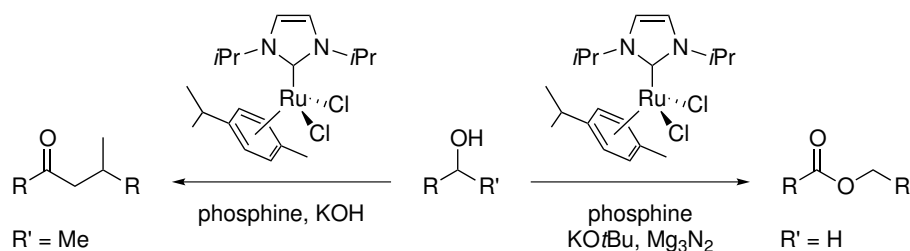
The experimental procedure was adapted from the work of Phillips *et al.*⁹⁹ NaOMe was synthesized by dissolving sodium (3 g, 130 mmol) in methanol (150 mL) and then the solvent was evaporated *in vacuo* (after the evaporation had been finished, the rotary evaporator was filled with argon instead of air). 3,5-dichloropyridine **39a** (2 g, 13.5 mmol) was dissolved in DMF (60 mL) and argon was bubbled through the solution for 1 h. NaOMe and a magnetic stirrer were added to the flask and it was placed in an oil bath ($T = 80\text{ }^{\circ}\text{C}$). During the reaction argon was bubbling through the solution. After 20 h KOMe (prepared similarly to NaOMe by dissolving potassium (0.7 g, 18 mmol) in methanol (25 mL)) was added and the reaction mixture was stirred for 1 additional day. Then, the mixture was poured into 150 mL of water. The aqueous phase was extracted with ether ($3 \times 70\text{ mL}$) and ethyl acetate ($2 \times 100\text{ mL}$). The combined organic fractions were dried with Na₂SO₄ and evaporated *in vacuo*. The residue was distilled *in vacuo* to give a bright-yellow liquid. Yield 2.57 g (55%). ¹H-NMR (300 MHz, CDCl₃): δ 3.83 (s, 6 H), 6.72 (t, 1 H, ³J_{H-H} = 2.6 Hz), 6.72 (d, 2 H, ³J_{H-H} = 2.6 Hz).

⁹⁸BUNCCEL, E.; KEUM, S.-R. *Tetrahedron* **1983**, *39*, 1091–1101.

⁹⁹PHILLIPS, S. T.; REZAC, M.; ABEL, U.; KOSSENJANS, M.; BARTLETT, P. A. *J. Am. Chem. Soc.* **2002**, *124*, 58–66.

3 Ruthenium–*N*-Heterocyclic Carbene Catalyzed Self-Coupling of Primary and Secondary Alcohols

THIS PART OF THE DISSERTATION discusses two ruthenium-catalyzed self-coupling reactions of primary and secondary alcohols (Scheme 3.1). It was previously reported that pentan-1-ol was fully converted into pentyl pentanoate upon reflux in mesitylene for 18 h.¹⁰¹ However, for benzylic alcohols the esterification was accompanied by significant decarbonylation of the intermediate aldehyde which was presumably caused by the high reaction temperature. Therefore, it was decided to reinvestigate the ester formation with complex **1** in an attempt to achieve the reaction at a lower temperature. During these studies a new dehydrogenative self-coupling of secondary alcohols was discovered which proceeded by alkylation in the β -position and dehydrogenation to the ketone.



Scheme 3.1: Ruthenium-catalyzed self-coupling of primary and secondary alcohols.

¹⁰¹SØLVHØJ, A.; MADSEN, R. *Organometallics* **2011**, *30*, 6044–6048.

3.1 Introduction

3.1.1 Ruthenium-Catalyzed Esterification Reactions

The amidation reaction discussed in the previous chapter is only one of the examples of a dehydrogenative coupling of alcohols with nucleophiles. An alcohol could also play the role of the second coupling partner if there are no other nucleophiles in the system, hence, transforming the reaction into a self-coupling which leads either to esters or to acetals depending on the conditions.

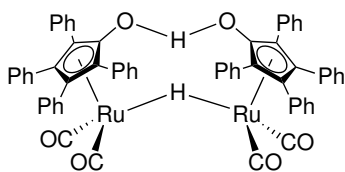


Figure 3.1: Structure of the Shvo catalyst.

The first works on the ruthenium-catalyzed esterification reaction was published in 1981.^{102,103} Blum *et al.* reported that in the presence of diphenylacetylene as a hydrogen scavenger, benzyl alcohol and pentan-1-ol were converted into the corresponding esters with a high yield. They proposed that diphenylacetylene not only traps hydrogen but also transforms $\text{Ru}_3(\text{CO})_{12}$ into an active species. Murahashi *et al.* claimed that $\text{RuH}_2(\text{PPh}_3)_4$ catalyzed formation of esters and lactones from the corresponding alcohols in the absence of any hydrogen scavengers in toluene at 180 °C. Several years later, Blum *et al.* proposed that based on thermodynamic parameters of the reaction ($\Delta H = 18.8 \text{ kcal/mol}$), it is impossible to form esters from primary alcohols in the absence of a hydrogen scavenger.¹⁰⁴ They also proposed that in the reaction reported by Murahashi in 1981, hydrogen gas was not liberated but was trapped by PPh_3 since H_2 formation was not proved in the paper. However, in 1985 they refuted their own propositions and reported the acceptorless self-coupling of primary alcohols catalyzed by the Shvo catalyst (Figure 3.1).¹⁰⁵ Two years later Murahashi and coworkers reported another examples of the acceptorless esterification catalyzed by $\text{RuH}_2(\text{PPh}_3)_4$ in non-polar solvents along with some mechanistic investigations.¹⁰⁶

These reactions were carried out with a catalytic loading of 2 mol% (based on a monomeric ruthenium species) in mesitylene at 180 °C (Murahashi)

¹⁰²BLUM, Y.; RESHEF, D.; SHVO, Y. *Tetrahedron Lett.* **1981**, 22, 1541–1544.

¹⁰³MURAHASHI, S.-I.; ITO, K.-I.; NAOTA, T.; MAEDA, Y. *Tetrahedron Lett.* **1981**, 22, 5327–5330.

¹⁰⁴BLUM, Y.; SHVO, Y. *J. Organomet. Chem.* **1984**, 263, 93–107.

¹⁰⁵BLUM, Y.; SHVO, Y. *J. Organomet. Chem.* **1985**, 282, C7–C10.

¹⁰⁶MURAHASHI, S.-I.; NAOTA, T.; ITO, K.; MAEDA, Y.; TAKI, H. *J. Org. Chem.* **1987**, 52, 4319–4327.

or under solvent-less conditions at various temperatures depending on the boiling point of an alcohol (Blum). Under these conditions aliphatic and aromatic alcohols were converted into the corresponding esters with high to excellent yields. In several cases aldehydes, acetals and ethers were also detected in low amounts (< 5%). Olefin bonds were hydrogenated under the reaction conditions to give saturated esters.

Only 1,4- and 1,5-diols could be transformed to lactones, whereas the reaction with other α,ω -diols afforded the corresponding polyester. Interestingly, in the presence of 1 equiv. of acetonitrile 1,5-pentandiol was self-coupled to give 5-hydroxypentyl 5-hydroxypentanoate as if it had only one OH-group.¹⁰⁶ This indicated that both oxygen atoms had to be coordinated to ruthenium in order to form a lactone what was impossible in the presence of CH_3CN because it was a better ligand than an OH group.

The cross-esterification with two different alcohols was also studied in the above-mentioned works. In the reaction between two primary alcohols no selectivity was observed and a statistical mixture of all four possible esters was formed. If a primary alcohol reacted with phenol or a secondary alcohol, then an ester from the self-coupling was formed as a major product and only traces of the corresponding cross-ester were detected.

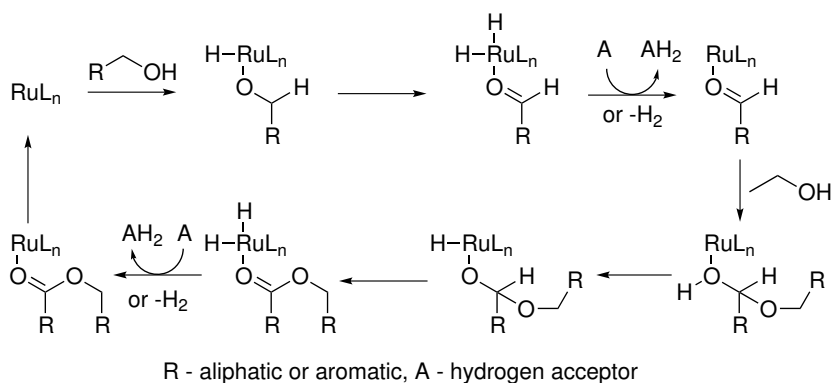
Aldehydes could couple with primary alcohols to give ester and dihydrogen as was shown by Blum and Murahashi.^{104,106} For example, the reaction of benzaldehyde with an equimolar amount of benzyl alcohol catalyzed by $\text{RuH}_2(\text{PPh}_3)_4$ gave benzylbenzoate with 85% yield. Attempts to make the cross-condensation between an alcohol (RCH_2OH) and a different aldehyde ($\text{R}'\text{CHO}$) selectively failed and gave a mixture of all four possible esters. Based on their mechanistic investigations, Murahashi and coworkers proposed that the aldehyde was hydrogenated to the alcohol which could participate in the esterification. They supported this idea by a cross-coupling in the presence of a hydrogen acceptor, such as mesityl oxide, which prevented the aldehyde from being hydrogenated. Under these conditions a cross-ester was obtained selectively in moderate yield.

These groups proposed two similar mechanisms for the esterification reaction (Scheme 3.2). The difference was in the way how hydrogen was removed from the system: it was either abstracted by a hydrogen acceptor or liberated in the form of dihydrogen. The cycle was based on a $\text{Ru}(0)/\text{Ru}(\text{II})$ redox process. First, $\text{Ru}(0)$ species oxidatively inserts into the O–H bond, then the

¹⁰⁴BLUM, Y.; SHVO, Y. *J. Organomet. Chem.* **1984**, 263, 93–107.

¹⁰⁶MURAHASHI, S.-I.; NAOTA, T.; ITO, K.; MAEDA, Y.; TAKI, H. *J. Org. Chem.* **1987**, 52, 4319–4327.

3.1 Introduction



Scheme 3.2: Proposed mechanism for the ruthenium-catalyzed esterification reaction.

alkoxide undergoes β -hydride elimination to give a species with a coordinated aldehyde. These steps are fast because considerable amount of an intermediate aldehyde is formed during the reaction.

After almost 20 years, studies of the ruthenium-catalyzed self-coupling of primary alcohols to give esters were resumed. Milstein and coworkers reported several new ruthenium PNP and PNN pincer complexes (Figure 3.2) which excelled the previously known catalysts in activity.^{107,108} Compounds **42a**, **42d** and **42c** in the presence of catalytic amounts of bases (0.1 mol% of KOH or 0.2 mol% of NaOiPr) converted aliphatic and aromatic primary alcohols into the corresponding esters effectively, giving almost quantitative yields after 24 h. Complex **42e** lost a molecule of N_2 upon heating and in the presence of NaOiPr was transformed into the active catalyst which performed as effectively as the other three. During the study, it was found that neither of these compounds catalyzed the esterification reaction in the absence of a base. Further investigation revealed that all these complexes were converted into the same active species **42b** which was later successfully synthesized. The authors demonstrated that this species did not require any base to catalyze the alcohol coupling. They also showed that when using **42b** the reaction significantly accelerated in comparison with other complexes and esters could be obtained in more than 90% yields after 2.5–6 h.

The authors undertook a mechanistic study and found that no Tischenko-type disproportionation was involved in the esterification reaction and that it more likely proceeds by hemiacetal formation with following β -hydride

¹⁰⁷ZHANG, J.; LEITUS, G.; BEN-DAVID, Y.; MILSTEIN, D. *J. Am. Chem. Soc.* **2005**, *127*, 10840–10841.

¹⁰⁸ZHANG, J.; GANDELMAN, M.; SHIMON, L. J. W.; MILSTEIN, D. *Dalton Trans.* **2007**, 107–113.

3.1.1 Ruthenium-Catalyzed Esterification Reactions

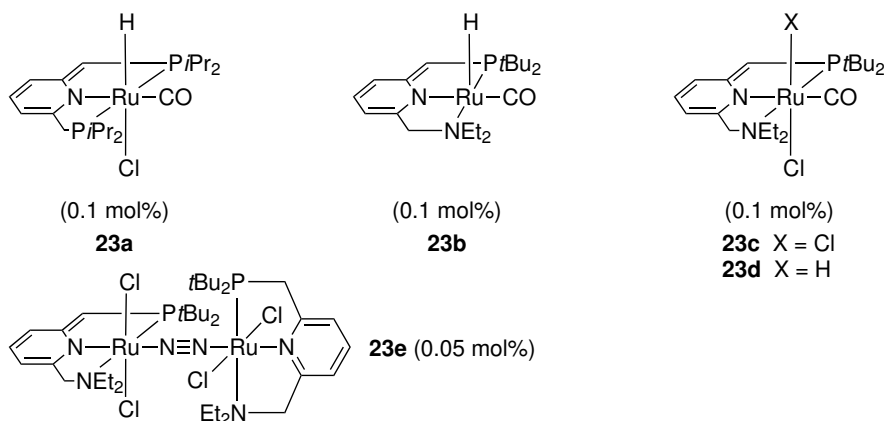


Figure 3.2: Structures of PNP and PNN pincer complexes employed in the dehydrogenative esterification of alcohols.

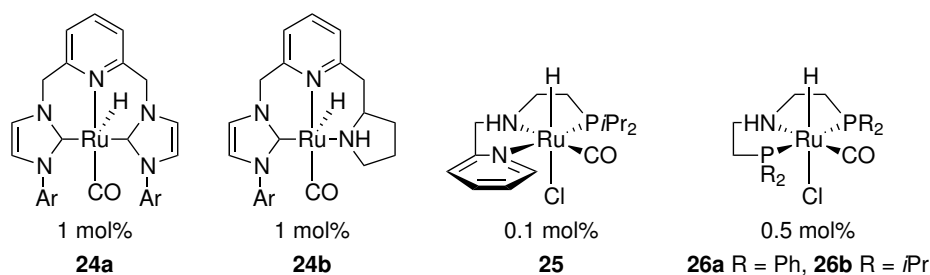


Figure 3.3: Structures of pincer complexes employed in the esterification reaction.

elimination to give an ester. They supported this idea by two experiments. In one of them 100 equivalents of benzaldehyde were heated in toluene with **42b** in the absence of benzyl alcohol. This experiment did not lead to the formation of benzyl benzoate. However, when the experiment was repeated with a 1:1 mixture of benzaldehyde and benzyl alcohol, then after 12 h the ester was formed in 100% yield. It is worth noting that this reaction proceeds according to the mechanism similar to the one discussed earlier (Scheme 3.2).

Compounds **42a–42e** are not the only type of ruthenium–pincer complexes which effectively catalyze acceptorless self-coupling of primary alcohols (Figure 3.3). In 2011, Sánchez and coworkers reported a family of combined NHC–pincer complexes **43a** and **43b**.¹⁰⁹ The authors showed that with 1 mol% catalytic loading and in some cases with 1 mol% of KOH aliphatic alcohols

¹⁰⁹ DEL POZO, C.; IGLESIAS, M.; SÁNCHEZ, F. *Organometallics* **2011**, *30*, 2180–2188.

3.1 Introduction

were converted into esters within 3–72 h with up to 100% yields. One year later, Gusev and coworkers discovered another pincer complex **44** which under neat conditions in a loading as low as 0.1 mol% with 0.5 mol% of KOtBu effectively catalyzed the esterification reaction.¹¹⁰ For example, heptyl heptanoate was obtained in 86% yield after 1 h (TOF is 4300 h⁻¹). Two other very active catalysts **45a** and **45b** were reported by Beller and coworkers.¹¹¹ With only 25 ppm of either of these two complexes and 1.3 mol% of NaOEt, the dehydrogenation of ethanol to give ethyl acetate proceeded under neat conditions with the TOF value slightly higher 1100 h⁻¹ which corresponds to a yield of 64% after 2 h. The authors studied the mechanism of esterification and found that aldehyde present in solution inhibited the reaction. From this observation they concluded that after outer-sphere dehydrogenation of the starting alcohol, the aldehyde stayed in the vicinity of the ruthenium catalyst, then another molecule of the alcohol attacked to give the hemiacetal which then underwent β -hydride elimination. They also speculated whether it was the alkoxide and not the alcohol that attacked the aldehyde because the amount of the catalytic alkoxide had a crucial role on the reactivity of the system.

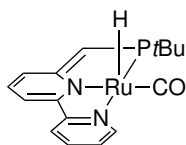


Figure 3.4: Structure of complex **46**.

Another catalytic system capable of dehydrogenative esterification of primary alcohols was recently developed in our group.¹⁰¹ It is based on ruthenium complex **1** which was also used for the amidation reaction discussed in Chapter 1. Self-coupling of aliphatic alcohols catalyzed by 2.5 mol% of **1**, 4.5 mol% of PCy₃ and 10 mol% of KOH in refluxing mesitylene (bp = 163 °C) afforded the corresponding esters in 49–97% after 18 h.

The reactions with aromatic alcohols had lower yields mostly due to concurrent decarbonylation of the aldehyde intermediate. A mechanistic study revealed that the reaction proceeded by essentially the same mechanism as other ruthenium-catalyzed self-coupling reactions (Scheme 3.2). It was also shown that the catalytically active species was a ruthenium dihydride.

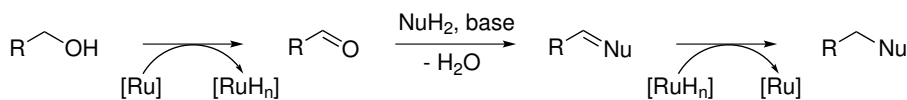
As we discussed before, attempts to perform a cross-coupling of the different alcohols failed. Recently, Milstein and coworkers published a successful cross-esterification of primary alcohols with secondary alcohols.¹¹² A reaction of

¹⁰¹SØLVHØJ, A.; MADSEN, R. *Organometallics* **2011**, *30*, 6044–6048.

¹¹⁰SPASYUK, D.; SMITH, S.; GUSEV, D. G. *Angew. Chem. Int. Ed.* **2012**, *51*, 2772–2775.

¹¹¹NIELSEN, M.; JUNGE, H.; KAMMER, A.; BELLER, M. *Angew. Chem. Int. Ed.* **2012**, *51*, 5711–5713.

3.1.2 Ruthenium-Catalyzed Alkylation Reactions Involving Alcohols



Scheme 3.3: Mechanism of the “hydrogen borrowing” process.

various primary alcohols (mostly aliphatic, one example with benzyl alcohol) with two-fold excess of a secondary alcohol in boiling toluene (bp = 110 °C) catalyzed by 1 mol% of complex **46** (Figure 3.4) gave esters in 46–99% yields after 24 h.

3.1.2 Ruthenium-Catalyzed Alkylation Reactions Involving Alcohols

The reaction mechanisms discussed in the previous chapter have several common steps, such as oxidation of an alcohol via β -hydride elimination to give an aldehyde followed by the attack of various *O*- and *N*-nucleophiles. Besides these, different reactions with carbon nucleophiles have also been discovered. After the nucleophilic addition, a double bond is formed which afterwards gets hydrogenated (Scheme 3.3). This transformation is usually called “hydrogen borrowing” process because the double bond “borrows” hydrogen atoms from the starting alcohol.

This methodology was applied to perform an indirect Wittig reaction. Various aromatic alcohols reacted with cyanoylide $\text{Ph}_3\text{P}=\text{CHCN}$ to give saturated nitriles in good yields (65–85%) after 2 h under ruthenium-hydride-catalyzed conditions.¹¹³ A similar transformation was performed with another ylide $\text{Ph}_3\text{P}=\text{CHCOOR}$.¹¹⁴ With this reaction saturated esters were obtained in good yields.

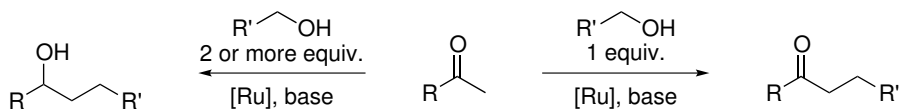
Not only homogeneous catalysts were developed for the hydrogen borrowing processes. In 2004, Kaneda and coworkers reported a ruthenium-hydrotalcite catalyzed α -alkylation of nitriles.¹¹⁵ Several aliphatic alcohols were coupled with aromatic nitriles to give the corresponding alkylated products in high to excellent yields. Ruthenium centers played the role of both

¹¹²SRIMANI, D.; BALARAMAN, E.; GNANAPRAKASAM, B.; BEN-DAVID, Y.; MILSTEIN, D. *Adv. Synth. Catal.* **2012**, 354, 2403–2406.

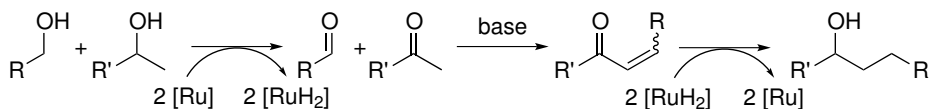
¹¹³BURLING, S.; PAINE, B. M.; NAMA, D.; BROWN, V. S.; MAHON, M. F.; PRIOR, T. J.; PREGOSIN, P. S.; WHITTLESEY, M. K.; WILLIAMS, J. M. J. *J. Am. Chem. Soc.* **2007**, 129, 1987–1995.

¹¹⁴EDWARDS, M. G.; JAZZAR, R. F. R.; PAINE, B. M.; SHERMER, D. J.; WHITTLESEY, M. K.; WILLIAMS, J. M. J.; EDNEY, D. D. *Chem. Commun.* **2004**, 90–91.

3.1 Introduction



Scheme 3.4: Different pathways of the reaction between primary alcohols and ketones.



Scheme 3.5: Mechanism of β -alkylation of secondary alcohols with primary alcohols.

oxidant and reductant whereas basic centers of hydrotalcite activated the nitrile and allowed process to proceed without additional base.

Ketones and the corresponding enolates are another type of nucleophiles used in hydrogen borrowing transformations. Depending on the amount of the primary alcohol, the product of the reaction could be either a β -alkylated ketone or a secondary alcohol (Scheme 3.4). Shim and coworkers reported transformations of both types catalyzed by $\text{RuCl}_2(\text{PPh}_3)_3$. Benzyl alcohol reacted with equimolar amount of various ketones in the presence of 1 equivalent of 1-dodecene as a hydrogen acceptor and 1 equivalent of KOH as a base to give the corresponding benzylated ketones in high yields.¹¹⁶ When using a three-fold excess of the alcohol, the alkylated ketone intermediate was further reduced to give secondary alcohol.¹¹⁷ The authors proposed that under basic conditions the ruthenium dichloride complex was transformed into a dihydride species which was the active catalyst. This idea was later supported by the experiments with $\text{RuH}_2(\text{PPh}_3)_3\text{CO}$ reported by Williams and coworkers.¹¹⁸ In the absence of a base and with only 0.5 mol% catalytic loading, various aromatic primary alcohols effectively alkylated ketonitriles.

Ability of ruthenium complexes to oxidize alcohols to carbonyl compounds could be employed to replace the ketones for the coupling with the corresponding secondary alcohols. As opposed to alkylation of ketones, the product of the reaction with secondary alcohols is another secondary alcohol even if a ratio between reactants is 1:1. This is due to the fact that hydrogen abstracted

¹¹⁵MOTOKURA, K.; NISHIMURA, D.; MORI, K.; MIZUGAKI, T.; EBITANI, K.; KANEDA, K. *J. Am. Chem. Soc.* **2004**, *126*, 5662–5663.

¹¹⁶CHO, C. S.; KIM, B. T.; KIM, T.-J.; CHUL SHIM, S. *Tetrahedron Lett.* **2002**, *43*, 7987–7989.

¹¹⁷CHO, C. S.; KIM, B. T.; KIM, T.-J.; SHIM, S. C. *J. Org. Chem.* **2001**, *66*, 9020–9022.

¹¹⁸SLATFORD, P. A.; WHITTLESEY, M. K.; WILLIAMS, J. M. J. *Tetrahedron Lett.* **2006**, *47*, 6787–6789.

from the reactants retains in the system in the form of ruthenium-dihydride and is delivered back to the α,β -unsaturated ketone to give a saturated secondary alcohol (Scheme 3.5). Crabtree and coworkers, reported that alkylation of aromatic secondary alcohols with aliphatic and aromatic primary alcohols catalyzed by a ruthenium-terpyridine complex led to almost exclusive formation of alkylated alcohols in high yields. In some cases, the ketone was observed as a byproduct but the yield did not exceed 8%.¹¹⁹ Cho *et al.* reported that addition of hydrogen scavengers to the reaction catalyzed by $\text{RuCl}_2(\text{PPh}_3)_3$ did not prevent hydrogenation of the ketone but, on the contrary, favored formation of the corresponding alcohol.¹²⁰ In this case, the ketone was also only a byproduct and its maximum yield was 3%.

Finally, there were published several examples of metal-free coupling of two alcohols. More than one century ago, Guerbet reported that in the presence of strong bases, such as sodium alkoxides, primary and secondary alcohols underwent self-coupling to give β -alkylated alcohols.^{121,122} Recently, Allen and Crabtree reported β -alkylation of a secondary alcohol with a primary alcohol catalyzed by NaOH or KOH in air.¹²³ They proposed that the alcohols got oxidized by air and then reduced by means of Meerwein-Ponndorf-Verley reaction.

The field of ruthenium-catalyzed (and in general, metal-catalyzed) alkylation with primary alcohols is very broad and well-investigated. In this chapter we have discussed only several representative reactions from this area. More examples and details can be found in recent reviews.^{124–126}

3.2 Optimization of the Esterification Reaction

We started our study with the same catalytic system as was used in the mechanistic investigation of the dehydrogenative amidation of primary alcohols with amines (Section 1.2): $\text{RuCl}_2(\text{IiPr})(p\text{-cymene})$ **1** (5 mol%), $\text{PCy}_3 \cdot \text{HBF}_4$ **2**

¹¹⁹GNANAMGARI, D.; LEUNG, C. H.; SCHLEY, N. D.; HILTON, S. T.; CRABTREE, R. H. *Org. Biomol. Chem.* **2008**, *6*, 4442–4445.

¹²⁰CHO, C. S.; KIM, B. T.; KIM, H.-S.; KIM, T.-J.; SHIM, S. C. *Organometallics* **2003**, *22*, 3608–3610.

¹²¹GUERBET, M. C. R. *Acad. Sci.* **1899**, *128*, 1002–1004.

¹²²GUERBET, M. C. R. *Acad. Sci.* **1909**, *149*, 129–132.

¹²³ALLEN, L. J.; CRABTREE, R. H. *Green Chem.* **2010**, *12*, 1362–1364.

¹²⁴GUILLENA, G.; RAMÓN, D. J.; YUS, M. *Angew. Chem. Int. Ed.* **2007**, *46*, 2358–2364.

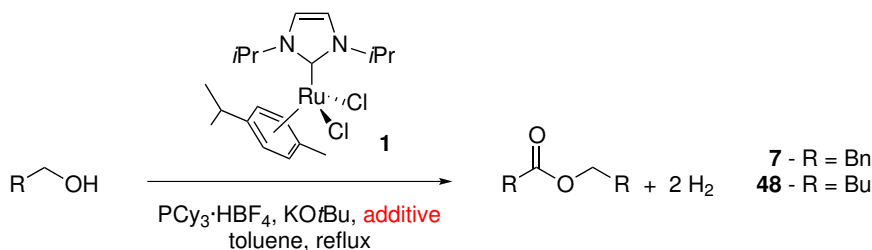
¹²⁵HAMID, M. H. S. A.; SLATFORD, P. A.; WILLIAMS, J. M. J. *Adv. Synth. Catal.* **2007**, *349*, 1555–1575.

¹²⁶NIXON, T. D.; WHITTLESEY, M. K.; WILLIAMS, J. M. J. *Dalton Trans.* **2009**, 753–762.

3.2 Optimization of the Esterification Reaction

(5 mol%) and KOtBu (15 mol%) in refluxing toluene. It was also reported that when different ammonia equivalents were used in this reaction, the corresponding ester was formed in various amounts. Particularly interesting was use of Mg₃N₂ as an NH₃ equivalent because it allowed to obtain the ester in quantitative yield when performing the reaction in refluxing toluene. To study this transformation in more detail we used Mg₃N₂ (**47**) as an additive in the esterification reaction and 2-phenylethanol (**7**) as a model substrate.

Table 3.1: Different conditions of the esterification reaction.



Entry	Alcohol	1 ^a	2 ^a	KOtBu ^a	Additive ^b	Time ^c	Conversion ^d	Yield ^d
1	7	5	5	15	–	24	100	64
2	7	5	5	15	47 (100)	24	100	84
3	7	5	0	10	47 (100)	24	23	14
4	7	5	5	5	47 (100)	24	21	1
5	7	5	5 ^e	10	47 (100)	24	89	66
6	7	5	5 ^f	10	47 (100)	24	82	65
7	48	1.25	1.25	3.75	47 (4.2)	2	–	36
8	48	1.25	1.25	3.75	47 (8.3)	2	–	61
9	48	1.25	1.25	3.75	47 (16.7)	2	–	78
10	48	1.25	1.25	3.75	47 (27)	2	–	61
11	48	1.25	1.25	3.75	47 (100)	2	–	49
12	7	2.5	2.5	7.5	MgO (50)	24	30	24
13	7	1.25	1.25	3.75	MgBr ₂ (50)	24	10	0
14	48	1.25	1.25	3.75	Ca ₃ N ₂ (16.7)	24	–	95
15	48	1.25	1.25	3.75	Li ₃ N (33)	24	–	80

See next page

Entry	Alcohol	1 ^a	2 ^a	KOtBu ^a	Additive ^b	Time ^c	Conversion ^d	Yield ^d
16	48	1.25	1.25	3.75	Cs ₂ CO ₃ (50)	24	–	11
17	48	1.25	1.25	3.75	K ₃ PO ₄ (33)	24	–	98
18	48	5	5	15	47 (16.7)	3	–	98
19	48	1.25	1.25	3.75	47 (16.7)	24	–	93
20	48	0.5	0.5	1.5	47 (16.7)	72	–	70
21	48 ^g	1.25	1.25	3.75	47 (16.7)	24	–	75
22	6a	1.25	1.25	3.75	47 (16.7)	24	33	27
23	6e	1.25	1.25	3.75	47 (16.7)	24	50	17
24	6e	2.5	2.5	7.5	47 (16.7)	24	65	33
25	6e	5	5	15	47 (16.7)	24	67	48
26	6e	5	5	15	47 (100)	24	100	81

a – in mol%, *b* – mol% in parentheses, *c* – in hours, *d* – determined by GC-MS, in %, *e* – PPh₃ instead of **2**, *f* – dppe instead of **2**, *g* – neat.

First, it was shown that both phosphine and a strong base were important components of the catalytic system (entries 2–4 in Table 3.1). Electron-rich phosphines facilitated formation of the ester since the reaction with PPh₃ or a bidentate phosphine 1,2-bis(diphenylphosphino)ethane (dppe) performed better than in the absence of a phosphine but worse than with **2** (entries 5 and 6). This also indicated that dppe might act as a monodentate ligand in this transformation because each of its phosphorus atoms have similar electronic properties to that of PPh₃ and the reactions with both dppe and PPh₃ gave similar yields.

Entries 2–6 demonstrate that the conversion of alcohol **7** was always higher than the yield of the ester which indicated that some side-reactions might have occurred. It was known that at a higher temperature (refluxing mesitylene) the same ruthenium complex could catalyze decarbonylation of alcohols.¹⁰¹ To verify if this process took place under the conditions used in the current study, the esterification reaction was performed with 2-(4-fluorophenyl)ethanol as a substrate instead of alcohol **7**. After 24 h a small amount of *p*-fluorotoluene was detected by GC-MS. This observation clearly demonstrated that the decarbonylation is one of the side reactions.

Next, the influence of additive **47** on the reactivity was studied. The substrate

3.2 Optimization of the Esterification Reaction

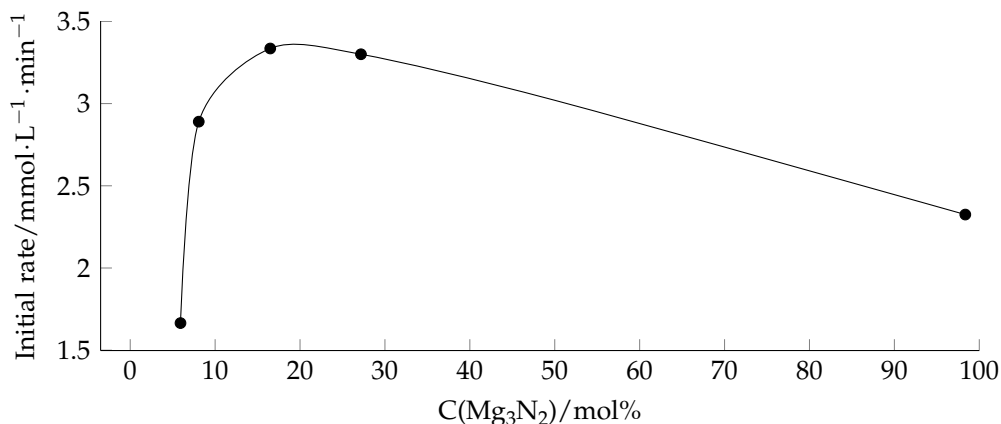


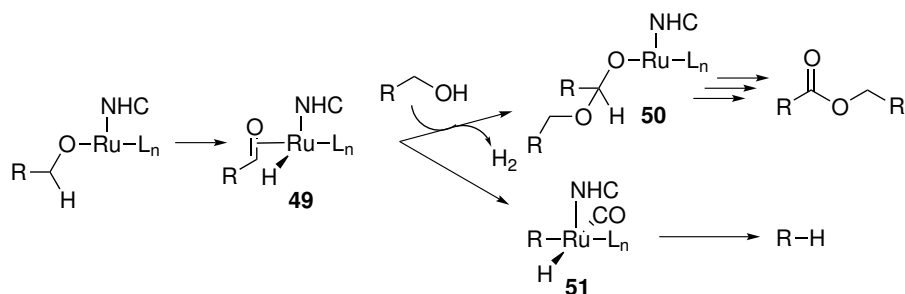
Figure 3.5: Dependence of the initial rate of the esterification on the amount of Mg₃N₂.

was changed from **7** to pentan-1-ol (**48**) to reduce the influence of the side reactions and the catalytic loading was lowered from 5 to 1.25 mol% to make the reaction proceed with a rate suitable for the kinetic measurements. The reaction had the highest initial rate and the highest yield when 16.7 mol% of **47** was used (Figure 3.5 and entries 7–11) which corresponded to 1/6 of the amount of alcohol **48**. This is an interesting number since 1 equivalent of Mg₃N₂ can theoretically react as a base with 6 equivalents of the alcohol. Thus, if basicity is the only important property of Mg₃N₂ in this transformation, then the optimal ratio between a base and an alcohol in the esterification reaction is 1:1.

To determine whether other properties are important, Mg₃N₂ was replaced with similar additives (entries 12–17). No ester was formed with MgBr₂ and only a low yield was observed with the weaker bases MgO and Cs₂CO₃ (entries 12, 13 and 16). On the contrary, high yields were achieved with the stronger bases Ca₃N₂, Li₃N and K₃PO₄ (entries 14, 15 and 17) and it appears that the most important property of the additive is basicity. The amount of complex **1** could be lowered to 0.5% at the expense of a longer reaction time and a slightly lower yield (entries 18–20). Thus, the conversion of pentan-1-ol into pentyl valerate has been achieved at a lower temperature and catalyst loading than in the previous study.¹⁰¹

The conditions were also applied to *p*-methoxybenzyl alcohol **6e** which gave the lowest yield of all substrates (19%) in the previous study due to extensive decarbonylation. With Mg₃N₂ as the additive the esterification of this alcohol

¹⁰¹SØLVHØJ, A.; MADSEN, R. *Organometallics* **2011**, *30*, 6044–6048.



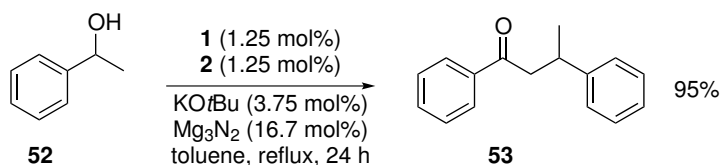
Scheme 3.6: Possible pathways of the aldehyde transformation.

was substantially improved and less decarbonylation was observed (entries 23–25). Using 100 mol% of Mg_3N_2 it was possible to achieve full conversion of **6e** and high yield of the corresponding ester (entry 26). With benzyl alcohol, however, the yield and conversion were essentially the same as in the previous study (entry 22).¹⁰¹

The role of Mg_3N_2 as a base could be explained from the mechanistic point of view. Assuming that the aldehyde formed during the reaction stays coordinated to the ruthenium center (as in the amidation reaction discussed in Chapter 1) two pathways for the further transformations could be proposed (Scheme 3.6). Once species **49** had been formed, the coordinated aldehyde could undergo several reactions. First, it could be attacked by an alcohol to form complex **50** with a bound hemiacetal which later was transformed to an ester. Second, if there was an empty site on ruthenium, species **49** could be decarbonylated to give compound **51** which could be further converted to a hydrocarbon R–H. If the formation of **50** is a rate-limiting step and the aldehyde bound to ruthenium does not tend to lose CO, then the ester formation is just a slow process and, in principle, will give ester in a high yield after a long period. However, if the aldehyde has a tendency to lose CO then the formation of R–H will be a concurrent or even dominating process. One of the possible reasons why the formation of **50** is slow could be that the hydride bound to ruthenium is not basic enough to rapidly pick up a proton from the attacking alcohol and form a molecule of H_2 . In this step, an external base can facilitate the proton abstraction making the formation of **50** faster. Comparing entries 1 and 2 it could be seen that Mg_3N_2 suppresses side reactions and increases the yield of the ester which supports the explanation about the role of the basic additive.

¹⁰¹SØLVHØJ, A.; MADSEN, R. *Organometallics* **2011**, *30*, 6044–6048.

3.3 Study of the Dehydrogenative Guerbet Reaction with Secondary Alcohols



Scheme 3.7: Unexpected Self-Condensation of 1-Phenylethanol.

At this point of the study, it was decided not to continue the investigations with other primary alcohols since the outcome most likely would be a rather predictable improvement of the previous substrate study. Instead, selective cross-esterifications were attempted which had never been done so far with complex **1**. First, an equimolar mixture of benzyl alcohol and 2-phenylethanol were reacted under the optimized conditions, but this only resulted in a statistical mixture of all four possible esters. Then, the cross-esterification was attempted with 2-phenylethanol and 1-phenylethanol **52** hoping that the increased basicity of the mixture would favor the reaction between the primary and the secondary alcohol. However, this only produced traces of the desired ester while 2-phenylethanol was almost completely converted into the symmetrical ester and 1-phenylethanol to acetophenone. Since the latter seems to be easily dehydrogenated under the reaction conditions, an experiment was also performed with 1-phenylethanol in the absence of a primary alcohol. Surprisingly, this now produced a 95% GC yield of ketone **53** (Scheme 3.7). This transformation can be envisioned as a dehydrogenative Guerbet reaction with a secondary alcohol – a reaction that to the best of our knowledge has not been described previously with a homogeneous catalyst. Hence, it was decided to study this reaction in more detail.

3.3 Study of the Dehydrogenative Guerbet Reaction with Secondary Alcohols

3.3.1 Optimization of the Reaction Conditions

For optimizing the reaction conditions heptan-2-ol **54** was selected as a model substrate. This alcohol only produced the corresponding ketone under the conditions in Scheme 3.7 and no dimerization was observed (entry **1** in Table 3.2). Most likely, it was due to the fact that Mg₃N₂ was a weak base and did not promote the aldol condensation of **56** to give enone **57** and other

3.3.1 Optimization of the Reaction Conditions

additives were therefore investigated. The screening of bases revealed that only strong bases catalyzed the transformation of **54** to **55** (entries 1–5 and 8–12). Apart from being a strong base the additive should also be a good drying agent to be able to trap water formed during the reaction (compare entries 3, 9, 10 and 12) which is why these additives cannot be used in catalytic amounts. The reaction without a base but just with a drying agent, however, did not give any product of the self-coupling (entries 6 and 7).

Table 3.2: Optimization of the secondary alcohols self-coupling.

Reaction scheme: **54** (secondary alcohol) reacts with **1** (2.5 mol%), phosphine (2.5 mol%), KOtBu (7.5%), additive, solvent, reflux to yield **55** (ketone), **56** (ketone), and **57** (enone).

Entry	Phosphine	Additive (mol%)	Solvent	55^a	56^a	57^a
1	2	Mg ₃ N ₂ (16.7)	Toluene	0	38	0
2	2	Ca ₃ N ₂ (16.7)	Toluene	0	30	0
3	2	Li ₃ N (33)	Toluene	86	12	2
4	2	K ₃ PO ₄ (33)	Toluene	0	99	1
5	2	K ₂ CO ₃ (50)	Toluene	0	64	0
6	2	4 Å mol. sieves	Toluene	0	67	0
7	2	Na ₂ SO ₄ (100)	Toluene	0	63	0
8	2	NaHCO ₃ (100)	Toluene	0	45	0
9	2	DBU (100)	Toluene	0	25	0
10	2	LDA ^b (100)	Toluene	56	6	5
11	2	KOtBu (100)	Toluene	78	0	0
12	2	NaH (100)	Toluene	92	2	2
13	no	Li ₃ N (33)	Toluene	50	1	10
14 ^c	2	Li ₃ N (33)	Toluene	76	17	6
15 ^d	2	Li ₃ N (33)	Toluene	44	16	8
16 ^e	PPh ₃	Li ₃ N (33)	Toluene	69	18	5
17 ^f	PPh ₃	Li ₃ N (33)	Toluene	26	16	4
18 ^e	dppe	Li ₃ N (33)	Toluene	34	10	4

See next page

3.3 Study of the Dehydrogenative Guerbet Reaction with Secondary Alcohols

Entry	Phosphine	Additive (mol%)	Solvent	55 ^a	56 ^a	57 ^a
19 ^e	py	Li ₃ N (33)	Toluene	23	2	9
20	2	Li ₃ N (33)	<i>o</i> -Xylene	39	0	1
21	2	Li ₃ N (33)	Heptane	7	0	5
22	2	Li ₃ N (33)	Benzene	18	21	3
23	2	Li ₃ N (33)	Dioxane	36	10	9
24	2	Li ₃ N (33)	Water	0	14	0
25	2	LiOH (100)	Toluene	0	64	0
26	2	NaOH (100)	Toluene	55	44	1
27	2	KOH (100)	Toluene	95	2	0
28 ^f	2	KOH (107.5)	Toluene	94	2	0
29 ^g	2	KOH (100)	Toluene	93	5	0
30 ^f	2	KOH (185)	Toluene	92	2	0
31 ^f	2	KOH (50)	Toluene	87	12	1
32 ^{f,h}	2	KOH (115)	Toluene	97	1	0
33 ^{f,i}	2	KOH (115)	Toluene	95	5	0

a – GC-MS yield after 24 h, *b* – 1.8 M solution in hexane, *c* – 2.5 mol% of KO^{*t*}Bu, *d* – KHMDS instead of KO^{*t*}Bu, *e* – 5 mol% of KO^{*t*}Bu, *f* – without KO^{*t*}Bu, *g* – 2 M solution of **54**, *h* – 1.25 mol% of **1** and 1.25 mol% of **2**, *i* – 5 mol% of **1** and 5 mol% of **2**.

Next, the role of the other components of the catalytic system was studied. As in the esterification reaction, a phosphine also played an important role in this transformation and the reaction performed better with more electron-rich phosphines (entries 16–19). In the absence of KO^{*t*}Bu, ketone **55** was formed in lower yields, presumably, because only a very strong base could effectively convert pre-catalyst **1** to the active catalyst (entries 14 and 17).

The reaction performed better in aromatic solvents because these solvents could temporarily bind to coordinatively unsaturated complexes and prevent their decomposition (entries 20–22). The reaction in 1,4-dioxane did not give as high yields as in toluene (entry 23) because 1,4-dioxane is a stronger coordinating solvent and could block the empty sites on ruthenium needed for the reaction. Water hydrolyzed both the active catalyst and Li₃N (entry 24).

The importance of basicity was clearly illustrated when KOH, NaOH and

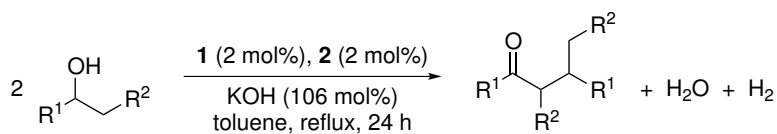
LiOH were compared, since the former gave ketone **55** as the major product while the latter only furnished heptan-2-one **56** (entries 25–27). With KOH it was possible to leave out KO*t*Bu and even lower the amount of complex **1** without compromising the yield of **55** (entries 28–30, 32 and 33). Only when lower amounts of KOH were employed did the yield of ketone **55** decrease slightly (entry 31).

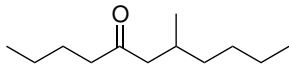
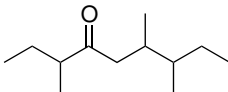
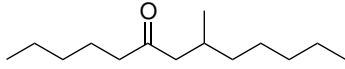
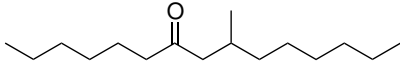
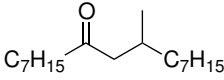
To conclude, the following catalytic system was found to be the most effective in the dehydrogenative Guerbet reaction with secondary alcohols: 2 mol% of complex **1**, 2 mol% of phosphine **2** and 106 mol% of KOH.

3.3.2 Scope and Limitations of the Reaction

After having optimized the reaction conditions, we moved further and explored the scope and limitations of the coupling. Various secondary alcohols with a boiling point above 110 °C were used in the study (Table 3.3).

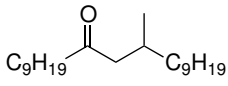
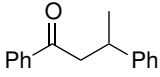
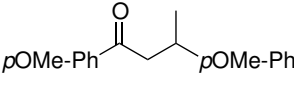
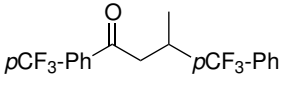
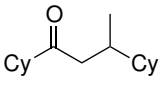
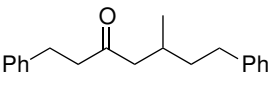
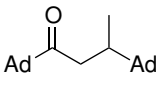
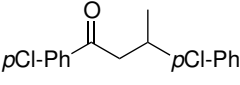
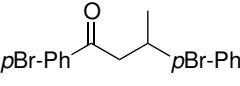
Table 3.3: Scope of the self-coupling reaction.



Entry	R ¹	R ²	Product	Yield ^a , %
1	<i>n</i> -C ₄ H ₉	H		95 ^a
2	<i>sec</i> -C ₄ H ₉	H		80 ^a
3	<i>n</i> -C ₅ H ₁₁	H		92 ^a
4	<i>n</i> -C ₆ H ₁₃	H		92 ^a
5	<i>n</i> -C ₇ H ₁₅	H		94 ^a

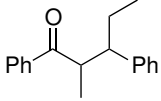
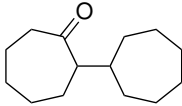
See next page

3.3 Study of the Dehydrogenative Guerbet Reaction with Secondary Alcohols

Entry	R ¹	R ²	Product	Yield ^a , %
6	<i>n</i> -C ₉ H ₁₉	H		60 ^b (87 ^{a,c})
7	<i>n</i> -C ₁₂ H ₂₅	H	none	0
8	Ph	H		95 ^a
9	<i>p</i> OMe-Ph	H		95 ^a
10	<i>p</i> CF ₃ -Ph	H		80 ^b (22 ^a)
11	Cy	H		92 ^a
12	BnCH ₂	H		88 ^a
13	Ad	H		20 ^b
14	C ₂ H ₅	CH ₃	none	0
15	<i>n</i> -C ₃ H ₇	CH ₃	none	0
16	<i>i</i> -C ₃ H ₇	CH ₃	none	0
17	<i>n</i> -C ₅ H ₁₁	<i>n</i> -C ₄ H ₉	none	0
18	<i>p</i> Cl-Ph	H		25 ^b
19	<i>p</i> Br-Ph	H		10 ^b
20	2-furyl	H	none	0
21	COOEt	H	none	0
22	Me	COOEt	none	0

See next page

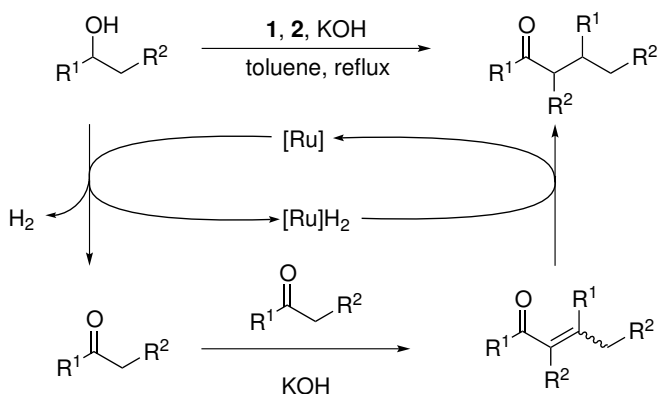
3.3.2 Scope and Limitations of the Reaction

Entry	R ¹	R ²	Product	Yield ^a , %
23	Ph	Me		5 ^b
24	Vinyl	<i>n</i> -C ₄ H ₉	none	0
25		-(CH ₂) ₅ -		70

a – isolated yield, *b* – GC-MS yield, *c* – after 65 h

Aliphatic alcohols with an OH-group in the 2 position (ranging from hexan-2-ol to nonan-2-ol) were converted to the corresponding ketones in high yields (entries 1–5). A further increase in the length of the aliphatic chain resulted in a lower reactivity as shown with undecan-2-ol and tetradecan-2-ol (entries 6 and 7). The former required a longer reaction time to give a good yield whereas the latter was only oxidized to the ketone and no aldol reaction was observed. Alcohols with one relatively bulky substituent underwent self-coupling in high yields (entries 11 and 12). However, introducing more bulky group, such as the adamantyl substituent led to a decrease in the yield (entry 13). Phenylethanols with a halogen substituent in the *para* position gave a mixture of various compounds due to partial dehalogenation of the substrates. The desired dihalogenated ketones were detected by GC-MS in low amounts (entries 18 and 19). However, if the *para* substituent tolerated the reaction conditions, the corresponding ketone was obtained in high yields regardless of the electronic properties the substituent (entries 8–10).

Surprisingly, no products of the self-coupling were obtained when alcohols with R¹ other than H were used (entries 14–17, 22 and 24). Even the more easily oxidized propiophenone only gave a very low yield of the coupling product (entry 23). Cycloalkanols, on the other hand, were completely transformed into the α -alkylated ketones. Unfortunately, cyclopentanol and cyclohexanol both gave a mixture of the monoalkylated and the α,α' -ketone where the ratio was 1:7 with cyclopentanol and 1:1 with cyclohexanol. No attempts were made to separate these product mixtures. Only cycloheptanol afforded exclusively the monoalkylated product which was isolated in good yield (entry 25). Reactions with other cyclic alcohols, such as 4-oxacyclohexanol



Scheme 3.8: Mechanism of the dehydrogenative self-coupling.

and 1,2,3,4-tetrahydronaphthalen-1-ol did not afford the corresponding self-coupled ketone.

In summary, the dehydrogenative dimerization of secondary alcohols with the ruthenium complex **1** worked well with a range of methyl carbinols while other acyclic secondary alcohols were not sufficiently reactive to undergo the coupling. Simple cyclic alcohols were transformed in good yield, but only cycloheptanol gives complete regioselectivity for the monoalkylated product.

3.3.3 Mechanistic Investigation

To better understand the mechanism of the reaction, several experiments have been undertaken. The reaction with 1-phenylethanol was monitored over time by GC-MS and both the intermediate ketone and the α,β -unsaturated enone could be observed (Scheme 2 and Figure 2). This confirmed that the C–C bond formation occurred by an aldol reaction followed by hydrogenation (Scheme 3.8 and Figure 3.6).

To gain more information about the ruthenium species involved in the catalytic cycle several NMR experiments were performed. Self-condensation of 1-phenylethanol was carried out in toluene- d_8 and after one hour several signals in the hydride region of the ^1H NMR spectrum were detected. Doublets at -22.13 ($^2J_{\text{P-H}} = 40$ Hz) and -22.24 ppm ($^2J_{\text{P-H}} = 35$ Hz) could be assigned to coordinatively unsaturated mono-hydride ruthenium species with PCy_3 trans to the carbene ligand and cis to the hydride.⁶⁷ The signals at -6.47 , -6.63 ,

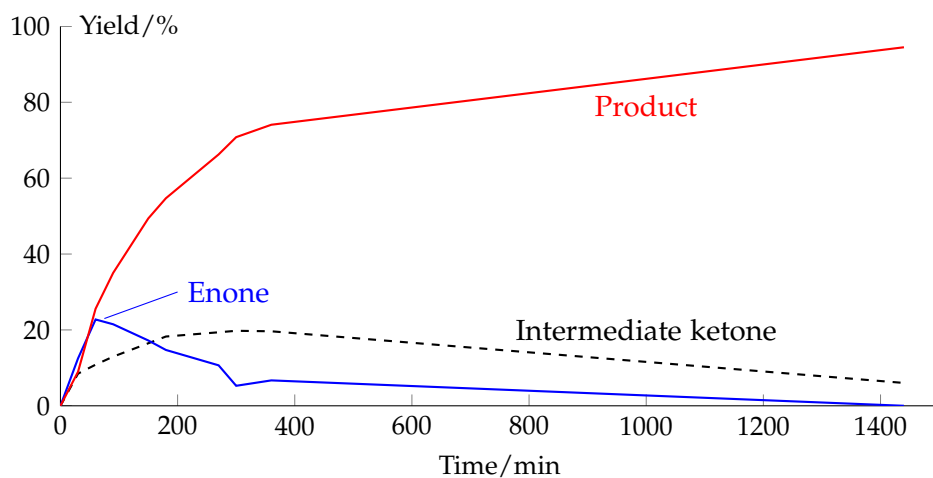


Figure 3.6: Profile of the dehydrogenative self-coupling.

–6.93 ppm could be assigned to dihydride species.^{127,128} Further evidence for the ruthenium dihydride species was provided by the experiments with a deuterated alcohol 1-deutero-1-phenylethanol. These experiments revealed that deuterium and hydrogen in the α -position were rapidly scrambled under self-coupling conditions. This fact indicated, first, that the oxidation of the alcohol is a reversible process and, second, that the complex formed after the oxidation of the alcohol is a dihydride species.

3.4 Conclusion

The ruthenium-catalyzed dehydrogenative self-coupling of primary alcohols to give esters and the previously unknown dehydrogenative Guerbet reaction with secondary alcohols to give ketones were studied. It was shown that in the presence of a basic additive Mg_3N_2 the esterification reaction proceeded at a lower temperature and with lower degree of the concurrent decarbonylation as compared with the earlier reported and similar ruthenium–NHC

⁶⁷LEE, H. M.; SMITH, D. C.; HE, Z.; STEVENS, E. D.; YI, C. S.; NOLAN, S. P. *Organometallics* **2001**, *20*, 794–797.

¹²⁷GIUNTA, D.; HOELSCHER, M.; LEHMANN, C. W.; MYNOTT, R.; WIRTZ, C.; LEITNER, W. *Adv. Synth. Catal.* **2003**, *345*, 1139–1145.

¹²⁸BURLING, S.; MAHON, M. F.; PAINE, B. M.; WHITTLESEY, M. K.; WILLIAMS, J. M. J. *Organometallics* **2004**, *23*, 4537–4539.

3.4 Conclusion

catalytic system. The conditions for the secondary alcohol self-coupling were optimized and the scope and the limitations of the reaction were studied. It was found that alkan-2-ols could be efficiently converted to the corresponding ketones with the liberation of one molecule of dihydrogen. The mechanistic investigation revealed that the reaction followed the oxidation–aldol condensation–reduction pathway and that the active ruthenium species was a dihydride.

3.5 Experimental Part

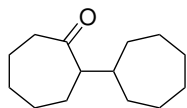
For the general experimental methods see Section 1.5 on page 49.

General Procedure for the Coupling of the Secondary Alcohols

A Schlenk tube was charged with $\text{RuCl}_2\text{I}(\text{p-cymene})$ **1** (46 mg, 1 mmol), $\text{PCy}_3\text{-HBF}_4$ **2** (36.8 mg, 0.1 mmol), KOH (298 mg, 5.3 mmol), and a stirring bar. A cold finger was attached and the tube was evacuated and refilled with Ar 3 times. The secondary alcohol (5 mmol) and nonane (321 mg, 2.5 mmol) were dissolved in toluene to give a 1 M solution of the alcohol (total volume 5 mL). This solution was transferred to the Schlenk tube which then was placed in a preheated oil bath ($T = 120^\circ\text{C}$). After 24 h the reaction mixture was cooled down to room temperature and filtered through a pad of Celite which was then washed with pentane. The collected solution was evaporated *in vacuo* and the resulting liquid was purified either by vacuum distillation or by column chromatography (eluent: pentane:EtOAc 50:1 to 15:1).

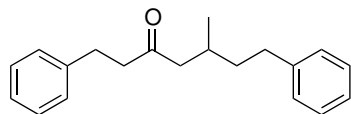
Characterization Data for the Compounds from Chapter 3

[1,1'-bi(cycloheptan)]-2-one



Distilled *in vacuo*, colorless liquid. Yield 364 mg (70%). $^1\text{H-NMR}$: δ 1.16–1.63 (m, 16 H), 1.76–1.91 (m, 5 H), 2.21–2.38 (m, 2 H), 2.43–2.53 (m, 1 H). $^{13}\text{C-NMR}$: δ 25.5, 26.8, 26.9, 27.6, 28.2, 28.3, 28.6, 30.3, 30.9, 32.9, 42.2, 43.4, 59.5, 217.4. IR (neat, cm^{-1}) 1705 (C=O). bp (5 mmHg) 136°C . HRMS (m/z) calcd for $[\text{C}_{14}\text{H}_{24}\text{O}+\text{H}]^+$ 209.1905, found 209.1895.

5-methyl-1,7-diphenylheptan-3-one

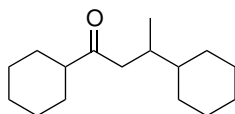


Purified by column chromatography, yellowish liquid. Yield 308 mg (88%). $^1\text{H-NMR}$: δ 0.86 (d, 3 H, $J_{\text{H-H}} = 6.4$ Hz), 1.32–1.58 (m, 2 H), 1.90–2.03 (m, 1 H), 2.13–2.21 (m, 1 H), 2.30–2.37 (m, 1 H), 2.41–2.64 (m, 4 H), 2.78–2.83 (m, 2 H), 7.07–7.22 (m, 10 H). $^{13}\text{C-NMR}$: δ 19.9, 29.1, 29.9, 33.5, 38.8, 44.9, 50.6, 125.9,

3.5 Experimental Part

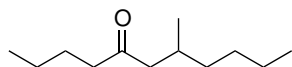
126.2, 128.5, 128.6, 141.3, 142.5, 209.9. **IR** (neat, cm^{-1}) 1712 (C=O). **HRMS** (m/z) calcd for $[\text{C}_{20}\text{H}_{24}\text{O}+\text{H}]^+$ 281.1905, found 281.1902.

1,3-dicyclohexylbutan-1-one



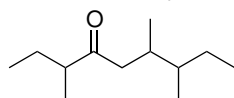
Distilled *in vacuo*, colorless liquid. Yield 543 mg (92%). **$^1\text{H-NMR}$** : δ 0.80 (d, 3 H, $J_{\text{H-H}} = 6.7$ Hz), 0.92–1.39 (m, 11 H), 1.59–1.96 (m, 11 H), 2.17–2.34 (m, 2 H), 2.44 (dd, 1 H, $J_{\text{H-H}} = 16.1$ Hz, $J_{\text{H-H}} = 4.8$ Hz). **$^{13}\text{C-NMR}$** : δ 16.8, 25.8, 25.9, 26.0, 26.8, 26.9, 28.5, 28.7, 29.2, 30.5, 33.9, 42.9, 45.6, 51.3, 214.7. **IR** (neat, cm^{-1}) 1705 (C=O). **bp** (5 mmHg) 146 °C. **HRMS** (m/z) calcd for $[\text{C}_{16}\text{H}_{28}\text{O}+\text{H}]^+$ 237.2218, found 237.2213.

7-methylundecan-5-one



Distilled *in vacuo*, colorless liquid. Yield 437 mg (95%). **$^1\text{H-NMR}$** : δ 0.85–0.92 (m, 9 H), 1.18–1.36 (m, 8 H), 1.88 (quint, 2 H, $J_{\text{H-H}} = 7.5$ Hz), 1.92–2.04 (m, 1 H), 2.14–2.22 (m, 1 H), 2.31–2.40 (m, 3 H). **$^{13}\text{C-NMR}$** : δ 14.0, 14.2, 20.0, 22.5, 23.0, 26.0, 29.3, 29.4, 36.8, 43.3, 50.5, 211.6. **IR** (neat, cm^{-1}) 1712 (C=O). **bp** (5 mmHg) 91 °C (reported¹²⁹ bp: 103–105 °C at 9 mmHg). **HRMS** (m/z) calcd for $[\text{C}_{12}\text{H}_{24}\text{O}+\text{H}]^+$ 185.1905, found 185.1899.

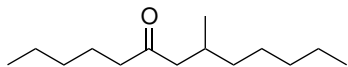
3,6,7-trimethylnonan-4-one



Distilled *in vacuo*, colorless liquid. Yield 368 mg (80%), mixture of diastereomers. **$^1\text{H-NMR}$** : δ 0.74–0.89 (m, 9 H), 1.03 (d, 3 H, $^3J_{\text{H-H}} = 6.0$ Hz), 1.07–1.41 (m, 3 H), 1.59–1.73 (m, 1 H), 2.01–2.48 (m, 3 H). **$^{13}\text{C-NMR}$** : δ 11.0, 11.8, 11.9, 12.2, 12.2, 14.5, 14.5, 14.8, 14.9, 15.9, 15.9, 16.0, 16.0, 16.1, 16.1, 17.3, 17.3, 19.9, 25.9, 25.9, 26.0, 26.1, 26.1, 26.5, 27.4, 32.2, 32.9, 33.0, 34.6, 35.9, 38.9, 38.9, 39.5, 45.0, 45.0, 46.0, 46.9, 48.2, 48.2, 48.3, 48.4, 214.9, 214.9, 215.1, 215.1. **IR** (neat, cm^{-1}) 1712 (C=O). **bp** (5 mmHg) 70 °C. **HRMS** (m/z) calcd for $[\text{C}_{12}\text{H}_{24}\text{O}+\text{H}]^+$ 185.1905, found .

¹²⁹KINDT-LARSEN, T.; BITSCH, V.; ANDERSEN, I. G. K.; JART, A.; MUNCH-PETERSEN, J. *Acta Chem. Scand.* **1963**, *17*, 1426–1432.

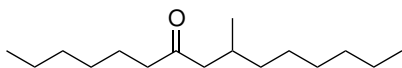
8-methyltridecan-6-one **55**



Distilled *in vacuo*, colorless liquid. Yield 488 mg (92%).

¹H-NMR: δ 0.85–0.90 (m, 9H), 1.19–1.34 (m, 12H), 1.55 (quint, 2H, $J_{\text{H-H}} = 7.5$ Hz), 1.92–2.04 (m, 1H), 2.14–2.22 (m, 1H), 2.33–2.40 (m, 3H). **¹³C-NMR:** δ 14.1, 14.2, 20.0, 22.6, 22.8, 23.6, 26.8, 29.4, 31.6, 32.1, 37.1, 43.5, 50.5, 211.7. **IR** (neat, cm^{-1}) 1708 (C=O). **bp** (5 mmHg) 111–112 °C. **HRMS** (m/z) calcd for $[\text{C}_{14}\text{H}_{28}\text{O}+\text{H}]^+$ 213.2218, found 213.2212.

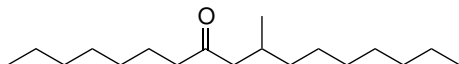
9-methylpentadecan-7-one **62**



Distilled *in vacuo*, colorless liquid. Yield 552 mg (92%).

¹H-NMR: δ 0.84–0.89 (m, 9H), 1.16–1.34 (m, 16H), 1.50–1.59 (m, 2H), 1.92–2.03 (m, 1H), 2.14–2.21 (m, 1H), 2.32–2.39 (m, 3H). **¹³C-NMR:** δ 14.17, 14.24, 20.0, 22.6, 22.8, 23.9, 27.1, 29.1, 29.4, 29.6, 31.8, 32.0, 37.1, 43.6, 50.5, 211.7. **IR** (neat, cm^{-1}) 1713 (C=O). **bp** (5 mmHg) 130–131 °C ¹H-NMR data is in accordance with literature values.¹³⁰

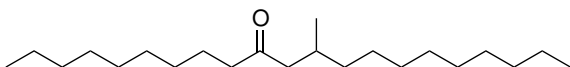
10-methylheptadecan-8-one **63**



Distilled *in vacuo*, colorless liquid. Yield 630 mg (94%).

¹H-NMR: δ 0.84–0.89 (m, 9H), 1.18–1.31 (m, 20H), 1.50–1.59 (m, 2H), 1.92–2.03 (m, 1H), 2.14–2.21 (m, 1H), 2.31–2.39 (m, 3H). **¹³C-NMR:** δ 14.18, 14.22, 20.0, 22.76, 22.81, 24.0, 27.1, 29.2, 29.36, 29.40, 29.5, 29.9, 31.8, 32.0, 37.1, 43.5, 50.5, 211.6. **IR** (neat, cm^{-1}) 1713 (C=O). **bp** (5 mmHg) 154 °C. **HRMS** (m/z) calcd for $[\text{C}_{18}\text{H}_{36}\text{O}+\text{H}]^+$, found

12-methylhenicosan-10-one **64**



Distilled *in vacuo*, colorless liquid that crystallized after a while. Yield 705 mg (87%).

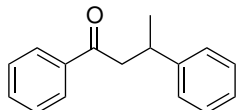
¹H-NMR: δ 0.84–0.89 (m, 9H), 1.25 (br. s., 28H), 1.50–1.59 (m, 2H), 1.94–2.03 (m, 1H), 2.14–2.22 (m, 1H), 2.33–2.40 (m, 3H). **¹³C-NMR:** δ 14.26, 14.27, 20.1,

¹³⁰BROWN, H. C.; KULKARNI, S. V.; RACHERLA, U. S.; DHOKTE, U. P. *J. Org. Chem.* **1998**, *63*, 7030–7036.

3.5 Experimental Part

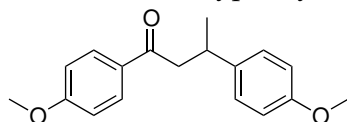
22.82, 22.84, 24.0, 27.1, 29.4, 29.5, 29.6, 29.70, 29.76, 29.81, 29.85, 29.94, 32.02, 32.06, 37.1, 43.6, 50.5, 211.7. **IR** (neat, cm^{-1}) 1714 (C=O). **bp** (5 mmHg) 197 °C. **HRMS** (m/z) calcd for $[\text{C}_{22}\text{H}_{44}\text{O}+\text{H}]^+$, found

1,3-diphenylbutan-1-one **53**



Purified by column chromatography, yellow solid. Yield 532 mg (95%). NMR data is in accordance with literature values.¹³¹

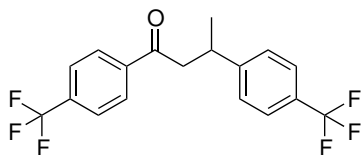
1,3-bis(4-methoxyphenyl)butan-1-one **65**



Purified by column chromatography, colorless liquid. Yield 675 mg (95%).

¹H-NMR: δ 1.30 (d, 3 H, $J_{\text{H-H}} = 6.9$ Hz), 3.05–3.24 (m, 2 H), 3.39–3.50 (m, 1 H), 3.78 (s, 3 H), 3.85 (s, 3 H), 6.84 (d, 2 H, $J_{\text{H-H}} = 8.7$ Hz), 6.91 (d, 2 H, $J_{\text{H-H}} = 8.9$ Hz), 7.19 (d, 2 H, $J_{\text{H-H}} = 8.7$ Hz), 7.91 (d, 2 H, $J_{\text{H-H}} = 8.9$ Hz). **¹³C-NMR**: δ 22.2, 35.1, 47.1, 55.4, 55.6, 113.8, 114.0, 127.9, 130.4, 130.5, 130.7, 138.9, 158.0, 163.5, 197.9. **IR** (neat, cm^{-1}) 1672 (C=O). **HRMS** (m/z) calcd for $[\text{C}_{18}\text{H}_{20}\text{O}_3+\text{H}]^+$ 285.1481, found 285.1488.

1,3-bis(4-methoxyphenyl)butan-1-one **66**



After 24 h the reaction solution was passed through a plug of Celite which was then washed with pentane. The resulting solution was evaporated *in vacuo* to give 701 mg of a red liquid. NMR spectrum showed that the sample contained approx. 85% of the desired product, GCMS also showed that the desired ketone was the major product. However, attempts to isolate quantitatively the product by column chromatography failed (probably, due to the partial decomposition of the compound). Two passes through a column with silica gel (eluent pentane:EtOAc from 50:1 to 15:1) gave a reddish liquid. Yield 198 mg

¹³¹KANAZAWA, Y.; TSUCHIYA, Y.; KOBAYASHI, K.; SHIOMI, T.; ITOH, J.-I.; KIKUCHI, M.; YAMAMOTO, Y.; NISHIYAMA, H. *Chem. Eur. J.* **2005**, *12*, 63–71.

(22%). **¹H-NMR:** δ 1.29 (d, 3 H, $J_{\text{H-H}} = 7.0$ Hz), 3.11–3.30 (m, 2 H), 3.45–3.56 (m, 1 H), 7.29 (d, 2 H, $J_{\text{H-H}} = 8.0$ Hz), 7.47 (d, 2 H, $J_{\text{H-H}} = 8.3$ Hz), 7.62 (d, 2 H, $J_{\text{H-H}} = 8.3$ Hz), 7.92 (d, 2 H, $J_{\text{H-H}} = 8.0$ Hz). **¹³C-NMR:** δ 22.0, 35.3, 46.9, 125.5–125.9 (m), 127.4, 128.3, 128.5, 129.4, 139.7, 150.3, 197.5. **¹⁹F-NMR:** δ –62.77, –62.02. **IR** (neat, cm^{-1}) 1692 (C=O). **HRMS** (m/z) calcd for $[\text{C}_{18}\text{H}_{14}\text{F}_6\text{O}+\text{H}]^+$ 361.1027, found 361.1028.

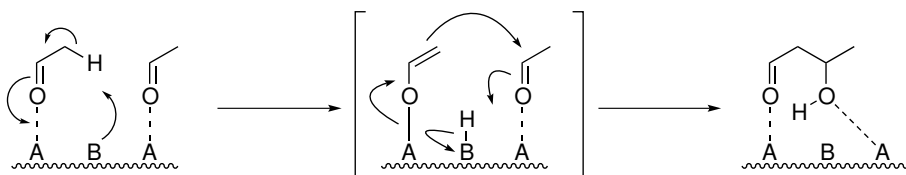
4 Study of the Acetaldehyde Transformations over Zeolite-Type Heterogeneous Catalysts

THIS CHAPTER DISCUSSES THE WORK performed during the three-month stay at the chemical company Haldor Topsøe A/S. The work was divided into two projects. The aim of one of them was to study the transformation of acetaldehyde over different heterogeneous catalysts such as metal oxides and zeolites. Another project dealt with elucidating the mechanism of the trioses to methyl lactate conversion catalyzed by Sn-Beta zeolite. Experiments with isotopically labeled sugars were employed as a major tool for the mechanistic study. The mechanistic part of the work will not be covered in this dissertation.

4.1 Introduction

The aldol reaction is one of the most fundamental transformations in organic chemistry and a great variety of methods for performing this reaction in solution with homogeneous catalysts have been discovered.¹³² There have also been reported heterogeneous catalytic systems that are capable of catalyzing the aldol reaction. Various silica-supported metal oxides, such as WO_x ,¹³³ MoO_x ,¹³³ ZrO_2 ,^{133,134} MgO .¹³⁴ could be used as a catalyst in the vapor-phase aldol reaction. Metal oxides (Al_2O_3 , CeO_2 , TiO_2),¹³⁵ type X zeolites,¹³⁶ MFA zeolites¹³⁷ were also reported to be effective catalysts of the aldol reaction in a vapor phase. Examples of the liquid phase aldol reaction promoted by heterogeneous catalysts are rare.¹³⁸

From the chemical point of view, the main difference between a homogeneous and heterogeneous variants of the aldol reaction is that the vast majority of heterogeneous catalysts combine both Lewis acidic and Brønsted basic centers, as opposed to the homogeneous counterpart which usually carries only one of these functionalities. This combination makes it possible to perform the reaction more effectively.



Scheme 4.1: Mechanism of the aldol reaction over a heterogeneous catalyst with Lewis acidic (A) and Brønsted basic (B) centers.

A mechanism of the aldol reaction over a heterogeneous catalyst with Lewis acidic and Brønsted basic centers is represented in Scheme 4.1. Depending on the conditions and catalysts, the reaction could proceed further to give different products. Several possible pathways are shown in Scheme 4.2. Over

¹³² In *Modern Aldol Reactions*, MAHRWALD, R., Ed.; WILEY-VCH Verlag GmbH & Co. KGaA: Weinheim, 2004; Vol. 1, 2.

¹³³ JI, W.; CHEN, Y.; KUNG, H. H. *Appl. Catal. A: Gen.* **1997**, 161, 93–104.

¹³⁴ ORDOMSKY, V. V.; SUSHKEVICH, V. L.; IVANOVA, I. I. *J. Mol. Catal. A* **2010**, 333, 85–93.

¹³⁵ RASKÓ, J.; KISS, J. *Appl. Catal. A: Gen.* **2005**, 287, 252–260.

¹³⁶ CHANG, Y.-C.; KO, A.-N. *Appl. Catal. A: Gen.* **2000**, 190, 149–155.

¹³⁷ DUMITRIU, E.; HULEA, V.; FECHETE, I.; AUROUX, A.; LACAZE, J.-F.; GUIMON, C. *Microporous and Mesoporous Materials* **2001**, 43, 341–359.

¹³⁸ KAGUNYA, W.; JONES, W. *Appl. Clay Sci.* **1995**, 10, 95–102.

basic catalysts acetaldehyde AcH could be transformed not only to aldol **70** but also to ethyl acetate **69** via a Tischenko reaction.^{133,134} Aldol **70** could be further converted to several compounds: by Meerwein-Ponndorf-Verley reduction to diol **71**; on the acidic sites of the catalyst to crotonaldehyde **72** (which is usually the major product of the reaction^{133–139}) or by a hydride shift to 1-hydroxybutanone-3 **73**. Each of these compounds could undergo further transformation. Diol **71** could react with acetaldehyde **67** to give acetal **76** (yield about 4 mol% was reported for the reaction over SiO₂/ZrO₂¹³⁴). Crotonaldehyde **72** could be reduced by Meerwein-Ponndorf-Verley reduction to allyl alcohol **77** or react with one or more molecules of **67** to form conjugated unsaturated aldehydes **78**^{134,136} and **80** (concentration of C₆ and C₈ oligomers was reported to be approximately 25 mol%¹³⁸). Compound **73** undergoes retro-aldol reaction to give acetone **74** and formaldehyde **75** or loses a molecule of water to give methylvinylketone **79**. It is worth noting that only titanium oxide¹⁴⁰ and silica supported zirconium (IV) oxide¹³⁴ can catalyze the isomerization of **70** to **73**.

The latter isomerization as well as several above-mentioned transformations proceed via Meerwein-Ponndorf-Verley reduction–Oppenauer oxidation (MPVO reactions, Scheme 4.3) that could be described as a main group metal-catalyzed hydride transfer from an alcohol to a carbonyl compound to give the corresponding carbonyl compound and another alcohol. Application of heterogeneous catalysts in this transformation was studied extensively. It was shown that different zeolites are capable of catalyzing MPVO reactions. Van Bekkum and coworkers found zeolite BEA and titanium Beta to be a very effective catalysts for this transformation.^{141,142} They also demonstrated that the activity of the catalyst depended on the configuration of the Lewis acidic aluminum sites in the zeolites.¹⁴¹ Zhu *et al.* reported that zirconium-Beta could give alcohols by MPVO reactions in high yields in a short reaction time.¹⁴³

¹³³Ji, W.; Chen, Y.; Kung, H. H. *Appl. Catal. A: Gen.* **1997**, *161*, 93–104.

¹³⁴ORDOMSKY, V. V.; SUSHKEVICH, V. L.; IVANOVA, I. I. *J. Mol. Catal. A* **2010**, *333*, 85–93.

¹³⁵RASKÓ, J.; KISS, J. *Appl. Catal. A: Gen.* **2005**, *287*, 252–260.

¹³⁶CHANG, Y.-C.; KO, A.-N. *Appl. Catal. A: Gen.* **2000**, *190*, 149–155.

¹³⁷DUMITRIU, E.; HULEA, V.; FECHETE, I.; AUROUX, A.; LACAZE, J.-F.; GUIMON, C. *Microporous and Mesoporous Materials* **2001**, *43*, 341–359.

¹³⁸KAGUNYA, W.; JONES, W. *Appl. Clay Sci.* **1995**, *10*, 95–102.

¹³⁹YOUNG, R.; SHEPPARD, N. *J. Catal.* **1967**, *7*, 223–233.

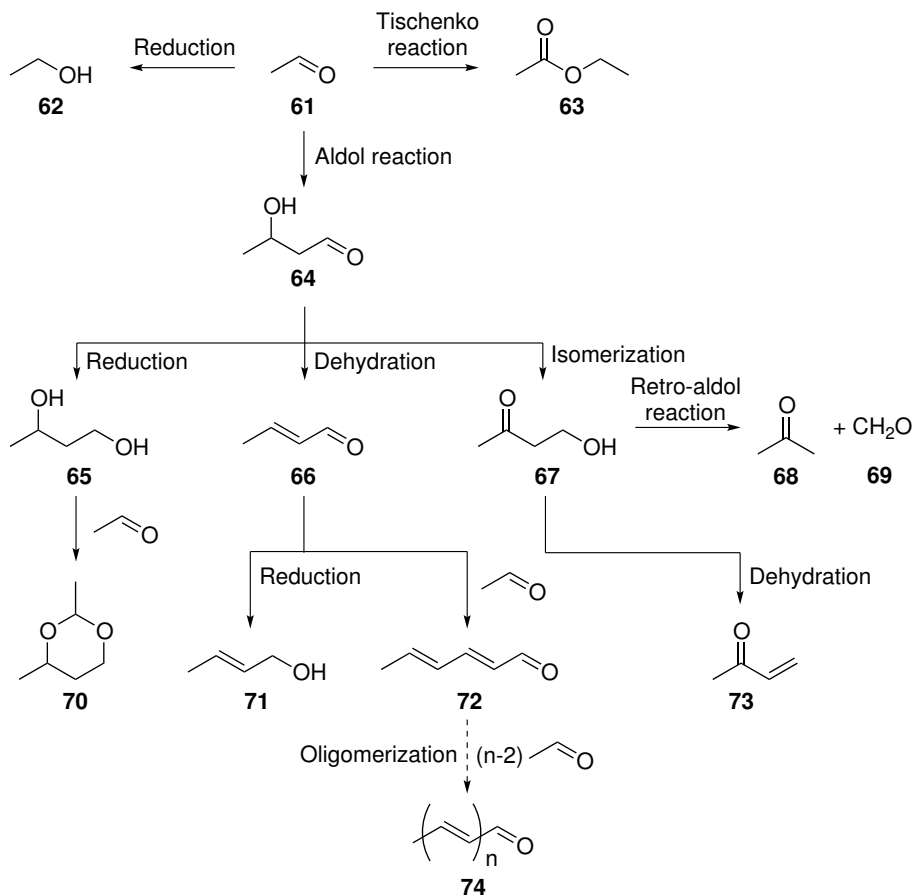
¹⁴⁰REKOSKE, J. E.; BARTEAU, M. A. *Ind. Eng. Chem. Res.* **2011**, *50*, 41–51.

¹⁴¹CREYGHTON, E.; GANESHIE, S.; DOWNING, R.; VAN BEKKUM, H. *J. Mol. Catal. A* **1997**, *115*, 457–472.

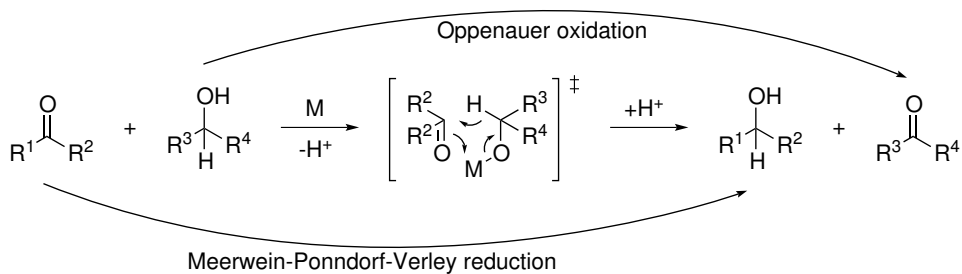
¹⁴²VAN DER WAAL, J. C.; KUNKELER, P.; TAN, K.; VAN BEKKUM, H. *J. Catal.* **1998**, *173*, 74–83.

¹⁴³ZHU, Y.; CHUAH, G.; JAENICKE, S. *J. Catal.* **2004**, *227*, 1–10.

4.1 Introduction



Scheme 4.2: Possible pathways of acetaldehyde transformations.



Scheme 4.3: Mechanism of Meerwein-Ponndorf-Verley reduction–Oppenauer oxidation reactions.

Tin-Beta zeolite was shown to be an excellent catalyst for this reaction.¹⁴⁴ An effect of the substituents in the carbonyl component was studied and it was demonstrated that the more crowded the environment around the carbonyl group is, the lower conversions could be achieved.^{144,145} Interestingly, it was also observed that aromatic groups present in a carbonyl compound decreased the reactivity of the substrate.¹⁴⁵ It was explained by the interaction of the aromatic ring with Lewis acidic sites which blocked some of these sites for coordination with the carbonyl group.

4.2 Results

As it was mentioned before, the aim of the project was to study the transformation of acetaldehyde over different heterogeneous catalysts. More precisely, it was interesting to explore the ability of Sn-Beta zeolite to catalyze the aldol reaction and subsequent transformations of acetaldehyde presented in Scheme 4.2. It was previously shown that Sn-Beta zeolite was an effective catalyst for the aldol and retro-aldol reactions. The Sn-Beta-catalyzed transformation of sugars to methyl lactate was proposed to proceed through a retro-aldol reaction in the case of hexoses¹⁴⁶ or several aldol-retro-aldol reactions in the case of pentoses.¹⁴⁷ As it was also mentioned in the introduction, tin-Beta is an excellent catalyst for MPVO reactions. All these facts made Sn-Beta a good candidate for catalyzing the acetaldehyde transformations.

Preparation of Sn-Beta zeolite is a time consuming process. As it took 21 days to synthesize Sn-Beta and the amount of the obtained catalyst was enough only to perform a limited number of reactions, the reaction conditions had to be considered thoroughly and optimized beforehand. For the optimization various compounds were used, such as MgO, CaO, titanium silicate-1 (TS-1). The experiments were carried out in a continuous flow reactor at 150 °C with a 10 wt% aqueous solution of acetaldehyde as the feed. It was rapidly discovered that CaO is an inappropriate compound for this system as it reacted with water to give Ca(OH)₂ which blocked up the reactor.

Further optimizations revealed that the optimal weight hourly space velocity

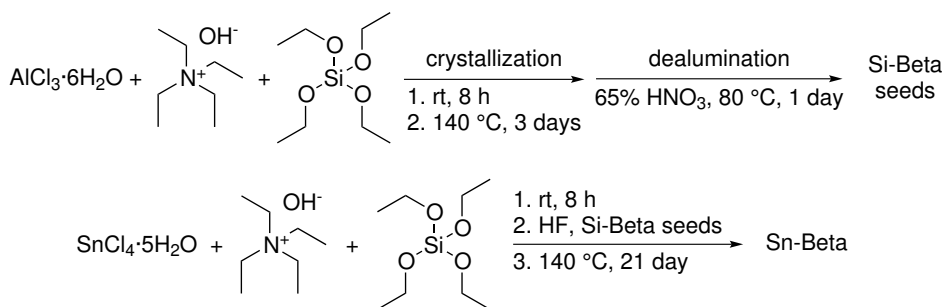
¹⁴⁴CORMA, A.; DOMINE, M. E.; NEMETH, L.; VALENCIA, S. *J. Am. Chem. Soc.* **2002**, *124*, 3194–3195.

¹⁴⁵CORMA, A.; DOMINE, M. E.; VALENCIA, S. *J. Catal.* **2003**, *215*, 294–304.

¹⁴⁶HOLM, M. S.; SARAVANAMURUGAN, S.; TAARNING, E. *Science* **2010**, *328*, 602–605.

¹⁴⁷HOLM, M. S.; PAGÁN-TORRES, Y. J.; SARAVANAMURUGAN, S.; RIISAGER, A.; DUMESIC, J. A.; TAARNING, E. *Green Chem.* **2012**, *14*, 702–706.

4.2 Results



Scheme 4.4: Synthesis of Sn-Beta zeolite.

(the ratio between the mass flow rate of the reactants and the mass of the catalyst in the reactor) was approximately $0.3\text{ g}_{\text{react}} \cdot \text{h}^{-1} \cdot \text{g}_{\text{cat}}^{-1}$. It was also found that the temperature of the coolant used for condensing the reaction products was $1\text{ }^\circ\text{C}$.

It is worth noting that the mass of the collected solution was always lower than the mass of the fed solution. In the case of MgO, most likely, only water was adsorbed or reacted with the catalyst, whereas when TS-1 was used it reacted with acetaldehyde too. This was concluded after examining the color of the catalyst before and after the reaction: white at the beginning TS-1 changed its color to green-blue in the end.

Next, the reaction was performed with Sn-Beta zeolite which was synthesized as follows (Scheme 4.4): first, zeolite Beta seeds were prepared from aluminum chloride and tetraethyl orthosilicate (TEOS) as a source of silicon. Tetraethylammonium hydroxide (TEAOH) was used as a base for hydrolysis of TEOS and as a template which determined the size of the pores in the seeds. After 3 days of crystallization in an autoclave at $140\text{ }^\circ\text{C}$, the seeds were dealuminated by heating in a concentrated solution of nitric acid, and then calcined at $550\text{ }^\circ\text{C}$. On the next step, the seeds were added to the mixture of SnCl₄·5H₂O, TEAOH and TEOS after the aging of the mixture had been complete. Three weeks of crystallization in an autoclave at $140\text{ }^\circ\text{C}$ followed by calcination at $550\text{ }^\circ\text{C}$ gave crystalline Sn-Beta zeolite (Figure 4.1).

The next step was to study the transformations of acetaldehyde **67** over the Sn-Beta catalyst (Table 4.1). The only product detected by GC in the experiment with a 10 wt% aqueous solution of **67** was crotonaldehyde **72** (entry 4). Another possible product could be aldol **70** which was dehydrated on a column during the GC analysis. Regardless of which of these two products was really formed, this result clearly showed that only two molecules

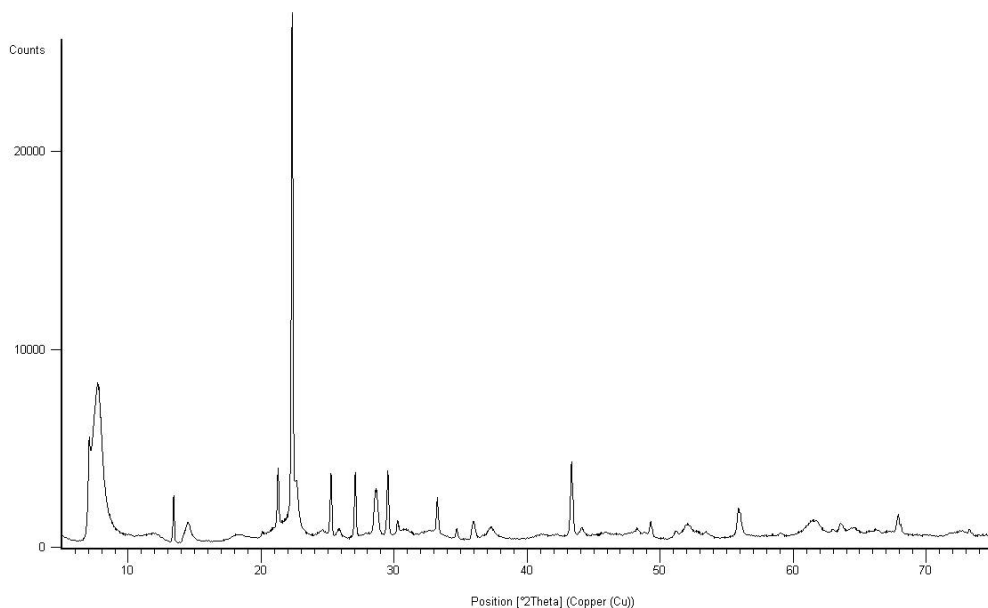


Figure 4.1: Powder X-ray diffraction pattern for the synthesized Sn-Beta.

of acetaldehyde were coupled without any further transformations represented in Scheme 4.2. Using a more concentrated solution or pure acetaldehyde as a feed increased the yield of crotonaldehyde but did not lead to any other transformations (entries 5 and 6). It was also shown that the yield of compound **72** was higher at higher temperatures (entries 6–8) but again crotonaldehyde was the only detected product.

Two other Beta-zeolites with Lewis acidic centers (Al-Beta and Ti-Beta, entries 9 and 10) as well as amorphous Sn-MCM-41 (entry 11) were tested and it was found that neither of them were capable of catalyzing any additional transformations as compared with Sn-Beta.

There could be several explanations of the low yields of crotonaldehyde obtained in the reaction and the fact that no further transformations were observed. First, this could be due to issues with the experimental set up, such as short contact time of acetaldehyde with a catalyst. During the study, the contact time was increased but it did not lead to higher yields. Probably, the flow rate should have been decreased more which would have led to longer contact time. Another reason could be the low concentration of the feed. Even though increasing the concentration did improve the yields it did not change the overall picture of the transformation and crotonaldehyde was still the

Table 4.1: Conditions of the acetaldehyde coupling reactions.

Entry	Catalyst	C(CH ₃ CHO), wt%	T, °C	Time, h	Yield, % ^a
1	MgO	10	150	2	0
2	TS-1	10	150	4	7.4
3	TS-1	20	150	4	7.6
4	Sn-Beta	10	150	4	1.2
5	Sn-Beta	20	150	2	1.5
6	Sn-Beta	100	150	2	2.6
7	Sn-Beta	100	125	2	1.3
8	Sn-Beta	100	175	2	5.6
9	Al-Beta	20	150	2	0.7
10	Ti-Beta	20	150	2	1.4
11	Sn-MCM-41	100	150	2	1.1

^a – yield of crotonaldehyde

only product in a low yield. A low activity of the catalysts used in the aldol reaction with acetaldehyde could also explain the observed results. Finally, a very small amount of aldol **70** could have been formed which was not enough for effective participating in further Meerwein-Ponndorf-Verley reduction of the carbonyl compounds present in the reaction mixture.

Additional experiments are required for clarifying why the reaction performed poorly and for improving the transformation conditions.

4.3 Conclusion

During the study Sn-Beta zeolite was synthesized and its activity was tested in the aldol reaction and Meerwein-Ponndorf-Verley reduction of acetaldehyde. It was shown that this catalyst was only capable of producing crotonaldehyde in low yields. Several other heterogeneous catalysts were tested (Al-Beta, Ti-Beta, Sn-MCM-41, TS-1) but none of them demonstrated substantially higher activity in the studied transformations.

4.4 Experimental Part

4.4.1 General Methods

All chemicals used in the study were purchased from Sigma-Aldrich and used without further purification. GC-analysis was performed on an Agilent 6890N instrument with an FID-detector equipped with an HP-5 capillary column (30 m × 320 μm × 0.25 μm). A helium flow-rate of 6.0 mL·min⁻¹ pressurized at 1.498 bar was used.

4.4.2 Synthesis of the Catalysts

Synthesis of zeolite Beta seeds The synthesis was performed according to the work of Taarning *et al.*¹⁴⁸ AlCl₃·6H₂O (1.85 g, 7.6 mmol) was dissolved in water (4.33 g) and a solution of tetraethylammonium hydroxide (TEAOH) (45.24 g of a 35 wt% aqueous solution, 108 mmol) followed by addition of tetraethyl orthosilicate (TEOS) (40 g, 192 mmol). The resulting gel was aged for 9 h under stirring. The mixture was transferred to a Teflon cup with lid and fitted into a stainless steel autoclave for crystallization which took place for 3 days at 140 °C. The product was isolated and washed by centrifugation and then it was dried at 110 °C overnight. After that the product was dealuminated by heating under stirring in HNO₃ (60 wt% aqueous solution, approx. 50 g of the solution per 1 g of zeolite) at 80 °C for 24 h. The dealuminated zeolite was isolated by suction filtration, washed thoroughly with demineralized water and dried overnight at 110 °C. The zeolite was calcined in static air at 550 °C for 6 h using a ramp of 2 °C·min⁻¹ to remove the structure directing agent.

Synthesis of Sn-Beta The synthesis was performed according to the work of Taarning *et al.*¹⁴⁸ TEOS (30 g, 144 mmol) was mixed with TEAOH (33 g of a 35 wt% aqueous solution, 79 mmol) for 90 min. Then, a solution of SnCl₄·5H₂O (0.42 g, 1.6 mmol) in water (2.75 g) was added and the resulting gel was aged for 8 h under stirring. During this process ethanol formed from the hydrolysis of TEOS was evaporating. HF (3.86 g of a 40 wt% aqueous solution, 77.2 mmol) was added drop-wise under stirring which produced a rigid gel. Dealuminated zeolite Beta seeds (0.36 g) were sonicated in water (1.75 g) for 5 min and then added to the gel. It was manually homogenized

¹⁴⁸TAARNING, E.; SARAVANAMURUGAN, S.; HOLM, M. S.; XIONG, J.; WEST, R. M.; CHRISTENSEN, C. H. *ChemSusChem* **2009**, *2*, 625–627.

4.4 Experimental Part

with a plastic spatula before it was transferred to a Teflon cup with lid which was inserted into a stainless steel autoclave for crystallization at 140 °C for 21 day. After that the product was filtered off, washed with distilled water and dried overnight at 110 °C. The zeolite was calcined in static air at 550 °C for 6 h using a ramp of 2 °C·min⁻¹ to remove the structure directing agent.

4.4.3 Performing the Reactions

The reactions were carried out in a continuous flow reactor filled with a catalyst with a particle size from 200 to 250 microns placed in a preheated oven. The catalyst was tableted, crashed in a mortar and then sifted through 200–250 mesh. An aqueous solution of acetaldehyde was pumped into the system with a rate 0.2 mL·min⁻¹. When pure acetaldehyde was used, a carrier gas (N₂) was bubbled through a flask with acetaldehyde to take its vapors into the system. In all the experiments a carrier gas flow rate was 49 mL·min⁻¹. In the experiments, weight hourly space velocity varied from 0.2 to 1.5 g_{react}·h⁻¹·g_{cat}⁻¹. To collect the products of the reaction a condenser (coolant temperature from -15 to 1 °C depending on the reaction) was attached. The samples from the collector were analyzed by GC with 1-pentanol as a standard (was added to the sample before each GC run).

Conclusion

THE THESIS IS DIVIDED INTO FOUR PARTS describing the research conducted during the PhD study. The first part discusses the mechanistic investigation of the ruthenium-catalyzed dehydrogenative synthesis of amides from alcohols and amines. A combination of experimental and theoretical methods has been employed. The Hammett study, experiments with deuterium-labeled compounds, determination of the reaction orders and the kinetic isotope effect provided valuable information about the reaction which was further used in the DFT calculations. A plausible catalytic cycle was proposed accounting for all data obtained during the investigation.

In the second part, the proposed catalytic cycle was employed for the computer-based search for more effective carbene ligands. The initial selection of the ligands for the screening was done based on the Tolman electronic parameter. It was attempted to synthesize ruthenium complexes with promising reactivity.

The third part deals with a study of the ruthenium-catalyzed dehydrogenative self-coupling of primary and secondary alcohols. An improved protocol for the synthesis of esters from primary alcohols was developed. A new self-coupling reaction of secondary alcohols was discovered which proceeded through a sequence of oxidation–aldol condensation–reduction to give the corresponding alkylated ketone. The mechanism of this transformation was studied.

The final part describes the work performed during the external stay at the company Haldor Topsøe A/S. Transformations of acetaldehyde over several zeolite-type heterogeneous catalysts was studied.

To conclude, this thesis supports the idea that a thorough mechanistic investigation is a useful tool in developing and improving catalytic reactions. Although a more effective catalyst has not been synthesized, we believe that it was primarily due to the lack of time and not due to the ineffectiveness of the approach. This work also shows that there is always room for a serendipitous discovery such as the self-coupling of the secondary alcohols. Many parameters of the reaction were studied and optimized, while other were left untouched, for example, stereospecificity. Further development in this direction could make the reaction even more attractive.

5 Bibliography

- (1) NORDSTRØM, L. U.; VOGT, H.; MADSEN, R. *J. Am. Chem. Soc.* **2008**, *130*, 17672–17673.
- (2) CAREY, J. S.; LAFFAN, D.; THOMSON, C.; WILLIAMS, M. T. *Org. Biomol. Chem.* **2006**, *4*, 2337–2347.
- (3) *The Amide Linkage: Structural Significance in Chemistry, Biochemistry, and Materials Science*; GREENBERG, A., BRENNEMAN, C. M., LIEBMAN, J. F., Eds.; Wiley-Interscience: New York, 2000.
- (4) PATTABIRAMAN, V. R.; BODE, J. W. *Nature* **2011**, *480*, 471–479.
- (5) SMITH, P. A. S. In *Organic reactions*, 1946; Vol. 3.
- (6) GAWLEY, R. E. In *Organic reactions*, 1988; Vol. 35.
- (7) CONSTABLE, D. J. C.; DUNN, P. J.; HAYLER, J. D.; HUMPHREY, G. R.; LEAZER, JR., J. L.; LINDERMAN, R. J.; LORENZ, K.; MANLEY, J.; PEARLMAN, B. A.; WELLS, A.; ZAKS, A.; ZHANG, T. Y. *Green Chem.* **2007**, *9*, 411–420.
- (8) ARORA, R.; PAUL, S.; GUPTA, R. *Can. J. Chem.* **2005**, *83*, 1137–1140.
- (9) GOTO, A.; ENDO, K.; SAITO, S. *Angew. Chem. Int. Ed.* **2008**, *47*, 3607–3609.
- (10) MURAHASHI, S.-I.; NAOTA, T.; SAITO, E. *J. Am. Chem. Soc.* **1986**, *108*, 7846–7847.
- (11) EKOUE-KOVI, K.; WOLF, C. *Chem. Eur. J.* **2008**, *14*, 6302–6315.
- (12) QIAN, C.; ZHANG, X.; ZHANG, Y.; SHEN, Q. *J. Organomet. Chem.* **2010**, *695*, 747–752.
- (13) ALLEN, C. L.; DAVULCU, S.; WILLIAMS, J. M. *J. Org. Lett.* **2010**, *12*, 5096–5099.
- (14) NAOTA, T.; MURAHASHI, S.-I. *Synlett* **1991**, *1991*, 693–694.
- (15) WANG, Y.; ZHU, D.; TANG, L.; WANG, S.; WANG, Z. *Angew. Chem. Int. Ed.* **2011**, *50*, 8917–8921.
- (16) SOULÉ, J.-F.; MIYAMURA, H.; KOBAYASHI, S. *J. Am. Chem. Soc.* **2011**, *133*, 18550–18553.

5 Bibliography

- (17) GUNANATHAN, C.; BEN-DAVID, Y.; MILSTEIN, D. *Science* **2007**, *317*, 790–792.
- (18) GHOSH, S. C.; MUTHAIAH, S.; ZHANG, Y.; XU, X.; HONG, S. H. *Adv. Synth. Catal.* **2009**, *351*, 2643–2649.
- (19) DAM, J. H.; OSZTROVSZKY, G.; NORDSTRØM, L. U.; MADSEN, R. *Chem. Eur. J.* **2010**, *16*, 6820–6827.
- (20) NOVA, A.; BALCELLS, D.; SCHLEY, N. D.; DOBEREINER, G. E.; CRABTREE, R. H.; EISENSTEIN, O. *Organometallics* **2010**, *29*, 6548–6558.
- (21) PRADES, A.; PERIS, E.; ALBRECHT, M. *Organometallics* **2011**, *30*, 1162–1167.
- (22) SHIMIZU, K.-I.; OHSHIMA, K.; ATSUSHI, S.; SATSUMA, A. *Chem. Eur. J.* **2009**, *15*, 9977–9980.
- (23) ZHU, J.; ZHANG, Y.; SHI, F.; DENG, Y. *Tetrahedron Lett.* **2012**, *53*, 3178–3180.
- (24) GNANAPRAKASAM, B.; BALARAMAN, E.; BEN-DAVID, Y.; MILSTEIN, D. *Angew. Chem. Int. Ed.* **2011**, *50*, 12240–12244.
- (25) ZENG, H.; GUAN, Z. *J. Am. Chem. Soc.* **2011**, *133*, 1159–1161.
- (26) YAMAGUCHI, K.; KOBAYASHI, H.; OISHI, T.; MIZUNO, N. *Angew. Chem. Int. Ed.* **2012**, *51*, 544–547.
- (27) MUTHAIAH, S.; GHOSH, S. C.; JEE, J.-E.; CHEN, C.; ZHANG, J.; HONG, S. H. *J. Org. Chem.* **2010**, *75*, 3002–3006.
- (28) GNANAPRAKASAM, B.; ZHANG, J.; MILSTEIN, D. *Angew. Chem. Int. Ed.* **2010**, *49*, 1468–1471.
- (29) MAGGI, A.; MADSEN, R. *Organometallics* **2012**, *31*, 451–455.
- (30) HAMMETT, L. P. *J. Am. Chem. Soc.* **1937**, *59*, 96–103.
- (31) WILLIAMS, A., *Free Energy Relationships in Organic and Bio-Organic Chemistry*; Royal Society of Chemistry: Cambridge, 2003.
- (32) SWAIN, C. G.; LUPTON, E. C. *J. Am. Chem. Soc.* **1968**, *90*, 4328–4337.
- (33) YUKAWA, Y.; TSUNO, Y. *Bull. Chem. Soc. Jpn.* **1959**, *32*, 965–971.
- (34) TAFT, R. W. *J. Am. Chem. Soc.* **1952**, *74*, 3120–3128.
- (35) HANSCH, C.; LEO, A.; TAFT, R. W. *Chem. Rev.* **1991**, *91*, 165–195.
- (36) RASMUSSEN, T.; JENSEN, J. F.; OSTERGAARD, N.; TANNER, D.; ZIEGLER, T.; NORRBY, P.-O. *Chem. Eur. J.* **2002**, *8*, 177–184.

- (37) KEINICKE, L.; FRISTRUP, P.; NORRBY, P.-O.; MADSEN, R. *J. Am. Chem. Soc.* **2005**, *127*, 15756–15761.
- (38) FRISTRUP, P.; KREIS, M.; PALMELUND, A.; NORRBY, P.-O.; MADSEN, R. *J. Am. Chem. Soc.* **2008**, *130*, 5206–5215.
- (39) DEPREZ, N. R.; SANFORD, M. S. *J. Am. Chem. Soc.* **2009**, 11234–11241.
- (40) LEE, D.-H.; KWON, K.-H.; YI, C. S. *Science* **2011**, *333*, 1613–1616.
- (41) SIMMONS, E. M.; HARTWIG, J. F. *Angew. Chem. Int. Ed.* **2012**, *51*, 3066–3072.
- (42) GÓMEZ-GALLEGO, M.; SIERRA, M. A. *Chem. Rev.* **2011**, *111*, 4857–4963.
- (43) AMATORE, C.; JUTAND, A. *J. Organomet. Chem.* **1999**, *576*, 254–278.
- (44) KOZUCH, S.; SHAIK, S. *Acc. Chem. Res.* **2011**, *44*, 101–110.
- (45) KOZUCH, S.; SHAIK, S. *J. Am. Chem. Soc.* **2006**, *128*, 3355–3365.
- (46) KOZUCH, S.; SHAIK, S. *J. Phys. Chem. A* **2008**, *112*, 6032–6041.
- (47) UHE, A.; KOZUCH, S.; SHAIK, S. *J. Comp. Chem.* **2011**, *32*, 978–985.
- (48) LEACH, A. R., *Molecular Modelling: Principles and Applications*, 2nd ed.; Pearson Education Limited: 2001.
- (49) JENSEN, J. H., *Molecular Modeling Basics*; CRC Press: 2010.
- (50) HOHENBERG, P.; KOHN, W. *Phys. Rev.* **1964**, *136*, B864–B871.
- (51) KOHN, W.; SHAM, L. J. *Phys. Rev.* **1965**, *140*, A1133–A1138.
- (52) BECKE, A. D. *Phys. Rev. A* **1988**, *38*, 3098–3100.
- (53) LEE, C.; YANG, W.; PARR, R. G. *Phys. Rev. B* **1988**, *37*, 785–789.
- (54) BECKE, A. D. *J. Chem. Phys.* **1993**, *98*, 5648–5652.
- (55) KOHN, W.; BECKE, A. D.; PARR, R. G. *J. Phys. Chem.* **1996**, *100*, 12974–12980.
- (56) KOHN, W.; MEIR, Y.; MAKAROV, D. *Phys. Rev. Letters* **1998**, *80*, 4153–4156.
- (57) DOBSON, J. F.; MCLENNAN, K.; RUBIO, A. *Aust. J. Chem.* **2002**, *54*, 513–527.
- (58) GRIMME, S. *J. Comp. Chem.* **2004**, *25*, 1463–1473.
- (59) ZHAO, Y.; TRUHLAR, D. G. *Acc. Chem. Res.* **2008**, *41*, 157–167.
- (60) AVERKIEV, B. B.; ZHAO, Y.; TRUHLAR, D. G. *J. Mol. Catal. A* **2010**, *324*, 80–88.

- (61) ZHAO, Y.; TRUHLAR, D. G. *Theor. Chem. Acc.* **2008**, *120*, 215–241.
- (62) BANTREIL, X.; PRESTAT, G.; MORENO, A.; MADEC, D.; FRISTRUP, P.; NORBY, P.-O.; PREGOSIN, P. S.; POLI, G. *Chem. Eur. J.* **2011**, *17*, 2885–2896.
- (63) NETHERTON, M. R.; FU, G. C. *Org. Lett.* **2001**, *3*, 4295–4298.
- (64) CREAMY, X.; MEHRSHEIKH-MOHAMMADI, M. E.; McDONALD, S. J. *Org. Chem.* **1987**, *52*, 3254–3263.
- (65) BOSSON, J.; POATER, A.; CAVALLO, L.; NOLAN, S. P. *J. Am. Chem. Soc.* **2010**, *132*, 13146–13149.
- (66) ZHANG, Y.; CHEN, C.; GHOSH, S. C.; LI, Y.; HONG, S. H. *Organometallics* **2010**, *29*, 1374–1378.
- (67) LEE, H. M.; SMITH, D. C.; HE, Z.; STEVENS, E. D.; YI, C. S.; NOLAN, S. P. *Organometallics* **2001**, *20*, 794–797.
- (68) WERTZ, D. J. *Am. Chem. Soc.* **1980**, *102*, 5316–5322.
- (69) LAU, J. K. C.; DEUBEL, D. V. *J. Chem. Theory Comput.* **2006**, *2*, 103–106.
- (70) FRISTRUP, P.; TURSKY, M.; MADSEN, R. *Org. Biomol. Chem.* **2012**, *10*, 2569–2577.
- (71) ARANYOS, A.; CSJERNYIK, G.; SZABÓ, K. J.; BÄCKVALL, J.-E. *Chem. Commun.* **1999**, *2*, 351–352.
- (72) SOLARI, E.; GAUTHIER, S.; SCOPELLITI, R.; SEVERIN, K. *Organometallics* **2009**, *28*, 4519–4526.
- (73) SIEFFERT, N.; BÜHL, M. J. *Am. Chem. Soc.* **2010**, *132*, 8056–8070.
- (74) DAM, J. H. *Organometallic Reactions: Development, Mechanistic Studies and Synthetic Applications*, PhD Thesis, Technical University of Denmark, 2009, pp 87–110.
- (75) SCHLEY, N. D.; DOBEREINER, G. E.; CRABTREE, R. H. *Organometallics* **2011**, 4174–4179.
- (76) *Jaguar, version 7.8*, Schrödinger, LLC, New York, NY, 2011.
- (77) HAY, P. J.; WADT, W. R. *J. Chem. Phys.* **1985**, *82*, 270–283.
- (78) CHAIKIN, S. W.; BROWN, W. G. *J. Am. Chem. Soc.* **1949**, *71*, 122–125.
- (79) BENNETT, M. A.; SMITH, A. K. *J. Chem. Soc., Dalton Trans.* **1974**, 233–241.
- (80) JO, Y.; JU, J.; CHOE, J.; SONG, K. H.; LEE, S. *J. Org. Chem.* **2009**, *74*, 6358–6361.

- (81) ISHIHARA, K.; YANO, T. *Org. Lett.* **2004**, *6*, 1983–1986.
- (82) NORDSTRØM, L. U. *Methods for Transition Metal Catalyzed C–N Bond Formation and Organocatalytic Allylation of Aldehydes*, PhD Thesis, Technical University of Denmark, 2008.
- (83) TOLMAN, C. *Chem. Rev.* **1977**, *77*, 313–348.
- (84) KELLY III, R. A.; CLAVIER, H.; GIUDICE, S.; SCOTT, N. M.; STEVENS, E. D.; BORDNER, J.; SAMARDJIEV, I.; HOFF, C. D.; CAVALLO, L.; NOLAN, S. P. *Organometallics* **2008**, *27*, 202–210.
- (85) GUSEV, D. G. *Organometallics* **2009**, *28*, 763–770.
- (86) GUSEV, D. G. *Organometallics* **2009**, *28*, 6458–6461.
- (87) TONNER, R.; FRENKING, G. *Organometallics* **2009**, *28*, 3901–3905.
- (88) ALTENHOFF, G.; GODDARD, R.; LEHMANN, C. W.; GLORIUS, F. *Angew. Chem. Int. Ed.* **2003**, *42*, 3690–3693.
- (89) ALTENHOFF, G.; GODDARD, R.; LEHMANN, C. W.; GLORIUS, F. *J. Am. Chem. Soc.* **2004**, *126*, 15195–15201.
- (90) BUTULA, I.; KARLOVIĆ, G. *Liebigs Ann. Chem.* **1976**, 1455–1464.
- (91) LEVY, J.-N.; LATHAM, C. M.; ROISIN, L.; KANDZIORA, N.; DI FRUSCIA, P.; WHITE, A. J. P.; WOODWARD, S.; FUCHTER, M. J. *Org. Biomol. Chem.* **2012**, *10*, 512–515.
- (92) RAUBENHEIMER, H. G.; CRONJE, S. *Dalton Trans.* **2008**, 1265–1272.
- (93) SCHUSTER, O.; YANG, L.; RAUBENHEIMER, H. G.; ALBRECHT, M. *Chem. Rev.* **2009**, *109*, 3445–3478.
- (94) STRASSER, C. E.; STANDER-GROBLER, E.; SCHUSTER, O.; CRONJE, S.; RAUBENHEIMER, H. G. *Eur. J. Inorg. Chem.* **2009**, 1905–1912.
- (95) VOUTCHKOVA, A. M.; APPELHANS, L. N.; CHIANESE, A. R.; CRABTREE, R. H. *J. Am. Chem. Soc.* **2005**, *127*, 17624–17625.
- (96) DRÖGE, T.; GLORIUS, F. *Angew. Chem. Int. Ed.* **2010**, *49*, 6940–6952.
- (97) MARZI, E.; BIGI, A.; SCHLOSSER, M. *Eur. J. Org. Chem.* **2001**, 1371–1376.
- (98) BUNCCEL, E.; KEUM, S.-R. *Tetrahedron* **1983**, *39*, 1091–1101.
- (99) PHILLIPS, S. T.; REZAC, M.; ABEL, U.; KOSSENJANS, M.; BARTLETT, P. A. J. *Am. Chem. Soc.* **2002**, *124*, 58–66.
- (100) KOSOWER, E.; PATTON, J. J. *Org. Chem.* **1961**, *26*, 1318–1319.

5 Bibliography

- (101) SØLVHØJ, A.; MADSEN, R. *Organometallics* **2011**, *30*, 6044–6048.
- (102) BLUM, Y.; RESHEF, D.; SHVO, Y. *Tetrahedron Lett.* **1981**, *22*, 1541–1544.
- (103) MURAHASHI, S.-I.; ITO, K.-I.; NAOTA, T.; MAEDA, Y. *Tetrahedron Lett.* **1981**, *22*, 5327–5330.
- (104) BLUM, Y.; SHVO, Y. *J. Organomet. Chem.* **1984**, *263*, 93–107.
- (105) BLUM, Y.; SHVO, Y. *J. Organomet. Chem.* **1985**, *282*, C7–C10.
- (106) MURAHASHI, S.-I.; NAOTA, T.; ITO, K.; MAEDA, Y.; TAKI, H. *J. Org. Chem.* **1987**, *52*, 4319–4327.
- (107) ZHANG, J.; LEITUS, G.; BEN-DAVID, Y.; MILSTEIN, D. *J. Am. Chem. Soc.* **2005**, *127*, 10840–10841.
- (108) ZHANG, J.; GANDELMAN, M.; SHIMON, L. J. W.; MILSTEIN, D. *Dalton Trans.* **2007**, 107–113.
- (109) DEL POZO, C.; IGLESIAS, M.; SÁNCHEZ, F. *Organometallics* **2011**, *30*, 2180–2188.
- (110) SPASYUK, D.; SMITH, S.; GUSEV, D. G. *Angew. Chem. Int. Ed.* **2012**, *51*, 2772–2775.
- (111) NIELSEN, M.; JUNGE, H.; KAMMER, A.; BELLER, M. *Angew. Chem. Int. Ed.* **2012**, *51*, 5711–5713.
- (112) SRIMANI, D.; BALARAMAN, E.; GNANAPRAKASAM, B.; BEN-DAVID, Y.; MILSTEIN, D. *Adv. Synth. Catal.* **2012**, *354*, 2403–2406.
- (113) BURLING, S.; PAINE, B. M.; NAMA, D.; BROWN, V. S.; MAHON, M. F.; PRIOR, T. J.; PREGOSIN, P. S.; WHITTLESEY, M. K.; WILLIAMS, J. M. J. *J. Am. Chem. Soc.* **2007**, *129*, 1987–1995.
- (114) EDWARDS, M. G.; JAZZAR, R. F. R.; PAINE, B. M.; SHERMER, D. J.; WHITTLESEY, M. K.; WILLIAMS, J. M. J.; EDNEY, D. D. *Chem. Commun.* **2004**, 90–91.
- (115) MOTOKURA, K.; NISHIMURA, D.; MORI, K.; MIZUGAKI, T.; EBITANI, K.; KANEDA, K. *J. Am. Chem. Soc.* **2004**, *126*, 5662–5663.
- (116) CHO, C. S.; KIM, B. T.; KIM, T.-J.; CHUL SHIM, S. *Tetrahedron Lett.* **2002**, *43*, 7987–7989.
- (117) CHO, C. S.; KIM, B. T.; KIM, T.-J.; SHIM, S. C. *J. Org. Chem.* **2001**, *66*, 9020–9022.

- (118) SLATFORD, P. A.; WHITTLESEY, M. K.; WILLIAMS, J. M. J. *Tetrahedron Lett.* **2006**, 47, 6787–6789.
- (119) GNANAMGARI, D.; LEUNG, C. H.; SCHLEY, N. D.; HILTON, S. T.; CRABTREE, R. H. *Org. Biomol. Chem.* **2008**, 6, 4442–4445.
- (120) CHO, C. S.; KIM, B. T.; KIM, H.-S.; KIM, T.-J.; SHIM, S. C. *Organometallics* **2003**, 22, 3608–3610.
- (121) GUERBET, M. C. *R. Acad. Sci.* **1899**, 128, 1002–1004.
- (122) GUERBET, M. C. *R. Acad. Sci.* **1909**, 149, 129–132.
- (123) ALLEN, L. J.; CRABTREE, R. H. *Green Chem.* **2010**, 12, 1362–1364.
- (124) GUILLENA, G.; RAMÓN, D. J.; YUS, M. *Angew. Chem. Int. Ed.* **2007**, 46, 2358–2364.
- (125) HAMID, M. H. S. A.; SLATFORD, P. A.; WILLIAMS, J. M. J. *Adv. Synth. Catal.* **2007**, 349, 1555–1575.
- (126) NIXON, T. D.; WHITTLESEY, M. K.; WILLIAMS, J. M. J. *Dalton Trans.* **2009**, 753–762.
- (127) GIUNTA, D.; HOELSCHER, M.; LEHMANN, C. W.; MYNOTT, R.; WIRTZ, C.; LEITNER, W. *Adv. Synth. Catal.* **2003**, 345, 1139–1145.
- (128) BURLING, S.; MAHON, M. F.; PAINE, B. M.; WHITTLESEY, M. K.; WILLIAMS, J. M. J. *Organometallics* **2004**, 23, 4537–4539.
- (129) KINDT-LARSEN, T.; BITSCH, V.; ANDERSEN, I. G. K.; JART, A.; MUNCH-PETERSEN, J. *Acta Chem. Scand.* **1963**, 17, 1426–1432.
- (130) BROWN, H. C.; KULKARNI, S. V.; RACHERLA, U. S.; DHOKTE, U. P. *J. Org. Chem.* **1998**, 63, 7030–7036.
- (131) KANAZAWA, Y.; TSUCHIYA, Y.; KOBAYASHI, K.; SHIOMI, T.; ITOH, J.-I.; KIKUCHI, M.; YAMAMOTO, Y.; NISHIYAMA, H. *Chem. Eur. J.* **2005**, 12, 63–71.
- (132) In *Modern Aldol Reactions*, MAHRWALD, R., Ed.; WILEY-VCH Verlag GmbH & Co. KGaA: Weinheim, 2004; Vol. 1, 2.
- (133) JI, W.; CHEN, Y.; KUNG, H. H. *Appl. Catal. A: Gen.* **1997**, 161, 93–104.
- (134) ORDOMSKY, V. V.; SUSHKEVICH, V. L.; IVANOVA, I. I. *J. Mol. Catal. A* **2010**, 333, 85–93.
- (135) RASKÓ, J.; KISS, J. *Appl. Catal. A: Gen.* **2005**, 287, 252–260.
- (136) CHANG, Y.-C.; KO, A.-N. *Appl. Catal. A: Gen.* **2000**, 190, 149–155.

5 Bibliography

- (137) DUMITRIU, E.; HULEA, V.; FECHETE, I.; AUROUX, A.; LACAZE, J.-F.; GUILMON, C. *Microporous and Mesoporous Materials* **2001**, *43*, 341–359.
- (138) KAGUNYA, W.; JONES, W. *Appl. Clay Sci.* **1995**, *10*, 95–102.
- (139) YOUNG, R.; SHEPPARD, N. *J. Catal.* **1967**, *7*, 223–233.
- (140) REKOSKE, J. E.; BARTEAU, M. A. *Ind. Eng. Chem. Res.* **2011**, *50*, 41–51.
- (141) CREYGHTON, E.; GANESHIE, S.; DOWNING, R.; VAN BEKKUM, H. *J. Mol. Catal. A* **1997**, *115*, 457–472.
- (142) VAN DER WAAL, J. C.; KUNKELER, P.; TAN, K.; VAN BEKKUM, H. *J. Catal.* **1998**, *173*, 74–83.
- (143) ZHU, Y.; CHUAH, G.; JAENICKE, S. *J. Catal.* **2004**, *227*, 1–10.
- (144) CORMA, A.; DOMINE, M. E.; NEMETH, L.; VALENCIA, S. *J. Am. Chem. Soc.* **2002**, *124*, 3194–3195.
- (145) CORMA, A.; DOMINE, M. E.; VALENCIA, S. *J. Catal.* **2003**, *215*, 294–304.
- (146) HOLM, M. S.; SARAVANAMURUGAN, S.; TAARNING, E. *Science* **2010**, *328*, 602–605.
- (147) HOLM, M. S.; PAGÁN-TORRES, Y. J.; SARAVANAMURUGAN, S.; RIISAGER, A.; DUMESIC, J. A.; TAARNING, E. *Green Chem.* **2012**, *14*, 702–706.
- (148) TAARNING, E.; SARAVANAMURUGAN, S.; HOLM, M. S.; XIONG, J.; WEST, R. M.; CHRISTENSEN, C. H. *ChemSusChem* **2009**, *2*, 625–627.

Appendix A

Publications prepared during the PhD study

1. Makarov, I. S.; Fristrup, P.; Madsen, R. *Chem. Eur. J.* **2012**, *18*, 15683–15692.

Mechanistic Investigation of the Ruthenium–N-Heterocyclic-Carbene-Catalyzed Amidation of Amines with Alcohols

Ilya S. Makarov, Peter Fristrup,* and Robert Madsen*^[a]

Abstract: The mechanism of the ruthenium–N-heterocyclic-carbene-catalyzed formation of amides from alcohols and amines was investigated by experimental techniques (Hammett studies, kinetic isotope effects) and by a computational study with dispersion-corrected density functional theory (DFT/M06). The Hammett study indicated that a small positive charge builds-up at the benzylic position in the transition state of the turnover-limiting step. The kinetic isotope effect was determined to be

2.29(±0.15), which suggests that the breakage of the C–H bond is not the rate-limiting step, but that it is one of several slow steps in the catalytic cycle. Rapid scrambling of hydrogen and deuterium at the α position of the alcohol was observed with deuterium-labeled substrates, which implies that the

Keywords: amides • density functional calculations • isotope effect • reaction mechanisms • ruthenium

catalytically active species is a ruthenium dihydride. The experimental results were supported by the characterization of a plausible catalytic cycle by using DFT/M06. Both *cis*-dihydride and *trans*-dihydride intermediates were considered, but when the theoretical turnover frequencies (TOFs) were derived directly from the calculated DFT/M06 energies, we found that only the *trans*-dihydride pathway was in agreement with the experimentally determined TOFs.

Introduction

The (carbox)amide group constitutes one of the most-significant functional groups in organic chemistry. The synthesis of amides is usually performed from carboxylic acids and amines by using a coupling reagent or by prior conversion of the acid into an activated derivative. Recently, however, several new and fundamentally different approaches to amide synthesis have been developed.^[1] These emerging methods include the umpolung synthesis from α -bromonitroalkanes,^[2] the decarboxylative condensation of α -ketoacids and hydroxylamines,^[3] and the metal-catalyzed coupling of primary alcohols and amines.^[4–6] This latter reaction can be carried out by aerobic oxidation with heterogeneous gold catalysts^[4] or by dehydrogenation with various homogeneous and heterogeneous catalysts.^[5,6] The dehydrogenative synthesis of amides from alcohols and amines can be performed both in the presence or absence of a hydrogen acceptor, such as a ketone or an alkene.^[5,6] The most-attractive procedures would avoid the need for hydrogen scavengers altogether, which can be achieved with homogeneous ruthenium pincers,^[5a] carbenes,^[5b,c] and diamine–diphosphine^[5d] complexes, as well as with heterogeneous Ag/Al₂O₃^[5e] and Au/hydrothermalite catalysts.^[5f] To further develop these amidation

procedures, it is important to gain a better understanding of the underlying reaction mechanisms. So far, the umpolung approach with α -bromonitroalkanes and the decarboxylative pathway with α -ketoacids have been studied with ¹⁸O-labeled substrates,^[7] whilst the first step in the dehydrogenative reaction with ruthenium pincer complexes has been investigated by low-temperature NMR spectroscopy.^[8] In addition, computational studies have been performed on the ruthenium-catalyzed transformations with pincer and diamine–diphosphine complexes.^[9]

The amidation reaction between primary alcohols and amines catalyzed by ruthenium–N-heterocyclic-carbene complexes was first reported by our group in 2008;^[5b] since then, this transformation has been further investigated with regard to catalyst precursors and substrate scope.^[10] This reaction is most-effectively catalyzed by complex **1** (Figure 1) in the presence of PCy₃ and KO^tBu. No stoichiometric additives are necessary and the amidation reaction produces hydrogen gas as the only byproduct. The reaction is believed to proceed through dehydrogenation of the alcohol into the corresponding aldehyde, which stays coordinated to the ruthenium catalyst (Scheme 1). Then, nucleophilic attack by the amine forms the hemiaminal, which is dehydrogenated to afford the amide. The fact that the intermediate aldehyde remains coordinated to the ruthenium center is an important observation that has been confirmed experimentally by a cross-

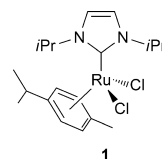
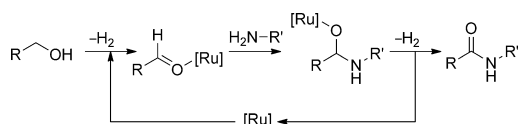


Figure 1. Structure of compound **1**.

[a] I. S. Makarov, Dr. P. Fristrup, Prof. Dr. R. Madsen
Department of Chemistry, Building 201
Technical University of Denmark, 2800 Kgs. Lyngby (Denmark)
Fax: (+45) 4593-3968
E-mail: pf@kemi.dtu.dk
rm@kemi.dtu.dk

Supporting information for this article is available on the WWW under <http://dx.doi.org/10.1002/chem.201202400>.



Scheme 1. Dehydrogenative synthesis of amides from alcohols and amines.

over experiment.^[10c] However, the mechanism of the amidation reaction has not previously been subjected to a more-thorough examination.

Herein, we report a combined experimental and theoretical mechanistic investigation of the formation of amides from alcohols and amines catalyzed by ruthenium–N-heterocyclic-carbene complex **1**.

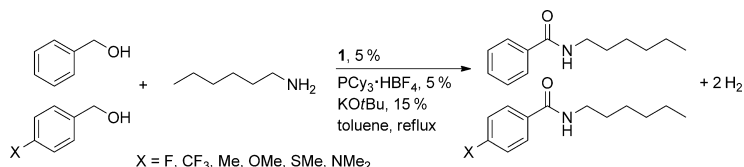
Results and Discussion

For the experimental study, the catalyst system was modified slightly to obtain more-accurate and reproducible results. Tricyclohexylphosphine is easily oxidized by air and commercial samples contain various amounts of impurities that are difficult to remove. To solve this problem, Netherton and Fu replaced trialkylphosphines with their corresponding HBF₄ salts in several metal-catalyzed reactions.^[11] These salts are air-stable and the phosphine can be released into the reaction with a Brønsted base. Moreover, because a base is already required for the amidation reaction, we decided to replace PCy₃ with PCy₃·HBF₄ and increase the amount of KO^tBu accordingly. This modification gave more-consistent results and, therefore, the experimental mechanistic study was performed on the following system: [RuCl₂(*i*Pr)(*p*-cymene)] (5 mol %), PCy₃·HBF₄ (5 mol %), and KO^tBu (15 mol %) in refluxing toluene.

Hammett study: We have previously used Hammett studies with *para*-substituted benzaldehydes to analyze the turnover-limiting step in several metal-mediated reactions.^[12] This method makes it possible to determine the change in charge at the benzylic position between the starting material and the transition state. Subsequently, the development of charge can be simulated *in silico*, based on a proposed catalytic cycle, and can be used to discriminate between different mechanistic scenarios. In this case, the Hammett study will be comprised of a series of competition reactions between benzyl alcohol and various *para*-substituted benzyl alcohols with hexylamine as the amine component (Scheme 2). First, the amidation reactions of hexylamine with different *para*-substituted benzyl alcohols were carried out and the reaction was found to proceed cleanly and in

high yield with both electron-donating and electron-withdrawing groups in the *para* position (Table 1).

Because the amidation reaction occurs with the negligible formation of byproducts, the course of the competition reactions could be followed by measuring the disappearance of the alcohols by using GC. Assuming that all of the substrates react according to the same mechanism and that the reaction is first order in the alcohol, their relative reactivi-



Scheme 2. Competition experiments for the amidation of benzyl alcohol versus that of *para*-substituted benzyl alcohols **2b–2g**.

Table 1. Amidation of *para*-substituted benzyl alcohols **2a–2g**.

Entry	Compound	X	Yield [%] ^[a]
1	2a	H	90
2	2b	CF ₃	70
3	2c	F	80
4	2d	Me	94
5	2e	OMe	100
6	2f	SMe	88
7	2g	NMe ₂	100

[a] Yield of isolated product after 24 h.

ties (k_X/k_H) can be obtained as the slope of the line when $\ln(c_0/c)$ for one *para*-substituted benzyl alcohol is plotted against the same values for benzyl alcohol. This plot resulted in good linear correlations for all six *para*-substituted benzyl alcohols (Figure 2), which confirmed the assumption that the amidation reaction was first order in the alcohol. In each case, the correlation coefficient was ≥ 0.99 and the benzyl alcohols with electron-donating *para* substituents reacted faster than alcohols with electron-withdrawing groups. The slopes could then be used to construct the Hammett plot based on σ values from the literature^[13] (Figure 3). The best correlation was achieved with σ^+ values, which afforded a straight line with a small negative slope ($\rho = -0.15$). This result indicates that a small positive charge is build-up at the benzylic position in the transition state of the turnover-limiting step. The correlation with Creary's σ' values was poor and, therefore, a radical intermediate is not involved in the amidation reaction. The oxidation of an alcohol into an amide is likely to proceed through two consecutive β -hydride eliminations, which result in the formation of an aldehyde and an amide, respectively. Either of these elimination steps are good candidates for the turnover-limiting step be-

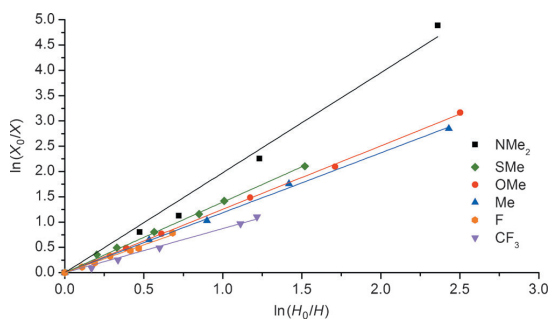


Figure 2. Kinetic data for the amidation of *para*-substituted benzyl alcohols **2b–2g** in competition with compound **2a** (“0” denotes initial concentration, X is the concentration of compounds **2b–2g**, and H is the concentration of compound **2a**).

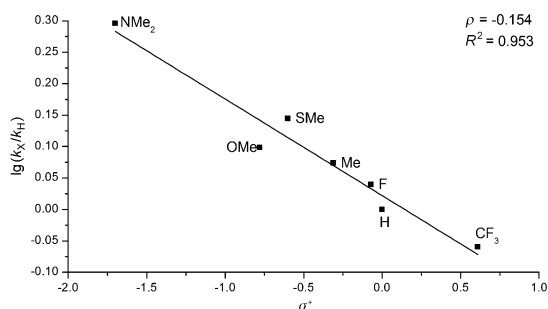


Figure 3. Hammett plot for the amidation of alcohols **2a–2g**.

cause, in both cases, a partial positive charge is formed at the benzylic position in the transition state.

Reaction order: To gain more information about the role of each component, we sought to determine the kinetic order in these constituents. First, the order in the amine was examined by varying the concentration of hexylamine from 0.2–0.5 M whilst keeping the concentration of benzyl alcohol (0.5 M) and the ruthenium catalyst (25 mM) constant. The initial rate of the reaction was determined for each concentration of amine and the rates were plotted against the amine concentrations to give a straight line, thus indicating a first-order dependence in the amine (Figure 4a).

The reaction order in phosphine was examined by varying the concentration of PCy_3 from 0–5 mM whilst keeping the concentrations of benzyl alcohol and hexylamine constant (0.2 M). A non-linear dependence was observed and an order of 0.5 in phosphine was derived from a double-logarithmic plot (Figure 4b). This reaction order will be further addressed in the computational study and used to pinpoint the role of phosphine in the reaction mechanism.

Attempts to establish the reaction order in the ruthenium catalyst were initially met with difficulties. At low catalyst loadings ($\leq 2\%$ or 10 mM), the amidation either proceeded with a long initiation period or did not proceed at all, which

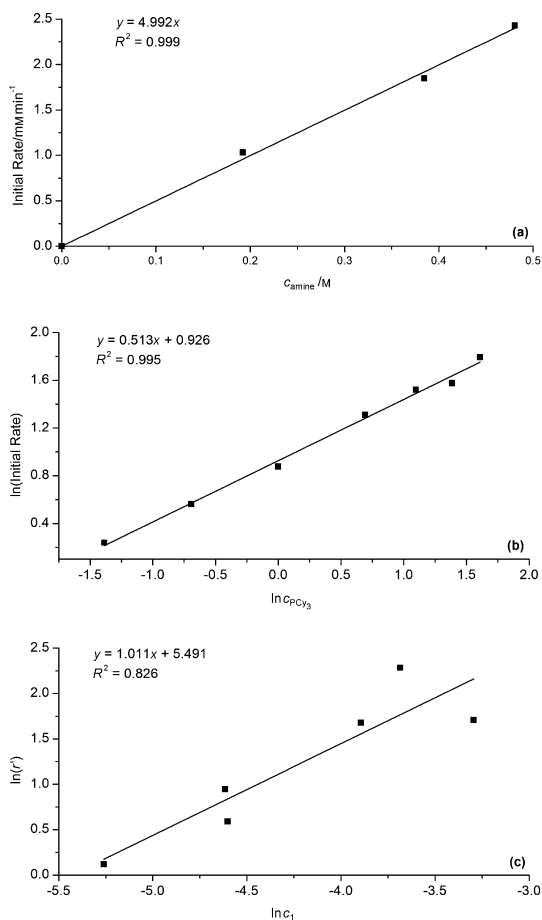


Figure 4. a) Plot of c_{amine} versus r_{init} ; b) plot of $\ln c_{\text{PCy}_3}$ versus $\ln r_{\text{init}}$; c) Plot of $\ln c_1$ versus $\ln r_{\text{init}}$.

made it impossible to obtain reproducible results. At higher loadings ($> 6\%$), the initial rate measurements were also accompanied by significant uncertainties. After some experimentation, we found that more-reproducible results could be obtained if complex **1** was treated with $\text{PCy}_3\text{-HBF}_4$ and $\text{KO}t\text{Bu}$ in refluxing toluene for 45 min before the alcohol and the amine were added. With this modification, the concentration of compound **1** was varied from 5–37 mM, whilst the concentrations of benzyl alcohol and hexylamine were kept constant (0.5 M). These data resulted in a straight line, as shown in Figure 4c, thus indicating a first-order dependence on the ruthenium catalyst. The experiments in Figure 4a were repeated under these slightly modified conditions and the same linear dependence was observed, which illustrates that the overall kinetics of the reaction have not been altered. The minimum amount of ruthenium catalyst for complete conversion under these conditions was about 1%, where the complete amidation of hexylamine with 2-

phenylethanol was observed in 24 h. This result should be compared to 0.1% loading with a ruthenium pincer complex^[5a] and to 4–5% loading with ruthenium–triazolyli-dine^[5c] and diamine–diphosphine^[5d] complexes.

Deuterium-labeled substrates: Initially, we planned to determine the kinetic isotope effect (KIE) by using competition experiments in a similar way to the Hammett study. [α,α -D₂]Benzyl alcohol would be allowed to compete with benzyl alcohol in a reaction with hexylamine and the KIE would be calculated by measuring the disappearance of the two alcohols, which would be separable by GC. However, we quickly discovered that this simple experiment was not feasible because a rapid scrambling of deuterium and hydrogen occurred at the α position of the alcohol under the amidation conditions. Accordingly, we decided to study this scrambling in more detail and, to exclude a possible side-reaction with benzylic radicals, these experiments were performed with 2-phenylethanol (**3**) as the alcohol substrate.

First, the source of the atom scrambling was determined (Table 2). The reaction between non-deuterated 2-phenylethanol and benzylamine was performed in [D₈]toluene and

Table 2. Experiments to determine the positions of the scrambled atoms.

$$\text{Ph-CH(OH)-CH}_2\text{-R}^1 + \text{Ph-NH-CH}_2\text{-R}^2 \xrightarrow[\text{solvent, reflux}]{\text{1, 5\% PCy}_3\text{:HBF}_4, \text{ 5\% KOtBu, 15\%}} \text{Ph-CH(O-CH}_2\text{-R}^1\text{)-C(=O)-CH}_2\text{-R}^2 + \text{H}_2/\text{D}_2$$

Entry	R ¹	R ²	Solvent
1	H (3)	H (4)	[D ₈]toluene
2	H (3)	D ([D ₂]- 4)	toluene
3	D ([D ₂]- 3)	H (5)	toluene

the relative amounts of non-deuterated, mono-deuterated, and di-deuterated alcohols were monitored by GCMS. This experiment showed no change in the deuterium content of the alcohol during the reaction, which demonstrates that no exchange with the solvent occurs (Figure 5, entry 1).

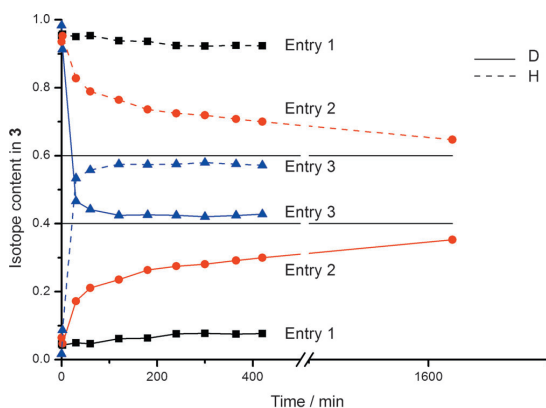


Figure 5. Experiments with deuterium-labeled substrates.

As a result, the exchangeable protons are most likely the two α protons on the primary alcohol, the O–H proton, and the two N–H protons in the primary amine. In a second experiment, non-deuterated 2-phenylethanol was reacted with BnND₂ and the deuterium content in the starting alcohol was monitored again as the reaction progressed (Figure 5, entry 2). This experiment showed that two hydrogen atoms in the alcohol were exchanged with deuterium and that the reaction must occur with the α protons because exchange of the O–H proton cannot be measured by GCMS. The scrambling occurred in such a fashion that an equilibrium was slowly reached at which the hydrogen/deuterium ratio for the two α protons was 3:2. This ratio is the same as that between the exchangeable hydrogen and deuterium atoms in the starting materials and confirms that all five protons take part in the scrambling. This result was verified by repeating the experiment with [D₂]- α,α -2-phenylethanol and non-deuterated benzylamine (Figure 5, entry 3). Again, equilibrium was reached at which the hydrogen/deuterium ratio for the two α protons in the alcohol was 3:2. However, in this case, the exchange occurred much more rapidly and was observed even before the amide had started to form. This result means that there is a reversible step at the beginning of the reaction, which most-likely involves a β -hydride elimination and a migratory insertion. More significantly, the scrambling implies that a ruthenium–dihydride species is involved in the catalytic cycle.

This result suggests that the two chloride ligands in complex **1** are not present in the catalytically active species, which, instead, is likely to be a ruthenium–dihydride species. To gain further support for this rationale, the two chloride atoms in complex **1** were replaced with a different halogen group. It has previously been shown that diiodide complexes [RuL₂(NHC)(*p*-cymene)] (NHC = IMe, IPr, and ICy) will also catalyze the amidation reaction,^[10e,h] although the yields vary, possibly owing to the lower stabilities of these complexes. However, when we measured the initial rate with complex [RuL₂(IPr)(*p*-cymene)] under the standard conditions with benzyl alcohol and hexylamine, we obtained a value of 3.09 mmmin⁻¹. This value is essentially the same as with complex **1** (3.37 mmmin⁻¹), which strongly suggests that the halides are not bound to the ruthenium center in the catalytic cycle.

Kinetic isotope effect: With the knowledge of the deuterium scrambling and the atoms that are involved in this process in hand, we designed an experiment to determine the KIE of the overall reaction. First, the hydrogen atoms at the exchangeable positions in both the alcohol and the amine were replaced with deuterium and the initial rates for both the deuterated and non-deuterated substrates were then measured in two separate experiments. For convenience, commercially available and fully deuterated [D₁₀]-1-butanol was selected as the alcohol, whilst BnND₂ was chosen as the amine part. The initial rate with these deuterated substrates was 6.44(±0.02) mmmin⁻¹, whilst the rate with non-deuterated 1-butanol and benzyl amine was 14.77(±0.96) mmmin⁻¹.

These values gave an experimental KIE of $2.29(\pm 0.15)$, which suggests that the breakage of the C–H bond is not the rate-limiting step, but instead is one of several slow steps in the catalytic cycle (see below).

NMR spectroscopy: The amidation reaction was also analyzed by NMR spectroscopy to identify possible intermediates during the transformation. First, we studied whether *p*-cymene stayed coordinated to the ruthenium center throughout the catalytic cycle. The reaction between compounds **3** and **4** was performed in $[D_8]$ toluene at 110°C with 15 mol% of compound **1** and with PPH_3 instead of $\text{PCy}_3\cdot\text{HBF}_4$ to avoid the presence of additional signals in the aliphatic region of the spectrum. Samples were removed from the reaction mixture and analyzed at ambient temperature. We found that, after only 3 min, 85% of *p*-cymene was in the solution in its unbound form and, after 10 min, *p*-cymene had completely decoordinated from the ruthenium atom.

Then, the reaction between 2-phenylethanol and benzylamine was monitored in $[D_8]$ toluene with the NMR probe temperature set at 70°C . A rather high catalyst loading was employed in this experiment with 40% of compound **1**, 40% of $\text{PCy}_3\cdot\text{HBF}_4$, and 120% of $\text{KO}t\text{Bu}$. During the reaction, several clusters of signals were detected in the hydride region of the spectrum. After 3 h, this cluster included low-intensity signals at $\delta = -7.44$ and -7.54 ppm, very low-intensity signals in the range $\delta = -10.66$ to -11.13 ppm, high-intensity doublets from $\delta = -17.41$ to -17.89 ppm ($J(\text{P,H}) \approx 20$ Hz), as well as a high-intensity doublet at $\delta = -18.04$ ppm ($J(\text{H,H}) = 7.1$ Hz). These observations clearly reveal that several hydride species are formed during the amidation reaction.^[10b] Moreover, the doublet at $\delta = -18.04$ ppm shows that there is a dihydride species that does not contain a phosphine group. The doublets from $\delta = -17.41$ to -17.89 ppm and their coupling constants suggest the presence of ruthenium–hydride complexes in which one phosphine group is coordinated *cis* to the hydride atom. Over time, the intensity of the signals decreased and some of them disappeared.

To study the reaction under conditions that were more similar to the actual setup, the amidation reaction was repeated in refluxing $[D_8]$ toluene with a catalyst loading of 20%. After 30 min, a sample was withdrawn and analyzed by ^1H and ^{31}P NMR spectroscopy at room temperature. In the ^1H NMR spectrum, several additional signals as well as the signals given above were observed in the hydride region, including a singlet at $\delta = -9.70$ ppm, a doublet at -15.04 ppm ($J(\text{P,H}) = 22.5$ Hz), and signals at $\delta \approx -17.8$ ppm. The presence of these signals also suggests the formation of several complexes in which the phosphine is *cis* to the hydride atom, as well as a complex without phosphine. The ^{31}P NMR spectrum reveals a group of signals in the range $\delta = 46$ – 51 ppm, a low-intensity signal at $\delta = 57.2$ ppm, and a high-intensity signal at $\delta = 10$ ppm. This latter signal is from free PCy_3 , whereas the others may be assigned to ruthenium intermediates that contain coordinat-

ed phosphine. Therefore, these spectroscopic data provide further support for the formation of mono- and dihydride–ruthenium species during the reaction. In addition, the NMR spectroscopy experiments have demonstrated that complexes both with and without phosphine are present in the reaction mixture.

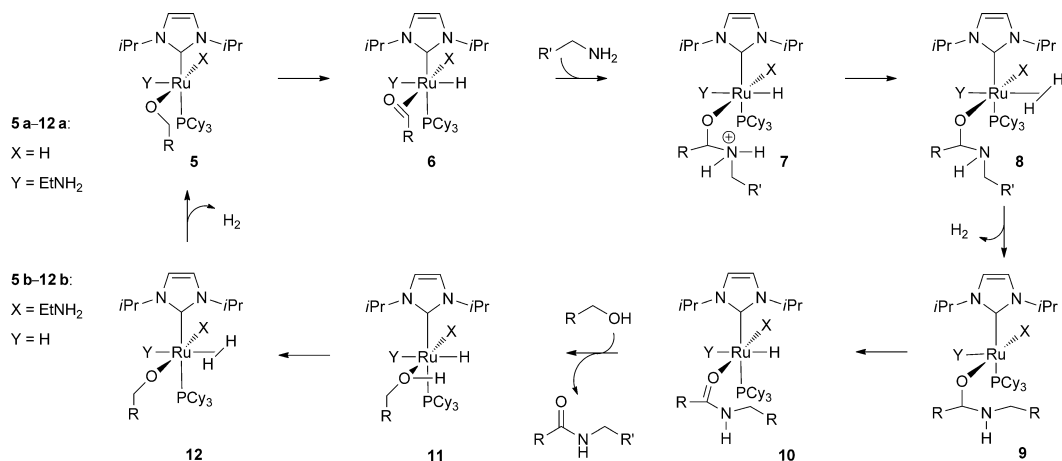
Computational study: To increase our understanding of the reaction pathway, our investigation was extended by performing a computational study, in line with earlier work.^[12] A simplified system was chosen in which ethylamine and benzyl alcohol were used as reactants and 1,3-diisopropylimidazol-2-ylidene (*iPr*) and PCy_3 were coordinated to the ruthenium atom. All of these calculations were performed by using the M06 functional, which includes non-bonding interactions (not the case with DFT/B3LYP). In all of these calculations, the total energy (ΔG_{tot}) was represented by a combination of gas-phase energy (E_{scf}), solution-phase energy (E_{solv}), and Gibbs free energy (ΔG), as shown in [Eq. (1)]. This approach was first suggested by Wertz^[14] and has later been applied in several studies of transition-metal-catalyzed reactions.^[12a,b,15] This procedure avoids the time-consuming and error-prone calculation of numerical frequencies in the solution phase.

$$\Delta G_{\text{tot}} = \Delta G - E_{\text{scf}} + E_{\text{solv}} \quad (1)$$

First, we were interested in identifying the ligands that could be coordinated to the ruthenium center during the catalytic cycle. The precursor complex (**1**) is an 18-electron ruthenium(II) species, which loses *p*-cymene during the initiation step. Another possible ligand is the amine moiety, which is present in stoichiometric amounts. The DFT calculations show that the coordination of one molecule of amine is very favorable, with a decrease in ΔG_{tot} from -31 to -107 kJ mol^{-1} , depending on the other ligands on the ruthenium atom. This result strongly implies that an amine is bound to the metal center throughout the reaction. However, the coordination of a second molecule of amine at the apical position of the complex is less favorable than the coordination of a phosphine at this position (ΔG_{tot} increases from 6 to 40 kJ mol^{-1} , depending on the other ligands on ruthenium atom).

A detailed study of the initiation of the reaction is beyond the scope of this investigation. However, for similar ruthenium(II)–dichloride complexes, it has been established that, in the presence of alcohols, the chloride ligands can be replaced with alkoxide and hydride groups.^[16] Thus, because the experimental study indicates that both chloride anions are replaced by other ligands, we decided to use 16-electron complex **5**, in which a hydride and an alkoxide ligand are coordinated to the ruthenium atom, as a starting point.

Our calculations show that complex **5** adopts a distorted octahedral orientation in which the two bulky ligands (*iPr* and phosphine) are in the apical positions and the amine, alkoxide, and hydride groups occupy the equatorial positions (Scheme 3). The alkoxide group must have an adjacent



Scheme 3. Proposed catalytic cycle (**a**: *cis*-dihydride pathway; **b**: *trans*-dihydride pathway).

empty site for β -hydride elimination to occur. As a consequence, the amine and hydride groups can be positioned in two different ways and, thus, form two isomers (**5a** and **5b**). Either of these isomers can serve as an entry point into the catalytic cycle.

Interestingly, these two isomers, compounds **5a** and **5b**, have almost the same energy ($\Delta\Delta G_{\text{tot}}(\mathbf{5a}-\mathbf{5b}) = 5.8 \text{ kJ mol}^{-1}$), which means that they can both be formed at the beginning of the reaction. To distinguish between these two possible pathways for the reaction, the entire catalytic cycles starting from either isomer **5a** or isomer **5b** were calculated. We expected that, by direct comparison between their experimental results and their calculated energy profiles, it would be possible to reach a conclusion about the orientation of the ligands. From the experiments with the deuterated substrates, it is known that deuterium scrambling takes place before the formation of the amide and that the rate of exchange is much higher than the rate of the amide-forming reaction. Most likely, the deuterium exchange occurs in the first β -hydride-elimination step when a dihydride species (**6**) is formed. The calculations show that the formation of species **6a** is exothermic, whereas the formation of species **6b** is endothermic (Figure 6). In addition, the activation energy for the reverse reaction is lower in the case of species **6b** ($\Delta\Delta E_a(\mathbf{6b}-\mathbf{6a}) = -30.4 \text{ kJ mol}^{-1}$), whilst the difference in energy between the two transition states (**TS2** and **TS1**) is lower with species **6a**

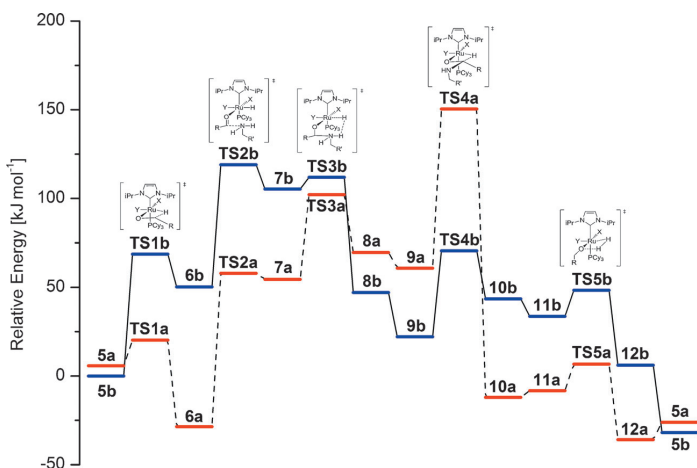


Figure 6. Energy profiles for the two possible catalytic cycles (**TS1a–TS5a**: X=H, Y=EtNH₂; **TS1b–TS5b**: X=EtNH₂, Y=H).

($\Delta E_a(\mathbf{TS2b}-\mathbf{TS1b}) = 48.9 \text{ kJ mol}^{-1}$, $\Delta E_a(\mathbf{TS2a}-\mathbf{TS1a}) = 18.5 \text{ kJ mol}^{-1}$). These facts suggest that the observed β -hydride elimination is more plausible in the case of isomer **6b** than with isomer **6a**. Consequently, the noted equilibrium between deuterated and non-deuterated substrates will be determined by the **b** pathway in the first β -hydride-elimination step.

To gain additional support for the **b** route, the two pathways were compared quantitatively by calculating the turn-over frequencies (TOFs) with the energetic span model. The concept of energetic span was introduced by Amatore and Jutand^[17] and further developed by Kozuch and Shaik.^[18]

This model replaces the classical Curtin–Hammett principle of the rate-limiting step in the catalytic cycle with the rate-limiting states, that is, the TOF-determining transition

state (TDTS) and the TOF-determining intermediate (TDI). The AUTOF program^[19] was used to calculate the TOFs from the computationally obtained energy states. These calculations show that, for the **a** pathway, **TS4a** is the TDTS and species **6a** is the TDI, whereas, for the **b** pathway, **TS2b** is the TDTS and species **5b** is the TDI. In other words, the rate of the reaction is defined by the difference in energy (energetic span) between species **6a** and **TS4a** ($\Delta E = 189.1 \text{ kJ mol}^{-1}$) for the **a** pathway and between species **5b** and **TS2b** for the **b** pathway ($\Delta E = 119.0 \text{ kJ mol}^{-1}$). As a result of the large differences in energetic span between the two pathways, the calculated TOF for the catalytic cycle that proceeds through the **a** pathway is $1.04 \times 10^{-8} \text{ h}^{-1}$, whereas the TOF for the catalytic cycle that proceeds through the **b** pathway is a factor of $\times 10^6$ higher ($7.38 \times 10^{-1} \text{ h}^{-1}$). This large difference between the calculated TOFs, along with the data on deuterium scrambling, clearly indicates that the orientation of the ligands in the **b** pathway is consistent with the experimental results, whereas that in the **a** pathway is not. Moreover, the calculated TOF is close to the average experimental value of $8.00 \times 10^{-1} \text{ h}^{-1}$, which lends further support to the conclusion that the **b** cycle is the dominant product-forming pathway in this reaction. The *trans* orientation of the hydrides in this route makes the species less stable and, consequently, more reactive.

For the **b** pathway, the ability to dissociate a molecule of phosphine was examined to explain the spectroscopic observations (see above). Calculations were performed for all of the intermediates (**5b–12b**) and revealed that one intermediate (**6b**) was more stable without a coordinated phosphine (Table 3).

Table 3. Energy of PCy₃ dissociation from intermediates **5b–12b**.

Compound	5b	6b	7b	8b	9b	10b	11b	12b
ΔG_{dissoc} [kJ mol ⁻¹]	41.2	-6.4	29.4	61.1	63.7	16.0	43.8	15.7

However, the barrier for the addition of an amine to this species (without a coordinated phosphine) is 21.7 kJ mol^{-1} higher than that to species **6b**, which, in total, makes the pathway without phosphine 15.3 kJ mol^{-1} less favorable. Because species **6b** is located between two rate-limiting states, the concentration of this intermediate will have a strong influence on the overall rate of the reaction. This result correlates with the experimental observations, where the addition of phosphine shifts the equilibrium towards species **6b** and increases the overall rate, but the order of the reaction with respect to phosphine is less than one because some phosphine dissociates off. In addition, the doublet in the ¹H NMR spectrum at $\delta = -18.04 \text{ ppm}$ can be assigned to the dihydride species that is formed by PCy₃ dissociation from species **6b**.

Having determined the orientation of the ligands, the next step was to establish the geometrical details of the species that are involved in the catalytic cycle. All of the compounds in the catalytic cycle are 18-electron complexes, except for two intermediates, **5b** and **9b**, which both have

an empty site and undergo β -hydride elimination. Notably, when molecular hydrogen has dissociated from species **12b** to form species **5b**, the alkoxide ligand changes its coordination from η^1 to η^3 by engaging in an agostic interaction between Ru and the α -C–H bond of the alkoxide. This interaction has also previously been observed in computational studies of the β -hydride elimination with alkoxides.^[20] As shown in Figure 7, the Ru–H bond length changes from

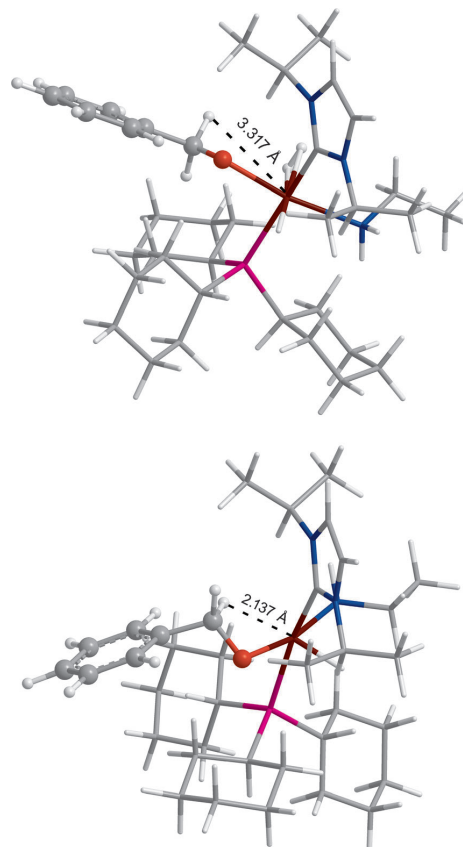
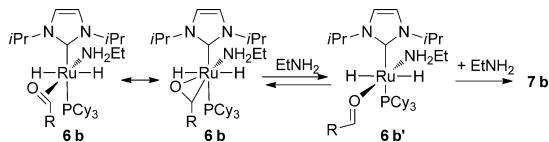


Figure 7. Calculated structures of compounds **12b** (top) and **5b** (bottom).

3.317 Å (**12b**) to 2.137 Å (**5b**). A similar agostic interaction is observed in the transformation from species **8b** into species **9b**. This result indicates that, during the catalytic cycle, ruthenium is electron poor and can be stabilized by receiving electron density from its ligands. This conclusion is also supported by experimental observations because amides are formed faster and in higher yields when electron-rich phosphines and NHCs, as well as benzyl alcohols, with electron-donating substituents in the *para* position are used (see above).

After the first β -hydride elimination, complex **6b** is formed. In this intermediate, the aldehyde acts as a η^2

ligand by binding to the ruthenium center through the π system of the C=O bond (Scheme 4). However, the geometry of the carbonyl carbon atom is close to that of an sp^3 hybrid-



Scheme 4. Equilibrium between the isomers of compound **6b**.

dized carbon atom (out-of-plane angle for the C–H bond: 136° , $d_{C=O}=1.309 \text{ \AA}$), which implies that complex **6b** is more-correctly represented by a three-membered oxaruthinacycle (Figure 8). In the subsequent addition of the amine, complex **6b** rearranges into the aldehyde η^1 isomer (**6b'**;

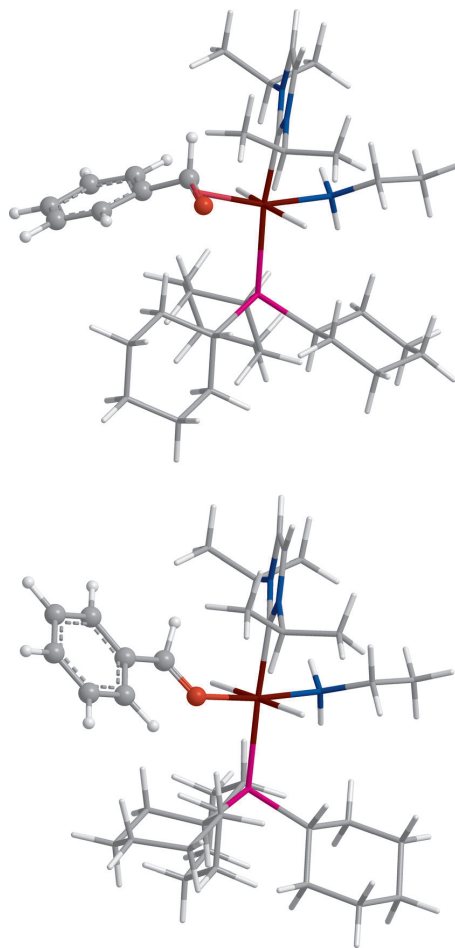


Figure 8. Calculated structures of compounds **6b** (top) and **6b'** (bottom).

out-of-plane angle for the C–H bond: 169° , $d_{C=O}=1.235 \text{ \AA}$), which is then attacked by the amine to form species **7b** (Scheme 4).

The energetic parameters for the transformations **5b**→**6b** and **6b**→**7b** determine the overall rate of the reaction. These steps have approximately equal energy ($E_a(\mathbf{5b-TS1b})=68.8 \text{ kJ mol}^{-1}$, $E_a(\mathbf{6b-TS2b})=68.7 \text{ kJ mol}^{-1}$) and, consequently, both steps should contribute equally to the limitations of the reaction. In the Hammett study, these two steps have opposite influence on the rate (and, hence, the ρ value) of the reaction. In the first step, electron-donating groups facilitate the β -hydride elimination, whereas, in the second step, they have the opposing effect in the nucleophilic addition to the aldehyde.

To model the Hammett study, the energy difference between the TDI and the TDTS was calculated for several benzyl alcohols with the following *para* substituents: NMe₂, OMe, SMe, Me, F, Cl, CF₃. Their relative reactivities were calculated by using Equation (2).

$$\lg \frac{k_X}{k_H} = \frac{\delta E_H - \delta E_X}{2.303RT}, \delta E = E(\text{TDTS}) - E(\text{TDI}) \quad (2)$$

Different calculated energies were used in [Eq. (2)], but only the gas-phase energies and solution-phase energies showed good correlation with the σ^+ values (Figure 9).

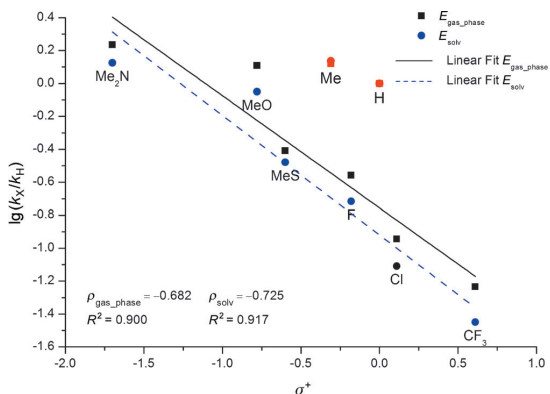


Figure 9. Hammett plot with calculated gas-phase and solvation energies (red points were excluded from the linear regression).

As can be seen from Figure 9, two substituents did not follow the overall good correlation; H and Me are both non-polar substituents and we ascribe the difference between these and the remaining polar substituents to inaccuracies in the solvation model. When examining the actual ρ values that were calculated by using the gas-phase energies ($\rho_{\text{gas phase}}=-0.68$) and the solution-phase energies ($\rho_{\text{solv}}=-0.73$), it is clear that the calculated slopes are somewhat higher than the experimental value ($\rho_{\text{exp}}=-0.15$). However, the calculated reactivity follows the same trend as the exper-

imental data, that is, that substrates with electron-donating substituents are more reactive than those with electron-withdrawing substituents.

The KIE for the reaction was also calculated by using the energetic-span model. In that case, the catalytic cycle with deuterated analogues had a δE value of 142.3 kJ mol⁻¹, which resulted in a TOF of 1.4·10⁻² h⁻¹. Thus, the KIE value was calculated as KIE = TOF_H/TOF_D = 3.78, which was significantly higher than that observed experimentally (KIE = 2.29). There may be several reasons for this discrepancy: First, benzyl alcohol was used in the computational model system whereas [D₁₀]-1-butanol was utilized in the experiment. This result indicates that the nature of the substituent on the α carbon atom of the alcohol does have a profound influence on the observed KIE value in the amidation reaction. Another way to calculate the KIE value is by using Equation (3).

$$\text{KIE} = \frac{k_{\text{H}}}{k_{\text{D}}} = e^{-\frac{\Delta G_{\text{H}}^{\ddagger} - \Delta G_{\text{D}}^{\ddagger}}{RT}}, \Delta G_{\text{a}} = \Delta G_{\text{tot}}(\text{TS2b}) - \Delta G_{\text{tot}}(\text{6b}) \quad (3)$$

The KIE value for the system with EtOH was calculated to be 3.27, which is very close to the value obtained by using the energetic span model. This result shows that either of these two models may be used for the KIE calculations.

However, the KIE value from these calculations is still higher than the experimental value (2.29); the reason for this difference may partially lie in the experimental determination of the KIE. Commercially available [D₁₀]-1-butanol was used for the KIE experiments and it contained a small amount of C₄D₉OH. The amidation reaction was performed with 5% of PCy₃·HBF₄, which, after deprotonation with KO^tBu, would exchange hydrogen and deuterium with [D₁₀]-1-butanol. Presumably, 5–10% of C₄D₉OH was present in the experiment with [D₁₀]-1-butanol and this isotopic impurity would lower the value of the experimentally determined KIE.

Conclusion

The mechanism of the Ru–NHC-catalyzed amidation reaction between alcohols and amines was investigated by using experimental and theoretical methods. A Hammett study indicates that a small positive charge is built-up at the benzylic position in the transition state of the turnover-limiting step. The small value indicates that the rate of the reaction is not dominated by a single elementary reaction; instead, it is likely that two steps with opposite electronic character both influence the reaction rate.

The kinetic isotope effect was experimentally determined to be 2.29(±0.15), which suggests that breakage of the C–H bond is not the rate-limiting step, but that it is one of several slow steps in the catalytic cycle. These experimental results were further supported by the characterization of a plausible catalytic cycle by using DFT/M06 calculations. Both *cis*-dihydride and *trans*-dihydride intermediates were considered,

but when the theoretical turnover frequencies (TOFs) were derived directly from the calculated DFT/M06 energies, we found that only the *trans*-dihydride pathway (Scheme 3, cycle **b**) was in agreement with the experimentally determined TOFs. The overall good agreement between the experimental and theoretical data illustrates that modern theoretical methods have matured to a point where their results can be used to predict and rationalize experimental observations. This result opens up the possibility for a number of new applications, such as in silico ligand screening, which is currently underway in our laboratory.

Computational Details

All calculations were performed with Jaguar^[21] (version 7.8, release 109) by using the M06^[22] or B3LYP functionals^[23] in combination with the LACVP* basis set.^[24] During our initial investigations, it became clear that the B3LYP functional did not adequately describe the non-bonded interactions that were responsible for discriminating between the possible reaction pathways; this deficiency of the B3LYP functional is well-known and the problem has been addressed previously by either appending a classic dispersion term^[25] or by using a functional that incorporates terms for kinetic energy density.^[26] Among the most-successful of these latter approaches are the M0x family of functionals reported by Truhlar and co-workers; herein, we chose the M06 functional, which has been optimized with a particular focus on organometallic systems and has been used successfully in an earlier study.^[27]

All of the structures were optimized in the gas phase and the single-point solvation energy was calculated for the optimized structures by using a standard Poisson–Boltzmann solver with suitable parameters for benzene as the solvent (dielectric constant: $\epsilon = 2.284$, probe radius: $r = 2.600$ Å). Gibbs free energies were obtained from the vibrational-frequency calculations for the gas-phase geometries at 298 K and 383 K. All of the transition states were characterized by the presence of one negative vibrational frequency.

Acknowledgements

We thank the Danish Council for Independent Research–Technology and Production Sciences (DFP) for financial support.

- [1] a) V. R. Pattabiraman, J. W. Bode, *Nature* **2011**, *480*, 471–479; b) C. L. Allen, J. M. J. Williams, *Chem. Soc. Rev.* **2011**, *40*, 3405–3415; c) C. Chen, S. H. Hong, *Org. Biomol. Chem.* **2011**, *9*, 20–26.
- [2] B. Shen, D. M. Makley, J. N. Johnston, *Nature* **2010**, *465*, 1027–1032.
- [3] J. W. Bode, R. M. Fox, K. D. Baucom, *Angew. Chem.* **2006**, *118*, 1270–1274; *Angew. Chem. Int. Ed.* **2006**, *45*, 1248–1252.
- [4] a) J.-F. Soulé, H. Miyamura, S. Kobayashi, *J. Am. Chem. Soc.* **2011**, *133*, 18550–18553; b) Y. Wang, D. Zhu, L. Tang, S. Wang, Z. Wang, *Angew. Chem.* **2011**, *123*, 9079–9083; *Angew. Chem. Int. Ed.* **2011**, *50*, 8917–8921.
- [5] a) C. Gunanathan, Y. Ben-David, D. Milstein, *Science* **2007**, *317*, 790–792; b) L. U. Nordstrøm, H. Vogt, R. Madsen, *J. Am. Chem. Soc.* **2008**, *130*, 17672–17673; c) A. Prades, E. Peris, M. Albrecht, *Organometallics* **2011**, *30*, 1162–1167; d) N. D. Schley, G. E. Doberiner, R. H. Crabtree, *Organometallics* **2011**, *30*, 4174–4179; e) K. Shimizu, K. Ohshima, A. Satsuma, *Chem. Eur. J.* **2009**, *15*, 9977–9980; f) J. Zhu, Y. Zhang, F. Shi, Y. Deng, *Tetrahedron Lett.* **2012**, *53*, 3178–3180.
- [6] a) T. Zweifel, J.-V. Naubron, H. Grützmacher, *Angew. Chem.* **2009**, *121*, 567–571; *Angew. Chem. Int. Ed.* **2009**, *48*, 559–563; b) A. J. A.

- Watson, A. C. Maxwell, J. M. J. Williams, *Org. Lett.* **2009**, *11*, 2667–2670.
- [7] a) J. P. Shackleford, B. Shen, J. N. Johnston, *Proc. Natl. Acad. Sci. USA* **2012**, *109*, 44–46; b) I. Pusterla, J. W. Bode, *Angew. Chem.* **2012**, *124*, 528–531; *Angew. Chem. Int. Ed.* **2012**, *51*, 513–516.
- [8] M. Montag, J. Zhang, D. Milstein, *J. Am. Chem. Soc.* **2012**, *134*, 10325–10328.
- [9] a) G. Zeng, S. Li, *Inorg. Chem.* **2011**, *50*, 10572–10580; b) H. Li, X. Wang, F. Huang, G. Lu, J. Jiang, Z. Wang, *Organometallics* **2011**, *30*, 5233–5247; c) A. Nova, D. Balcells, N. D. Schley, G. E. Dobreiner, R. H. Crabtree, O. Eisenstein, *Organometallics* **2010**, *29*, 6548–6558.
- [10] a) A. Maggi, R. Madsen, *Organometallics* **2012**, *31*, 451–455; b) C. Chen, Y. Zhang, S. H. Hong, *J. Org. Chem.* **2011**, *76*, 10005–10010; c) A. Sølvehøj, R. Madsen, *Organometallics* **2011**, *30*, 6044–6048; d) J. Zhang, M. Senthikumar, S. C. Ghosh, S. H. Hong, *Angew. Chem.* **2010**, *122*, 6535–6539; *Angew. Chem. Int. Ed.* **2010**, *49*, 6391–6395; e) J. H. Dam, G. Osztrovszky, L. U. Nordstrøm, R. Madsen, *Chem. Eur. J.* **2010**, *16*, 6820–6827; f) S. C. Ghosh, S. H. Hong, *Eur. J. Org. Chem.* **2010**, 4266–4270; g) S. Muthaiah, S. C. Ghosh, J.-E. Jee, C. Chen, J. Zhang, S. H. Hong, *J. Org. Chem.* **2010**, *75*, 3002–3006; h) Y. Zhang, C. Chen, S. C. Ghosh, Y. Li, S. H. Hong, *Organometallics* **2010**, *29*, 1374–1378; j) S. C. Ghosh, S. Muthaiah, Y. Zhang, X. Xu, S. H. Hong, *Adv. Synth. Catal.* **2009**, *351*, 2643–2649.
- [11] M. R. Netherton, G. C. Fu, *Org. Lett.* **2001**, *3*, 4295–4298.
- [12] a) P. Fristrup, M. Tursky, R. Madsen, *Org. Biomol. Chem.* **2012**, *10*, 2569–2577; b) P. Fristrup, M. Kreis, A. Palmelund, P.-O. Norrby, R. Madsen, *J. Am. Chem. Soc.* **2008**, *130*, 5206–5215; c) J. H. Dam, P. Fristrup, R. Madsen, *J. Org. Chem.* **2008**, *73*, 3228–3235; d) P. Fristrup, L. B. Johansen, C. H. Christensen, *Chem. Commun.* **2008**, 2750–2752.
- [13] a) C. Hansch, H. Gao, *Chem. Rev.* **1997**, *97*, 2995–3059; b) C. Hansch, A. Leo, R. W. Taft, *Chem. Rev.* **1991**, *91*, 165–195; c) X. Creary, M. E. Mehrsheikh-Mohammadi, S. McDonald, *J. Org. Chem.* **1987**, *52*, 3254–3263.
- [14] D. H. Wertz, *J. Am. Chem. Soc.* **1980**, *102*, 5316–5322.
- [15] J. K. C. Lau, D. V. Deubel, *J. Chem. Theory Comput.* **2006**, *2*, 103–106.
- [16] a) E. Solari, S. Gauthier, R. Scopelliti, K. Severin, *Organometallics* **2009**, *28*, 4519–4526; b) A. Aranyos, G. Csajnyik, K. J. Szabó, J.-E. Bäckvall, *Chem. Commun.* **1999**, 351–352.
- [17] C. Amatore, A. Jutand, *J. Organomet. Chem.* **1999**, *576*, 254–278.
- [18] S. Kozuch, S. Shaik, *Acc. Chem. Res.* **2011**, *44*, 101–110.
- [19] a) A. Uhe, S. Kozuch, S. Shaik, *J. Comput. Chem.* **2011**, *32*, 978–985; b) S. Kozuch, S. Shaik, *J. Phys. Chem. A* **2008**, *112*, 6032–6041; c) S. Kozuch, S. Shaik, *J. Am. Chem. Soc.* **2006**, *128*, 3355–3365.
- [20] N. Sieffert, M. Bühl, *J. Am. Chem. Soc.* **2010**, *132*, 8056–8070.
- [21] Jaguar, Version 7.8, Schrodinger, LLC, New York, NY, **2010**.
- [22] Y. Zhao, D. G. Truhlar, *Theor. Chem. Acc.* **2008**, *120*, 215–241.
- [23] a) A. D. Becke, *J. Chem. Phys.* **1993**, *98*, 5648–5652; b) C. Lee, W. Yang, R. G. Parr, *Phys. Rev. B* **1988**, *37*, 785–789.
- [24] P. J. Hay, W. R. Wadt, *J. Chem. Phys.* **1985**, *82*, 270–283.
- [25] a) S. Grimme, *J. Comput. Chem.* **2004**, *25*, 1463–1473; b) M. Elstner, P. Hobza, T. Frauenheim, S. Suhai, E. Kaxiras, *J. Chem. Phys.* **2001**, *114*, 5149–5155.
- [26] a) B. B. Averkiev, Y. Zhao, D. G. Truhlar, *J. Mol. Catal. A* **2010**, *324*, 80–88; b) Y. Zhao, D. G. Truhlar, *Acc. Chem. Res.* **2008**, *41*, 157–167.
- [27] X. Bantreil, G. Prestat, A. Moreno, D. Madec, P. Fristrup, P.-O. Norrby, P. S. Pregosin, G. Poli, *Chem. Eur. J.* **2011**, *17*, 2885–2896.

Received: July 5, 2012

Published online: October 15, 2012